Kite Turning

Ross Hughan Dawson

A thesis submitted in partial fulfilment
of the requirements for the degree of
Master of Engineering
in
Mechanical Engineering
at the
University of Canterbury,
Christchurch, New Zealand.

2011

Abstract

This thesis investigates the mechanisms behind the control of a typical two line kite, where the lines are attached to the kite side by side. This arrangement gives the kite flyer the ability to apply a roll angle to the kite, which then results in a yawing motion. The reason for this yaw rotation has not been adequately described previously.

The definitions of roll and yaw for a kite have been re-defined to match the real world behaviour of the kite-bridle-line system. Specifically, these are defined as rotations relative to the lines rather than the kite itself. This detail has been neglected in previous research, and has a significant effect on the turning behaviour of a kite.

A static model of a kite represented by flat disks was created. This model allows the out of balance forces and moments to be found for a kite when it is held at any position. When the kite is held with a roll angle applied, the disk angles of attack become unequal. This causes a change in the magnitude, direction, and point of action of the aerodynamic forces on each disk, which can lead to a yaw moment. While this does not give a complete picture of how a kite turns, it does explain one of the two mechanisms that cause a kite to begin to yaw when a roll angle is applied. The other mechanism is due to the velocity of the roll rotation, and is out of the scope of this thesis since a dynamic analysis would be required.

The static model showed that any variation to kite geometry or any parameter that affects the equilibrium position of the kite will affect turning response. The most important of these parameters for a simple kite represented by two disks is the dihedral angle. A minimum negative dihedral angle (or anhedral) is required for a kite to turn in the expected direction when a roll angle is applied. The value of the minimum anhedral angle required for this behaviour varies with other parameters, but is generally between 8°and 20°.

Other parameters such as bridle geometry also affect the turning response of a kite, primarily because they alter the equilibrium positions of the kite and line. Altering these equilibrium positions has a strong effect on turning response, since it changes the initial disk angles of attack. Additionally, if the kite and line are not aligned perpendicular to each other (which is a rare condition for a kite) a roll angle further changes the disk angles of attack, since the roll angle is applied about an axis relative to the line rather than the kite.

An investigation into the effect of varying wind velocity on turning response showed that it has an important effect. Some kites will reverse their response to a given roll angle at some wind velocities, which could make the kite very difficult to control. Additionally, some kites can alter their equilibrium positions sharply with wind velocity, again causing varying turning behaviour as the wind conditions change.

Future work should examine the dynamic turning response of kites. A dynamic simulation could be used to examine how the turning response of a kite is influenced by the rate at which a control input is applied. Additionally, the behaviour of the kite once the initial turning movement has begun could be assessed.

Acknowledgements

I would like to thank my supervisor, Dr. Keith Alexander, for the opportunity to work on such an interesting and challenging subject. His insight and enthusiasm for the subject have been invaluable.

I also wish to thank Graeme Harris for his valuable advice and assistance with wind tunnel testing, and Scott Amies for his help with the construction of the test rigs.

Finally, I would like to thank all my friends and family, of which there are too many to list here, for their support.

Contents

Nomenclature

A	Disk area
D	Drag force
L	Lift force
α	Disk angle of attack
β	Angle that bridles rotate through about their attachment to kite as the kite rolls.
Cd	Drag coefficient
Cl	Lift coefficient
d	Distance from the point where a kite line meets a bridle and the center of a kite.
F	Force. Superscripts indicate the coordinate system used, subsricpts identify the force.
g	Acceleration due to gravity
γ	Kite dihedral angle
l_a	Distance on kite between front and rear bridle line attachment points
l_f	Length of front bridle line
l_r	Length of rear bridle line
M	Moment. Superscripts indicate the coordinate system used, subscripts identify the moment axis.
m	Kite mass
p_i	Position vector of disk i of a multi disk kite relative to the kite center
φ	Kite roll angle
Φ	Line elevation angle

ψ	Kite yaw angle
ρ	Fluid density
R	Rotation matrix
r_{a-b}	Position vector, giving the vector between points a and b.
s	Kite span, defined as the distance between the disk centers for a two disk kite
τ	Kite twist angle
θ	Kite pitch angle
Θ	Line azimuth angle
V	Flow stream velocity

List of Figures

List of Tables

Chapter 1

Introduction

1.1 Project Aims

The primary purpose of this thesis is to develop an explanation as to how a kite with two lines turns. A two lined kite can be steered by pulling on one line to introduce a roll angle to the kite. This results in the kite yawing, which subsequently results in the kite moving off in a new direction. A well designed controllable kite will always yaw in one direction for a given roll direction – a pull on the left line (from the kite flyer's perspective), resulting in a roll rotation, causes the kite to turn towards the left. However, some kites will turn in the opposite direction, either consistently or only under certain conditions. The mechanism that causes this turning behaviour is not clear, and has not been adequately explained in previous studies.

To understand how a kite turns, a method of investigating the forces and moments acting on the kite and line in a given situation is required. Furthermore, the causes for variation of these forces and moments must be determined. Performing a complicated numerical dynamic simulation of a kite may indicate how a particular kite will respond to control inputs, but it would not facilitate an understanding of the fundamental mechanisms by which this response occurs. Rather, a static model of a kite was created, to allow the initial response to any perturbation to equilibrium conditions to be investigated. The calculations used for this static model can also be used as a starting point for any possible future work on the stability and dynamic control of kites.

The secondary purpose of this thesis is to investigate how changes to kite and bridle geometry affect the turning response of a kite. It is well known that many factors affect how a kite flies. For many flight parameters, such as equilibrium points and maximum altitudes, the effect of various kite setup parameters is well understood. However, how kite turning performance is affected by different kite and bridle geometry is not known, other than empirical information obtained essentially through trial and error by kite makers. It is hoped that the static model can be used to enable predictions to be made about what parameters are important for a kite's turning ability.

1.2 Background

1.2.1 History of Kite Research

The kite has been used in one form or another for around 2500 years. They were used by the Chinese and Indonesians for a variety of purposes, including fishing, warfare, religious rituals, and general amusement[1]. Research on how kites fly can be found dating back to the early 1800's, perhaps most notably George Pocock's work on using kites to lift or drag heavy objects. Pocock's accomplishments include lifting his children to heights of up to 82 metres and building and testing a kite powered buggy capable of speeds in excess of 30km/h[1, 2]. However, Pocock's work was all experimental.

The first rigorous treatment of the mechanics of kite flight is found in C.F. Marvin's 1897 Monograph on The Mechanics and Equilibrium of Kites[3]. This work covers the mechanics of kite flight in some detail. Marvin's work examines the forces acting on a kite, and how they interact with those acting on the line and tail. He examines conditions necessary for equilibrium of the kite-line system, as well as the stability of this equilibrium. Had two lined, steerable kites existed in his day, Marvin's work would have perhaps covered the content of this thesis to some extent. Marvin's work succeeds in breaking down the complexity of kite flight so that it can be understood in simple terms.

More recently, a similar approach was taken by K. Alexander and J. Stevenson in their paper investigating kite equilibrium points[4]. This included simulation of the kite-bridle-line system, rather than the simplified kite-line system used by Marvin. An important outcome of this work was the verification of the existence of multiple equilibrium positions for some kite-bridle-line systems, which had previously been shown to exist for simple kite-line systems by R.A. Adomaitis[5]. This work also showed how bridle geometry can be tuned to control a kite's equilibrium points in various wind conditions. The work was subsequently used to develop various methods of testing the performance of traction kites[6, 7, 8, 9].

G. Sánchez performed a dynamic analysis on a single-line kite-line system using a Lagrangian formulation[10]. A similar method could be used in the future to model a two-line kite-bridle-line system, using the work presented in this thesis as a starting point. Much of the other recent research relating to kites has concentrated on very specific aspects of kites and their flight, often with a specific goal in mind. For example, many articles can be found relating to the performance of kites used to lift meteorological instruments[11]. These kites are uncontrolled, single lined kites designed for stability. As such, research in this area has little relevance to kite turning.

The second area that has seen a large amount of research is that of traction kites, used for recreational purposes and increasingly proposed as a method of power generation. Many papers have been published modelling such kites, particularly with a

view to their use for power generation[12, 13, 14, 15, 16, 17]. While these are generally controllable kites, none of the research found contains an explanation for the turning mechanism being considered in this thesis. Rather, the kites modelled use direct manipulation of control surfaces or the entire kite surface to create asymmetries in the kite geometry. This is commonly achieved using four lines to control a kite, and has also been achieved by using motorised control surfaces and variable attachment points [12].

1.2.2 Development of Controllable Kites

Until comparatively recently, kites were only attached to the ground or kite flyer by one line. These single line kites are largely uncontrollable. In the 1930's, H. DeHaven patented kites that could be controlled from the ground by using two lines[18, 19]. The use of a second line allowed the user to control either the orientation or the angle of a rudder panel added to the kite. During the Second World War, dual line kites were further developed by P. Garber for the United States Navy[20]. Garber's kites were designed for use as anti-aircraft gunnery practice targets, and again utilised a movable rudder to control the movement of the kite.

Kites that are controllable without a separate, movable control surface first appeared in the early 1970's, having been developed by P. Powell in 1972 [1, 21]. Powell's kites were steerable by using two lines attached at a distance from each side of the centre of the kite, allowing the flyer to roll the kite by adjusting the relative lengths of the two lines. This roll leads to the kite yawing in the same manner as that caused by the rudder surface of Garber's kites, allowing the kite to be flown about the sky. The vast majority of two-line kites in use today use this same control mechanism.

The mechanism behind the yawing movement caused by the control surfaces of DeHaven's and Garber's kites is well understood – there is fundamentally very little difference between the actions of control surfaces on a kite and an aeroplane. However, the mechanism behind the operation of Powell's two line kites has not been rigorously explained. Anyone familiar with two line kites knows that pulling one line, thereby inducing a roll angle, causes a kite to yaw. The reason for this resulting yaw is not immediately apparent, and is the focus of this thesis.

Various explanations as to what happens to cause a yaw moment when a kite is rolled have been proposed – the most common explanation seems to be that the roll *velocity* induced by pulling on one line causes a change in the apparent wind direction of each side of the kite. This does without question occur, but a test flight with a common stunt kite will show that a slowly applied roll causes a yaw rotation just as effectively (sometimes more so) than a quickly applied one. This suggests the change in position of the kite is at least as important as the rate of change.

J. Stevenson postulated that the difference in line tensions created when rolling a kite causes the yaw moment [9]. As a kite is rolled, the load on the two lines becomes

unequal, and the location of the resultant force moves towards whichever side has the higher load. However, for this to create a yaw moment, the yaw axis must be assumed to be non-parallel to the lines – Stevenson assumed it was aligned perpendicular to the kite itself. This implies that as the kite yaws, it can alter the relative lengths of the lines without resistance, contradicting the assumption that the relative line lengths are controlled.

1.2.3 Modelling Kites Using Disks

The inspiration for the current research arose from J. Stevenson's thesis *Traction Kite Testing and Aerodynamics*[9]. This thesis primarily focused on devising a method of reliably testing traction kites. In later sections, it proposed investigating the behaviour of kites by using multiple circular plates to represent more complicated shapes. This removes many of the complications of modelling kites, since a disk's aerodynamic properties only vary with one parameter – the angle the wind makes to the disk surface, or angle of attack. Because of this property, a kite represented by a number of disks can be analysed relatively easily at any orientation to the wind by calculating the forces acting on each disk separately.

Stevenson performed a preliminary analysis using the disk method to investigate how kites are steered, but this was not a primary focus of the thesis. As mentioned above in section 1.2.2, it is thought that Stevenson's definition of the yaw axis is incorrect, and that the mechanism by which he describes a kite turning does not actually lead to a yaw moment.

Geraud LaFortune performed an analysis of kite turning using disk kites in his undergraduate research project *Fundamental Kite Motion* [22]. LaFortune assumed that the primary yaw moment causing a kite to turn is caused directly by the roll rotation induced in the kite by pulling on one line. This assumption seems to match observations of kite behaviour. However, as with Stevenson's work, LaFortune assumes that the kite rolls and yaws about axes relative to itself, not the lines. This is thought to be incorrect, as stated above.

1.2.4 Coordinate Systems for Kites

Because kites move in three dimensions in a complicated manner, the choice of coordinate system(s) has a great impact on the difficulty of performing any level of analysis. The choice of an appropriate coordinate system depends on what assumptions are made and how many degrees of freedom the kite system is allowed. As such, there is no universally accepted convention for coordinate systems used on kites. For example, Stephen Hobbs used a coordinate system fixed to the kite chord in his Two-dimensional simulation of kite flight [11], while Podgaets and Ockels have utilised both ground and kite

fixed coordinate systems in their three-dimensional simulation of the laddermill system [15].

Chapter 2

Defining the Position of a Kite

The seemingly simple kite is in fact a rather awkward object to define in three dimensions. Previous studies and simulations performed on kites have used many different coordinate systems to describe the position of the kite. None of the examples of kite simulation found, or any other convention found, are suited to investigating the turning behaviour of kites - mostly because simplifications have been made that limit the degrees of freedom available. To investigate the turning behaviour of a traditionally controlled kite (i.e. using multiple lines, rather than a single line with control surfaces added to the kite), its position and orientation need to be defined without making simplifications that limit movement.

2.1 Coordinate Systems

When describing a kite, it is useful to use three separate coordinate systems, as shown in Figure 2.1. Firstly, a coordinate system with the Z-axis aligned with the wind direction and the Y-axis normal to the ground (assumed level and flat) is used as the global coordinate system. Secondly, a coordinate system aligned with the kite itself is used when working with the aerodynamics of the kite. The origin of this coordinate system is either set at the centre of mass of the kite (as shown in Figure 2.1) or at the point where the bridle joins the line(s). A coordinate system based on the line is also used. The use of this coordinate system simplifies defining the rotational position of a kite with more than one line, since the lines restrict rotational movement about one or more axes that are not necessarily aligned with the kite based coordinate axes. This makes the Tait–Bryan yaw, pitch, and roll convention used for aircraft inappropriate [23].

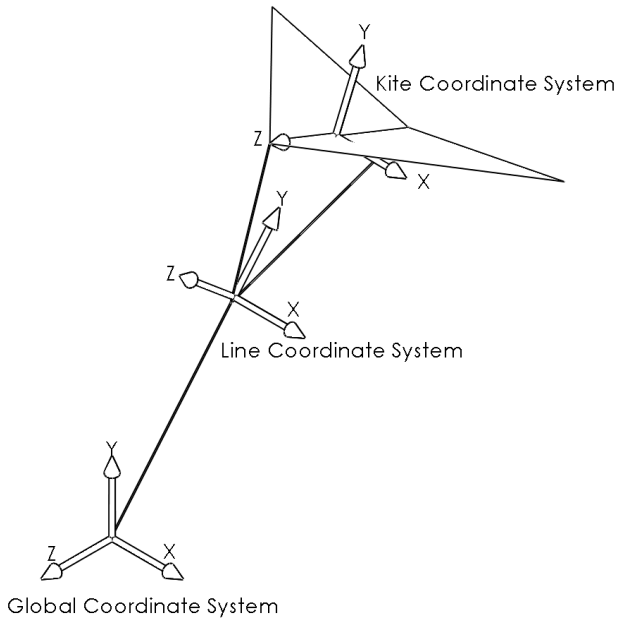

Figure 2.1 Diagram showing the three coordinate systems used in modelling a kite in three dimensions

2.2 Degrees of Freedom

2.2.1 General Case

The number of degrees of freedom of a kite depends on the number of lines used. In any case, the kite is split into two subsystems: the line(s) and the kite itself. For the purposes of the (static) calculations performed here, the lines are treated as one single line, and the extra constraints that the use of two or four lines place on the kite are simply added to the kite subsystem. This simplifies the calculations, although if a dynamic simulation were to be performed each line may need to be treated separately. The kite subsystem includes the structure of the kite and the bridles, which are assumed to be rigid with the exception of allowing the bridles to rotate about their attachment to the kite. The kite subsystem connects to the line subsystem at the end of the bridles.

The line is restrained from positional displacement at the bottom end but is free to rotate about any axis, giving three degrees of freedom. One of these degrees of freedom is neglected, since the line rotating about its own y-axis has no effect on the system, leaving two degrees of freedom. The kite is constrained by the line, and thus shares the line's two degrees of freedom plus a number of extra degrees of freedom afforded by the kite's ability to rotate around the top of the line - the number of which depends on the number of lines used.

2.2.2 Single Line Kite

A kite with a single line has the most degrees of freedom, since the kite is unrestrained from rotational movements about the top end of the line. Thus the single line kite has 5 degrees of freedom: The line can rotate with respect to the ground about two axes, and the kite is free to pitch, roll and yaw about the bridle point.

2.2.3 Two Line Kite

With a two line kite, the roll angle of the kite is controlled by the relative lengths of the two lines. The kite remains free to pitch and yaw about the bridle point, leaving the system with four degrees of freedom.

2.2.4 Four Line Kite

A four line kite is constrained from both pitching and rolling about the bridle point, leaving three degrees of freedom. This configuration is generally only used on flexible kites, as it allows the kite to be steered by twisting the kite, leading to a different angle of attack on each side. This allows for more predictable steering behaviour than the banking method used for two lined kites. Using four lines does not change the turning ability of a rigid kite, and thus will not be further discussed here.

2.3 Parameters Used to Define a Kite's Position

2.3.1 Parameters Used to Describe the Orientation of the Line

The line effectively has two degrees of freedom, as explained in section 2.2, thus two parameters are required to fix its position. The line is described by an elevation angle, Φ, and an azimuth angle, Θ, relative to the global coordinate system. The definitions for elevation and azimuth have been chosen to be similar to conventions used when defining the position of an object in the sky (such as stars and satellites), and do not directly correspond to the angles between the global and line coordinate systems. This will be dealt with later in section 2.4.1.

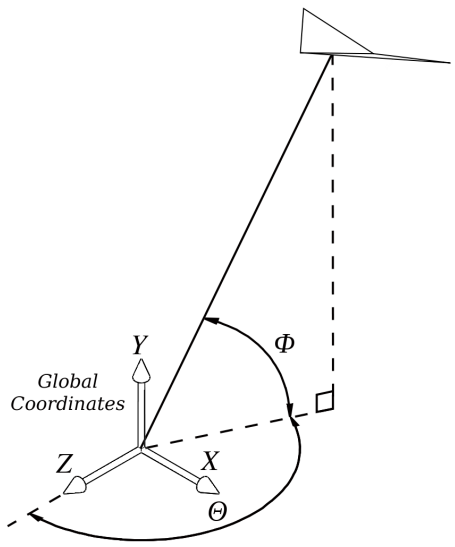

Figure 2.2 Diagram showing the definition of elevation angle Φ and an azimuth angle Θ for a kite

2.3.2 Parameters Used to Describe the Orientation of the Kite

Three parameters are required to fix the orientation of the kite on the end of the line. These will be referred to as pitch, roll and yaw, but their definition differs from the standard Tait-Bryan convention, as does the order in which they are applied. Firstly, a pitch angle is applied. This is defined as a rotation about the x-axis of the kite based coordinate system, and is analogous to the overall angle of attack of the kite with respect to the wind if no yaw or roll is applied. Next, a roll angle can be applied by rotating the kite about z-axis of the line based coordinate system. The line based coordinate system is used here to reflect what happens when a kite flier tugs one line on a two-line kite – the kite does not roll about its own z-axis, as is the case when using the Tait-Bryan convention, rather, it rolls about an axis perpendicular to the lines – the line based z-axis. Finally, a yaw angle can be applied. Again, this is applied by using the line based coordinate system, this time with a rotation about the y-axis, or the axis of the lines themselves.

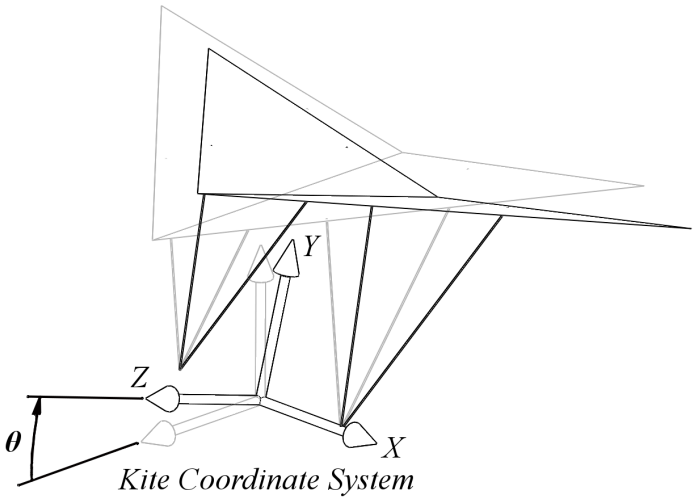

Figure 2.3 Diagram showing the definition of pitch angle, θ, for a kite, defined as a rotation about the kite X-Axis.

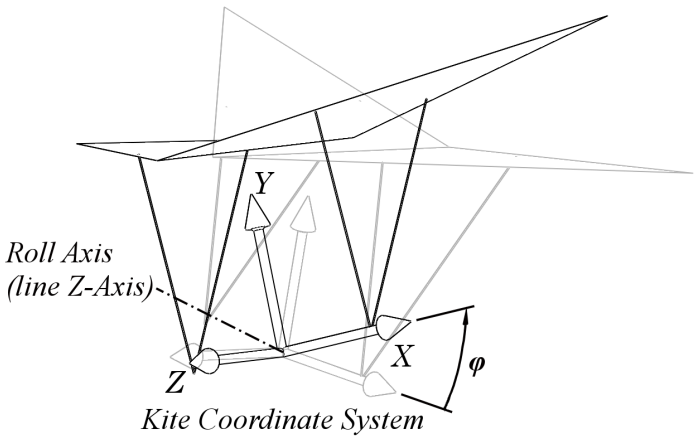

Figure 2.4 Diagram showing the definition of roll angle, φ, for a kite, defined as a rotation about the line Z-Axis. The bridles have been shown to be rigidly attached to the kite for clarity, whereas they can rotate about their attachment to the kite in reality, meaning that the kite does not rotate to the side as shown.

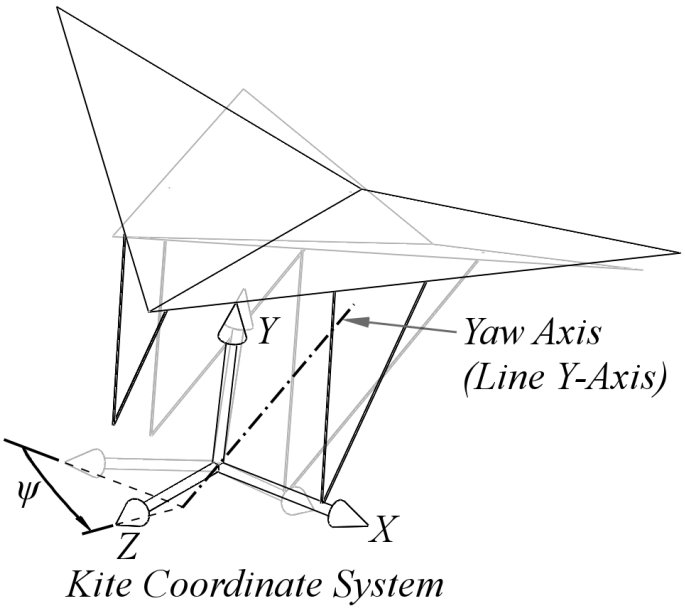

Figure 2.5 Diagram showing the definition of yaw angle, ψ, for a kite, defined as a rotation about the line Y-Axis.

2.4 Rotation Matrices

Rotation matrices are used to apply rotations to the kite and to switch between different coordinate systems. In a three dimensional space, any rotation can be represented by an orthogonal 3x3 matrix. This rotation matrix can be built from three basic rotation matrices about the x-, y-, and z-axes [23], or can be found directly for a rotation about an arbitrary axis. The three basic rotation matrices for a rotation ϑ are:

$$R_x(\vartheta) = \begin{bmatrix} 1 & 0 & 0 \\ 0 & \cos\vartheta & -\sin\vartheta \\ 0 & \sin\vartheta & \cos\vartheta \end{bmatrix} \tag{2.1}$$

$$R_y(\vartheta) = \begin{bmatrix} \cos\vartheta & 0 & \sin\vartheta \\ 0 & 1 & 0 \\ -\sin\vartheta & 0 & \cos\vartheta \end{bmatrix} \tag{2.2}$$

$$R_z(\vartheta) = \begin{bmatrix} \cos\vartheta & -\sin\vartheta & 0 \\ \sin\vartheta & \cos\vartheta & 0 \\ 0 & 0 & 1 \end{bmatrix} \tag{2.3}$$

When a rotation about some other axis is desired, Rodrigues rotation formula can be used rather than breaking the rotation down into x, y, and z components – this will

be useful in applying the roll and yaw angles to a kite[24]. Rodrigues rotation formula states that for a rotation ϑ about an axis given by the unit vector u:

$$R_u(\vartheta, \tilde{u}) = I + \tilde{u}\sin\vartheta + \tilde{u}^2(1 - \cos\vartheta) \tag{2.4}$$

Where I is the 3x3 Identity matrix and $\tilde{u}$ is the cross product matrix of u:

$$\tilde{u} = \begin{bmatrix} 0 & -u_z & u_y \\ u_z & 0 & -u_x \\ -u_y & u_x & 0 \end{bmatrix} \tag{2.5}$$

2.4.1 Rotation Matrix for the Line Coordinate System

The line coordinate system differs from the global coordinate system by a rotation about the global y-axis (found from the azimuth angle, Θ) and a rotation about the (now modified) x-axis (found from the elevation angle, Φ). The angles of rotation are not the same as the azimuth and elevation angles, as explained in section 2.3.1.

To change a vector defined in the global coordinate system to the line-based coordinate system, the vector needs to be rotated by the reverse of the azimuth and elevation angles. These rotations can both be performed using basic rotation matrices:

$$R_{azimuth} = \begin{bmatrix} \cos(\pi\text{-}\Theta) & 0 & \sin(\pi\text{-}\Theta) \\ 0 & 1 & 0 \\ -\sin(\pi\text{-}\Theta) & 0 & \cos(\pi\text{-}\Theta) \end{bmatrix} \tag{2.6}$$

$$R_{elevation} = \begin{bmatrix} 1 & 0 & 0 \\ 0 & \cos\left(\frac{\pi}{2} - \Phi\right) & -\sin\left(\frac{\pi}{2} - \Phi\right) \\ 0 & \sin\left(\frac{\pi}{2} - \Phi\right) & \cos\left(\frac{\pi}{2} - \Phi\right) \end{bmatrix} \tag{2.7}$$

Note that the angles used in the rotation matrices are modified due to the azimuth and elevation angles being defined by the angles made between the global axes and the line itself (rather than the line coordinate system), as described in section 2.3.1. The rotation matrix to change from the global coordinate system to the line coordinate system can be found by multiplying the azimuth and elevation matrices together in the correct order:

$$R_{line} = R_{elevation} \times R_{azimuth} \tag{2.8}$$

Since the line rotation matrix is essentially 'un-doing' the rotations by which the line coordinate system differs from the global coordinate system, the order of rotations is the reverse of the order described in section 2.3.1.

2.4.2 Rotation Matrix for the Kite Coordinate System

To change a vector defined in the global coordinate system into the kite coordinate system, three rotations are required: pitch, roll and yaw, as defined in section 2.3.2. As with the matrices defining the rotations of the line coordinate system, the negative of the angles are used to represent 'un-doing' the kite rotations, resulting in a matrix to transform a vector given in global coordinates to its equivalent in kite coordinates. The rotation matrix for the pitch rotation can be found using the basic rotation matrix for rotations about the x-axis:

$$R_{Pitch} = \begin{bmatrix} 1 & 0 & 0 \\ 0 & \cos(-\theta) & -\sin(-\theta) \\ 0 & \sin(-\theta) & \cos(-\theta) \end{bmatrix} \tag{2.9}$$

Since roll and yaw angles are not defined using the kite coordinate axes, Rodrigues rotation formula is used to find their rotation matrices. The kite rolls about an axis perpendicular to the line, equivalent to the z-axis of the line coordinate system. Since this rotation is applied after the pitch angle, the axis needs to be found in the pitched kite coordinate system – defined relative to the global coordinate system by R_{Pitch}. The roll axis in pitched kite coordinates is found by taking a vector in the z-direction in line coordinates, converting it into global coordinates, and then applying the pitch rotation:

$$u_{roll} = R_{Pitch} \times R_{line}^{-1} \times \begin{bmatrix} 0 \\ 0 \\ 1 \end{bmatrix} \tag{2.10}$$

The rotation matrix for the roll rotation can then be found using the cross product matrix of u_{roll} and the roll angle φ:

$$R_{roll} = I + \tilde{u}_{roll} \sin(-\varphi) + \tilde{u}_{roll}^2 (1 - \cos(-\varphi)) \tag{2.11}$$

The yaw angle is applied about an axis parallel to the line, or the y-axis of the line coordinate system. This rotation is applied after the pitch and roll rotations, and the axis of rotation is found in a similar manner as for the roll axis:

$$u_{yaw} = R_{roll} \times R_{Pitch} \times R_{line}^{-1} \times \begin{bmatrix} 0 \\ 1 \\ 0 \end{bmatrix} \tag{2.12}$$

Rodrigues rotation formula is then used to find the rotation matrix for the yaw rotation:

$$R_{yaw} = I + \tilde{u}_{yaw} \sin(-\psi) + \tilde{u}_{yaw}^2 (1 - \cos(-\psi)) \tag{2.13}$$

The rotation matrix to transform a vector defined in the global coordinate system to its equivalent in the kite coordinate system is found by multiplying the pitch, roll and yaw matrices together in the correct order.

$$R_{kite} = R_{yaw} \times R_{roll} \times R_{pitch} \tag{2.14}$$

As with the line rotation matrix, the order of rotation is the reverse of the order explained in section 2.3.2, since the rotations are being 'un-done' to change a vector expressed in global coordinates to one expressed in kite coordinates.

Chapter 3

Modelling a Kite in Three Dimensions

To determine how a kite responds to a control input in the form of an induced roll angle, it is necessary to model the system in three-dimensions. In this thesis, only the initial response to a control input is being investigated, therefore a static model is sufficient. The static model will determine the out of balance forces and moments acting on a kite when it is in a given position.

3.1 Representation of a Kite Using Disks

In order to find the forces and moments acting on a kite and how they are affected by changes in geometry, a simple 3D model is required. While Computational Fluid Dynamics (CFD) simulations could be performed on exact models of actual kites, the time required to run multiple simulations for the many parameters affecting a kite's flight would be excessive. In addition, a CFD simulation would effectively skip from question to answer, without providing the desired insight into the mechanisms behind the kite's behaviour. Instead, the forces and moments will be determined by breaking the kite up into sections and determining lift and drag forces and centre of pressure locations for each separately.

The aerodynamic forces acting on a general flat plate depend on its orientation to the wind in two dimensions – the angle of attack, and the orientation about an axis perpendicular to the surface. A rectangular plate may have a straight edge or a vertex pointing into the wind, or any angle in between. To avoid this, a disk is used. A disk's aerodynamic properties only vary with angle of attack, since rotating a circle about its own centre has no effect.

Using lift, drag and centre of pressure coefficients obtained through experiment at various angles of attack, the aerodynamic force acting on each disk of a kite made up of multiple disks can be found, and the resulting forces and moments acting on the kite structure determined [9]. This method allows the out of balance moments caused when a kite is held at a given orientation to the wind to be investigated with a minimum of computational effort. However, this method does have a number of limitations. Firstly,

the complexity of the kite shape is limited by the fact that one disk cannot lie behind another – a disk in the wake of another disk will exhibit quite different aerodynamic properties. A similar problem limits how close a disk can be positioned to the side of another disk, since their tip vortices may interfere with each other, leading to a change in the forces acting on the disks. Working within these limitations, a representation of a kite made up of disks can be used to investigate the effects that parameters like bridle lengths, dihedral angles, and basic shape have on the initial turning response of a kite.

3.1.1 Aerodynamic Properties of Disks

As mentioned in the previous section, the aerodynamic properties of a disk can be assumed to vary only with the disk's angle of attack with respect to the flow. While the properties do change with flow velocity, this need only be taken into account if the velocity is varying by orders of magnitude, or where a transition from laminar to turbulent flow regimes may occur. Since kites fly in a limited range of wind speeds, the effect of flow velocity on aerodynamic properties can be neglected. Using the standard lift and drag equations, the aerodynamic forces acting on a disk in a flow stream can be found:

$$L = \frac{\rho \cdot A \cdot Cl\,(\alpha) \cdot V^2}{2} \tag{3.1}$$

$$D = \frac{\rho \cdot A \cdot Cd\,(\alpha) \cdot V^2}{2} \tag{3.2}$$

Where L and D are the lift and drag forces, ρ is the density of the fluid, A is the reference area of the disk (in this case the plan-form area), $Cl\,(\alpha)$ and $Cd\,(\alpha)$ are the lift and drag coefficients at the angle of attack α, and V is the flow stream velocity. The lift and drag forces act at the centre of pressure, which lies on the chord line between the front edge and centre of the disk. The exact location of the centre of pressure is variable, again primarily as a function of the disk angle of attack α.

Lift and drag coefficients and centre of pressure locations for a 240mm diameter disk were previously found at various angles of attack by Justin Stevenson [9] using the Closed Circuit Wind Tunnel in the University of Canterbury Industrial Aerodynamics Laboratory. Further force coefficient and centre of pressure data was obtained using a disk with 120mm diameter in the Closed Circuit Wind Tunnel using a three-axis force balance. This data is comparable to that obtained for 240mm disks, as shown in Figures 3.1 and 3.2, indicating that the lift and drag coefficients are not sensitive to disk size over this range. These results were also compared to data published by the Engineering Sciences Data Unit [25], and were found to be very similar.

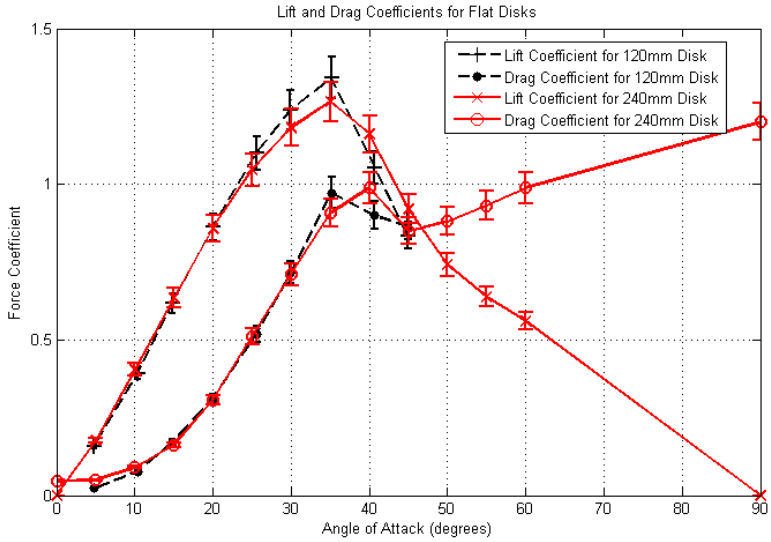

Figure 3.1 Chart showing the variation of lift and drag coefficients with angle of attack for two different sized disks, as measured in the closed-circuit wind tunnel

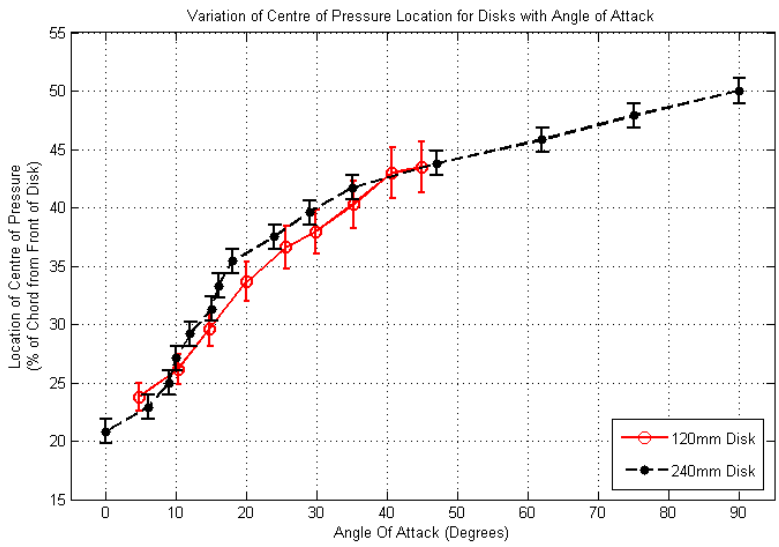

Figure 3.2 Chart showing the variation of centre of pressure location with angle of attack for two different sized disks, as measured in the closed-circuit wind tunnel

Using cubic spline interpolation, the results obtained by Stevenson can be smoothed to facilitate their use in modelling kite flight. This interpolation is performed using MATLAB's 'spline' function. The results of the interpolation are shown below in figures 3.3 and 3.4

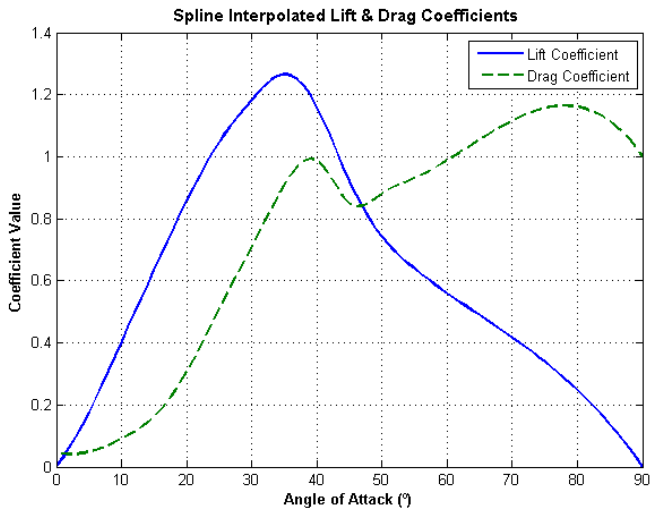

Figure 3.3 Chart showing interpolated values for lift and drag coefficients

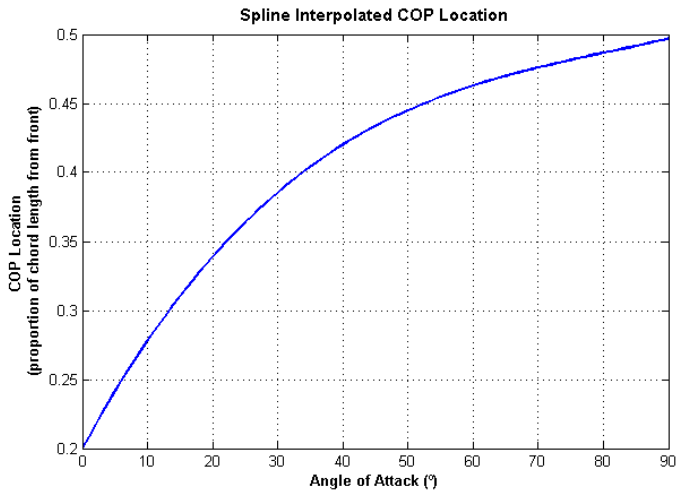

Figure 3.4 Chart showing interpolated values for centre of pressure location

3.1.2 Disk-Based Coordinate System

To calculate the forces acting on a kite made up of disks, it is useful to introduce a new coordinate system for each disk. These are aligned such that the disk surface lies on the x-z plane, with the origin set at the disk centre, as shown in figure 3.5. Each disk's coordinate system is defined initially relative to the kite coordinate system, thus the disk x-z plane is parallel to the kite x-z plane. From this position, up to two rotations are applied. The first of these is a rotation about the z-axis, leading to a dihedral angle. Following this rotation, a rotation about the disk's new x-axis can be applied – this will

be referred to as a twist angle.

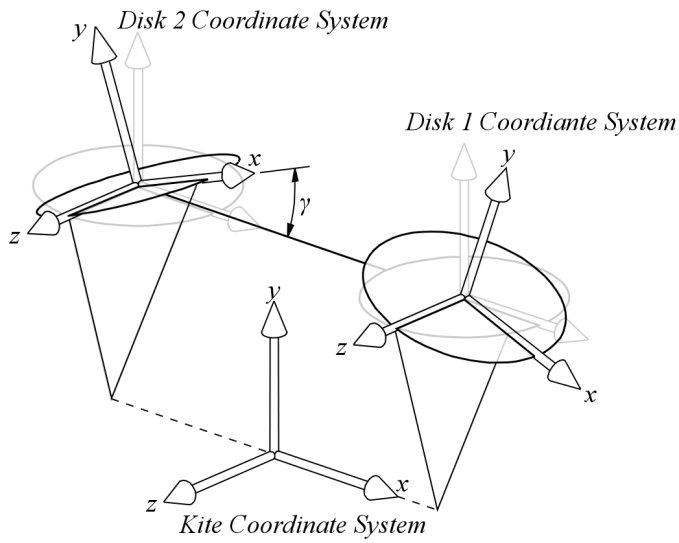

Figure 3.5 Diagram showing the disk-based coordinate systems for a two-disk kite with a dihedral angle γ

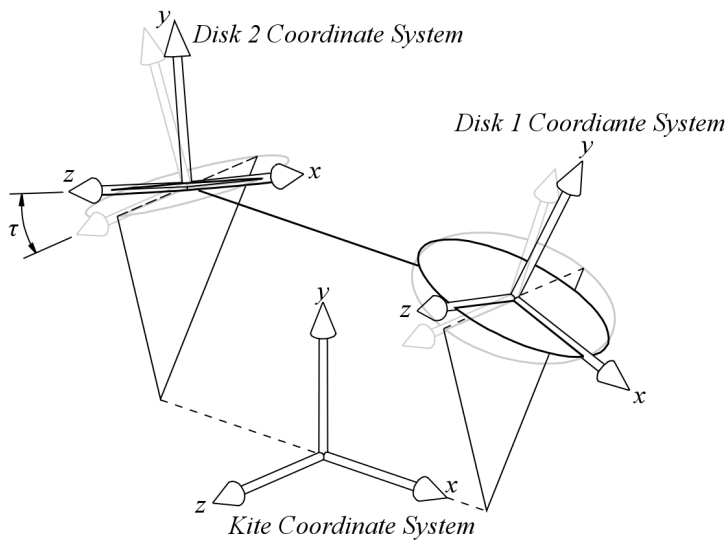

Figure 3.6 Diagram showing the disk-based coordinate systems for a two-disk kite with a twist angle τ

To change a vector given in the kite coordinate system to the disk coordinate system, the vector must be rotated through the reverse of the dihedral and twist angles:

$$R_{Dihedral(i)} = \begin{bmatrix} \cos\left(\left(-1^i\right)\gamma\right) & -\sin\left(\left(-1^i\right)\gamma\right) & 0 \\ \sin\left(\left(-1^i\right)\gamma\right) & \cos\left(\left(-1^i\right)\gamma\right) & 0 \\ 0 & 0 & 1 \end{bmatrix} \tag{3.3}$$

$$R_{Twist(i)} = \begin{bmatrix} 1 & 0 & 0 \\ 0 & \cos\left(-\tau_i\right) & -\sin\left(-\tau_i\right) \\ 0 & \sin\left(-\tau_i\right) & \cos\left(-\tau_i\right) \end{bmatrix} \tag{3.4}$$

Where γ is the dihedral angle and τ is the twist angle. These follow the standard right-hand rotation convention, such that a disk on the positive x-side of a dihedral kite has a positive dihedral angle, whereas the same disk on an anhedral kite has a negative dihedral value. The disks on the negative x side of the kite use equal but opposite dihedral angles to their positive side counterparts, since the kite is assumed to be symmetrical. The rotation matrix for transforming a vector from global coordinates to disk coordinates is found by multiplying the dihedral and twist rotation matrices with the kite rotation matrix in the correct order:

$$R_{Disk(i)} = R_{Twist(i)} \cdot R_{Dihedral(i)} \cdot R_{Kite} \tag{3.5}$$

3.2 Calculating the Yaw Moment Acting on a Disk Kite

When a kite flyer pulls on one line of a two line kite, a bank angle is induced in the kite as described in section 2.3.2. In a well designed two line kite, this results in an imbalance in the forces acting on the kite, causing it to yaw (or turn) in the intended direction and subsequently change position in the sky – this much is well known to any kite flyer. However, the direction and magnitude of this resulting yawing movement is presently only found by trial and error. In this section, the method used for calculating the forces and moments acting on a kite is outlined, and the yaw moment is subsequently identified.

3.2.1 Angle of Attack

To calculate the aerodynamic properties of each disk, their angles of attack must be found. This is found by calculating the angle between the global z-axis (i.e. the wind direction) and the x-z plane of the disk coordinate system (i.e. the disk surface). The angle ϑ between a vector W and a plane can be found by using a normal vector, N, to describe the plane:

$$\vartheta = \arcsin\left(\frac{W \bullet N}{|W| \cdot |N|}\right) \tag{3.6}$$

Using unit vectors in disk coordinates for both W and N to find the angle of attack, α, this reduces to:

$$\alpha_i = \arcsin\left(W_i^D \bullet \begin{bmatrix} 0 \\ 1 \\ 0 \end{bmatrix}\right) \tag{3.7}$$

Where W_i^D is a vector parallel with the wind in disk coordinates:

$$W_i^D = R_{Disk(i)} \cdot \begin{bmatrix} 0 \\ 0 \\ 1 \end{bmatrix} \tag{3.8}$$

The vector has been chosen to point into the wind (rather than with) it to result in a positive angle of attack.

3.2.2 Lift Force

To find the lift force vector acting on each disk in kite coordinates, the magnitude and direction must be found separately. The magnitude of the lift force for each disk is found using the standard formula for lift:

$$|L| = \frac{\rho \cdot A \cdot Cl\,(\alpha) \cdot V^2}{2} \tag{3.9}$$

Where $Cl\,(\alpha)$ is the lift coefficient for the disk at the current angle of attack α (found in equation 3.7).

The lift force acts along a vector given by the projection of a vector normal to the disk surface, S, onto the global x-y plane. The projection of a vector S onto a plane defined by its normal vector N is given by:

$$S \parallel N = S - (S \bullet N) \cdot N \tag{3.10}$$

In this case, the normal vector to the global x-y plane (i.e. the z-axis) needs to be converted into the disk-based coordinate system:

$$N^D = R_{Disk} \cdot \begin{bmatrix} 0 \\ 0 \\ 1 \end{bmatrix} \tag{3.11}$$

Where R_{Disk} is the rotation matrix found in section 3.1.2. A unit vector defining the

direction of the lift force can now be found:

$$\overrightarrow{L^D} = \begin{bmatrix} 0 \\ 1 \\ 0 \end{bmatrix} - \left(\begin{bmatrix} 0 \\ 1 \\ 0 \end{bmatrix} \bullet N^D \right) \cdot N^D \tag{3.12}$$

Which allows the lift force vector to be found in disk-based coordinates:

$$L^D = |L| \cdot \frac{\overrightarrow{L}}{\left|\overrightarrow{L}\right|} \tag{3.13}$$

And in kite-based coordinates:

$$L^K = R_{Kite} \cdot R_{Disk}^{-1} \cdot L^D \tag{3.14}$$

3.2.3 Drag Force

As with calculating the lift force vector, the drag force vector for each disk is found by calculating the magnitude and direction separately. The magnitude is found using the standard drag force equation:

$$|D| = \frac{\rho \cdot A \cdot Cd\,(\alpha) \cdot V^2}{2} \tag{3.15}$$

Where $Cd\,(\alpha)$ is the drag coefficient for the disk at the current angle of attack α (found in equation 3.7). Calculating the direction of the drag force vector is more straightforward than the lift force direction, as it simply acts along the global z-axis. Therefore, a unit vector in the direction of the drag force can be found in kite coordinates:

$$\overrightarrow{D^K} = R_{Kite} \cdot \begin{bmatrix} 0 \\ 0 \\ -1 \end{bmatrix} \tag{3.16}$$

And the drag force vector is:

$$D_i^K = |D|_i \cdot \overrightarrow{D^K} \tag{3.17}$$

3.2.4 Total Forces Acting on the Kite Structure

The sum of the lift and drag forces for each disk and the gravity force is resisted by the lines in the line Y-direction and causes the kite-bridle-line system to accelerate in other directions. The direction of this resulting force is important as it determines the equilibrium elevation angle for the kite line. Expressed using the kite-based coordinate

system, this force is:

$$F_T^K = \sum_{i=1}^{n} L_i^K + \sum_{i=1}^{n} D_i^K + F_{Gravity}^K \tag{3.18}$$

Where the gravity force is defined as:

$$F_{Gravity}^K = R_{Kite} \cdot \begin{bmatrix} 0 \\ -mg \\ 0 \end{bmatrix} \tag{3.19}$$

The sum of the aerodynamic and gravity forces is equal to the sum of the tension forces in the two kite lines for a kite at equilibrium. The proportion of this force that each line takes can be found using the z-component of the moments found in section 3.2.5, although this is not of interest when investigating the initial turning response of a kite.

3.2.5 3D Moments about the Bridle Point for a Simplified Two-Disk Kite

The sum of the moments about the centre of the bridle points, BP (shown in figure 3.7), is required to find the equilibrium pitch angle for a kite, in addition to calculating the response to a control input. Initially, a kite consisting of two disks with bridles attached to the disks will be used as a simple example. The out of balance moment in kite coordinates about BP, M^K, is:

$$M^K = \sum_{i=1}^{n} \left(\mathbf{r}_{BP-CPi}^K \times L_i^K\right) + \sum_{i=1}^{n} \left(\mathbf{r}_{BP-CPi}^K \times D_i^K\right) + \mathbf{r}_{BP-CM}^K \times F_{Gravity}^K \tag{3.20}$$

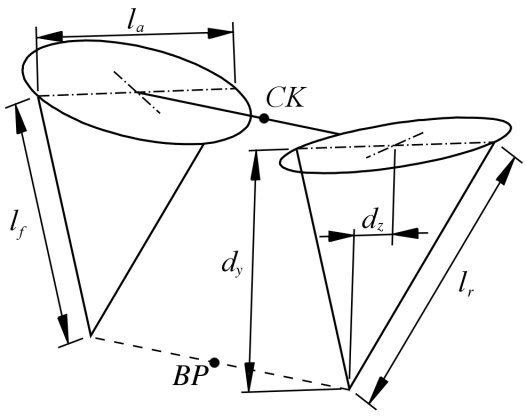

Figure 3.7 Diagram of a two-disk kite showing the location of the centre of the kite, CK, centre of bridle points BP, and bridle geometry

Where the vectors $\mathbf{r}^K_{BP-CPi}$ and $\mathbf{r}^K_{BP-CM}$ are vectors between the bridle point (BP) and the centres of pressure for each disk (CPi) and the centre of mass of the kite (CM), respectively. For this simplified two-disk kite, it is assumed that the centre of mass is located at the centre of the two disks, CK, therefore:

$$\mathbf{r}^K_{BP-CM} = \mathbf{r}^K_{BP-CK} \tag{3.21}$$

For a kite with no roll or yaw applied, the position vector for the centre of the kite relative to the bridle point, $\mathbf{r}^K_{BP-CK}$, can be found from the bridle lengths and the disk diameter. With some manipulation, the location of the bridle point with respect to the disk centre, as shown in Figure 3.7, can be shown to be:

$$\begin{aligned} d_y &= -\sqrt{l_f^2 - \left(\frac{l_f^2 - l_r^2 + l_a^2}{2 \cdot l_a}\right)^2} \\ d_z &= \frac{l_a}{2} - \frac{l_f^2 - l_r^2 + l_a^2}{2 \cdot l_a} \end{aligned} \tag{3.22}$$

If the kite has no roll or yaw angle, the x-component of the position vector for the centre of mass is zero, therefore the position vector $\mathbf{r}^K_{BP-CK}$ is:

$$\mathbf{r}^K_{BP-CK} = \begin{bmatrix} 0 \\ -d_y \\ -d_z \end{bmatrix} \tag{3.23}$$

However, if the kite has a nonzero roll and/or yaw angle, the bridles rotate about their attachment to the disk to align with the lines, as shown in Figure 3.8. The angle through which the bridles rotate is not necessarily equal to the roll angle, since they can only rotate about their attachment point, which may not be parallel to the roll axis. The bridles initially lie on a plane parallel to the kite y-z plane, thus the angle β through which the bridles rotate is equal to the angle between this plane and the kite lines:

$$\beta = -\arcsin\left(\begin{bmatrix} 1 \\ 0 \\ 0 \end{bmatrix} \bullet \left(R_{Kite} \cdot R_{line}^{-1} \cdot \begin{bmatrix} 0 \\ 1 \\ 0 \end{bmatrix}\right)\right) \tag{3.24}$$

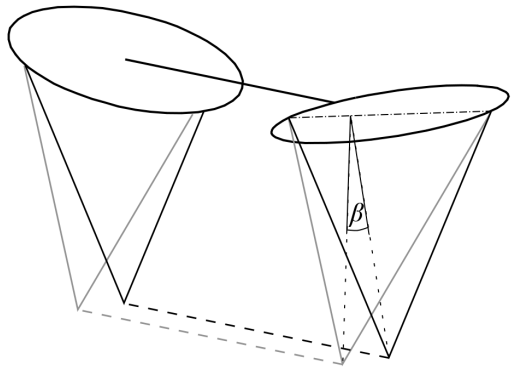

Figure 3.8 Diagram of a two-disk kite showing how the bridles can rotate when a roll and/or yaw angle is applied

The bridles rotate about an axis parallel to the kite z-axis, therefore a basic rotation matrix can be used to find the new position vector for the centre of mass, $\mathbf{r}^K_{BP-CK}$:

$$\mathbf{r}^K_{BP-CK} = \begin{bmatrix} \cos\beta & -\sin\beta & 0 \\ \sin\beta & \cos\beta & 0 \\ 0 & 0 & 1 \end{bmatrix} \cdot \begin{bmatrix} 0 \\ -d_y \\ -d_z \end{bmatrix} \tag{3.25}$$

To find the position vector for the centre of pressure of each disk, the position vector for the kite centre $\mathbf{r}^K_{BP-CK}$ can be used as a starting point. The position vectors for the centres of pressure are given by:

$$\mathbf{r}^K_{BP-CPi} = \mathbf{r}^K_{BP-CK} + \mathbf{r}^K_{CK-CDi} + \mathbf{r}^K_{CDi-CPi} \tag{3.26}$$

where $\mathbf{r}^K_{CK-CDi}$ is the position vector for the centre of disk i relative to the kite centre, and $\mathbf{r}^K_{CDi-CPi}$ is the position vector for the centre of pressure of disk i relative to the disk centre, both in kite coordinates. The vector $\mathbf{r}^K_{CK-CDi}$ is already defined – for the two-disk kite represented here, it is simply a vector along the kite x-axis with a length of half the span the between disk centres:

$$\mathbf{r}^K_{CK-CDi} = \begin{bmatrix} -1^{i+1} \cdot \frac{1}{2} \cdot s \\ 0 \\ 0 \end{bmatrix} \tag{3.27}$$

However, the vector $\mathbf{r}^K_{CDi-CPi}$ varies as the position of the kite varies. The scalar length of $\mathbf{r}^K_{CDi-CPi}$ is found from the aerodynamic properties of a disk determined by experiment, and varies with the disk angle of attack. The line on which the centre of pressure lies (the chord line) is found by taking a projection of a vector parallel to the wind onto the disk, as shown in figure 3.9. The vector $\mathbf{r}^K_{CDi-CPi}$ is found by multiplying

the scalar length $CoP(\alpha)$ and the normalised vector along the chord line $\overrightarrow{Chord}$:

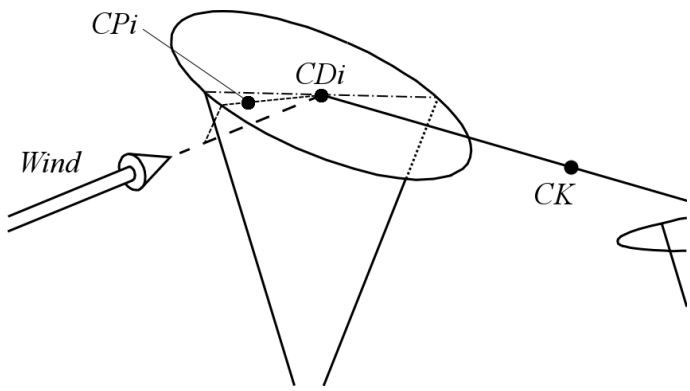

Figure 3.9 Diagram showing the location of the centre of pressure for disk two of a two-disk kite

$$\mathbf{r}^K_{CDi-CPi} = \frac{|CPi - CDi| \cdot \overrightarrow{Chord_i}}{\left|\overrightarrow{Chord_i}\right|} \tag{3.28}$$

Where the scalar $|CPi - CDi|$ is found using the coefficient for the centre of pressure location at the disk angle of attack and the disk diameter:

$$|CPi - CDi| = \frac{\emptyset_i}{2} - COP_i(\alpha) \cdot \emptyset_i \tag{3.29}$$

And the unit vector $\overrightarrow{Chord_i}$ is found using the projection formula:

$$\overrightarrow{Chord_i} = W^K - \left(W^K \bullet N_i^K\right) \cdot N_i^K \tag{3.30}$$

Where N is a vector normal to the disk surface and W is a vector parallel to the wind. These are found by applying the appropriate transformation matrices to unit vectors in the disk and global coordinate systems, respectively:

$$N_i^K = R_{Kite} \cdot R^{-1}_{diski} \cdot \begin{bmatrix} 0 \\ 1 \\ 0 \end{bmatrix} \tag{3.31}$$

$$W^K = R_{Kite} \cdot \begin{bmatrix} 0 \\ 0 \\ 1 \end{bmatrix} \tag{3.32}$$

The total moment about the centre of the bridle points in kite coordinates can now be found using equation 3.34. Since the kite is only free to yaw about the line y-axis, this

moment is transformed in to line coordinates to give a more useful result:

$$M^L = R_{Line} \cdot R_{Kite}^{-1} \cdot M^K \tag{3.33}$$

3.2.6 3D Moments about the Bridle Point for an n-Disk Kite

Most kites have shapes too complicated to be represented by only two disks. Further disks can be added to model kites with shapes more akin real ones with little modification to the method outlined in section 3.2.5. The angles of attack for each disk, along with the corresponding lift and drag forces, are calculated exactly as in sections 3.2.1 to 3.2.4. However, some additional calculations must be added to the subsequent steps to include the extra disks.

As stated in section 3.2.5, the moments about the centre of the bridle points (BP in figure 3.7) of a disk kite can be found using:

$$M^K = \sum_{i=1}^{n} \left(\mathbf{r}_{BP-CPi}^K \times L_i^K\right) + \sum_{i=1}^{n} \left(\mathbf{r}_{BP-CPi}^K \times D_i^K\right) + \mathbf{r}_{BP-CM}^K \times F_{Gravity}^K \tag{3.34}$$

The procedure for calculating the position vectors used in this equation is complicated by the fact that the centre of mass CM is longer at the centre of a line between two disk centres, as was assumed in section 3.2.5. For an n-disk kite, the centre of mass is defined by a position vector $\mathbf{r}_{CK-CM}^K$ in kite coordinates relative to the centre of the kite, CK. Additionally, the bridle attachment points are no longer assumed to be attached to the centre lines of two disks. Instead, their position is independently defined by a line of

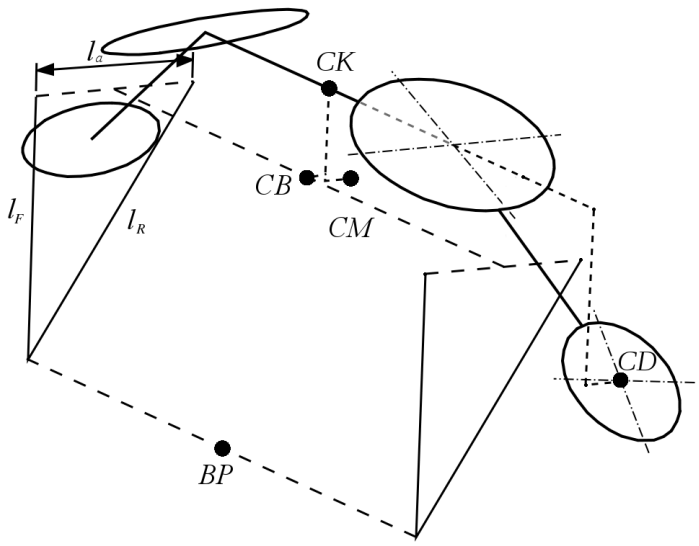

Figure 3.10 Diagram showing geometry of a disk kite and position vectors used to define locations

length l_a, parallel to the kite z-axis. The z- and y-locations for the centre of this line are defined by the point CB, which is defined by the position vector $\mathbf{r}^K_{CK-CB}$. Before finding position vectors between the centre of the bridle points, BP, and the centre of mass and disk centres, the position vector between BP and the centre of the kite, CK, must be found:

$$\mathbf{r}^K_{BP-CK} = \mathbf{r}^K_{BP-CB} - \mathbf{r}^K_{CK-CB} \tag{3.35}$$

The vector $\mathbf{r}^K_{CK-CB}$ is part of the definition of the kite geometry, and the vector $\mathbf{r}^K_{BP-CB}$ can be found using the bridle geometry in a manner similar to that used in equation 3.36:

$$\mathbf{r}^K_{BP-CB} = \begin{bmatrix} \cos\beta & -\sin\beta & 0 \\ \sin\beta & \cos\beta & 0 \\ 0 & 0 & 1 \end{bmatrix} \cdot \begin{bmatrix} 0 \\ -d_y \\ -d_z \end{bmatrix} \tag{3.36}$$

Where the angle β is given by equation 3.24, and the distances d_y and d_z are given by equation 3.22. The position vector $\mathbf{r}^K_{BP-CM}$ used to calculate the moment arising from the mass of the kite can now be found:

$$\mathbf{r}^K_{BP-CM} = \mathbf{r}^K_{BP-CK} + \mathbf{r}^K_{CK-CM} \tag{3.37}$$

The position vectors for the disk centres of pressure can also be found:

$$\mathbf{r}^K_{BP-CPi} = \mathbf{r}^K_{BP-CK} + \mathbf{r}^K_{CK-CDi} + \mathbf{r}^K_{CDi-CPi} \tag{3.38}$$

Where $\mathbf{r}^K_{CDi-CPi}$ is defined in equations 3.28 to 3.32. The moments about the centre of the bridle points can now be found as in equation 3.34, and transformed into line coordinates as in equation 3.33.

3.3 Use of MATLAB to Investigate Turning Behaviour

To investigate the effect of changing kite geometry on kite turning, the calculations outlined in section 4.2 have been implemented in MATLAB code. Using MATLAB, variables can be altered and their effect on the forces and moments acting on the kite can be graphed. In addition, equilibrium line and kite angles can be found for a given configuration.

3.3.1 Structure of Code to Find Kite Forces and Moments

The main code for calculating the forces and moments acting on a disk kite, as described in section 4.2, is implemented in a file called ndisk.m (see Appendix B). This file requires 12 input variables, which are listed in table 3.1, and calls on five sub-functions, which are listed in table 3.2. Schematics of the function and the sub-functions it calls are given in figures 3.11 and 3.12.

Table 3.1 Required input parameters for ndisk.m

Input	**Description**	Symbol
pitch	Kite pitch angle	θ
roll	Kite roll angle	φ
yaw	Kite yaw angle	ψ
dihedral	$\frac{n}{2} \times 1$ array containing dihedral angles of disks on positive x-side of kite	γ
twist	$\frac{n}{2} \times 1$ array containing twist angles of disks on positive x-side of kite	τ
elevation	Elevation angle of line	Φ
lbf	Length of front bridle lines	l_f
lbr	Length of rear bridle lines	l_r
DD	$\frac{n}{2} \times 1$ array containing diameters of disks on positive x-side of kite	$\emptyset$
P	$\frac{n}{2} \times 3$ array containing locations of disk centres on positive x-side of kite	$\mathbf{r}^K_{CK-CDi}$
PB	2×3 array containing locations of bridle line attachment points	$\mathbf{r}^K_{CK-CB}, l_a$
wind	Wind velocity	V
m	Kite mass	m
n	Number of disks	$-$

Table 3.2 functions called by ndisk.m

Function	**Description**
transformMTX.m	Finds matrices to change between global, line, kite and disk coordinate systems
aeroprops.m	Finds Cl, Cd, and centre of pressure for a disk given it's angle of attack
coplocation.m	Finds the location of the centre of pressure for a disk in kite coordinates
liftvector.m	Finds a unit vector in the direction of the lift force for a disk in kite coordinates
findbpoint.m	Finds the location of the centre of bridle points in kite coordinates

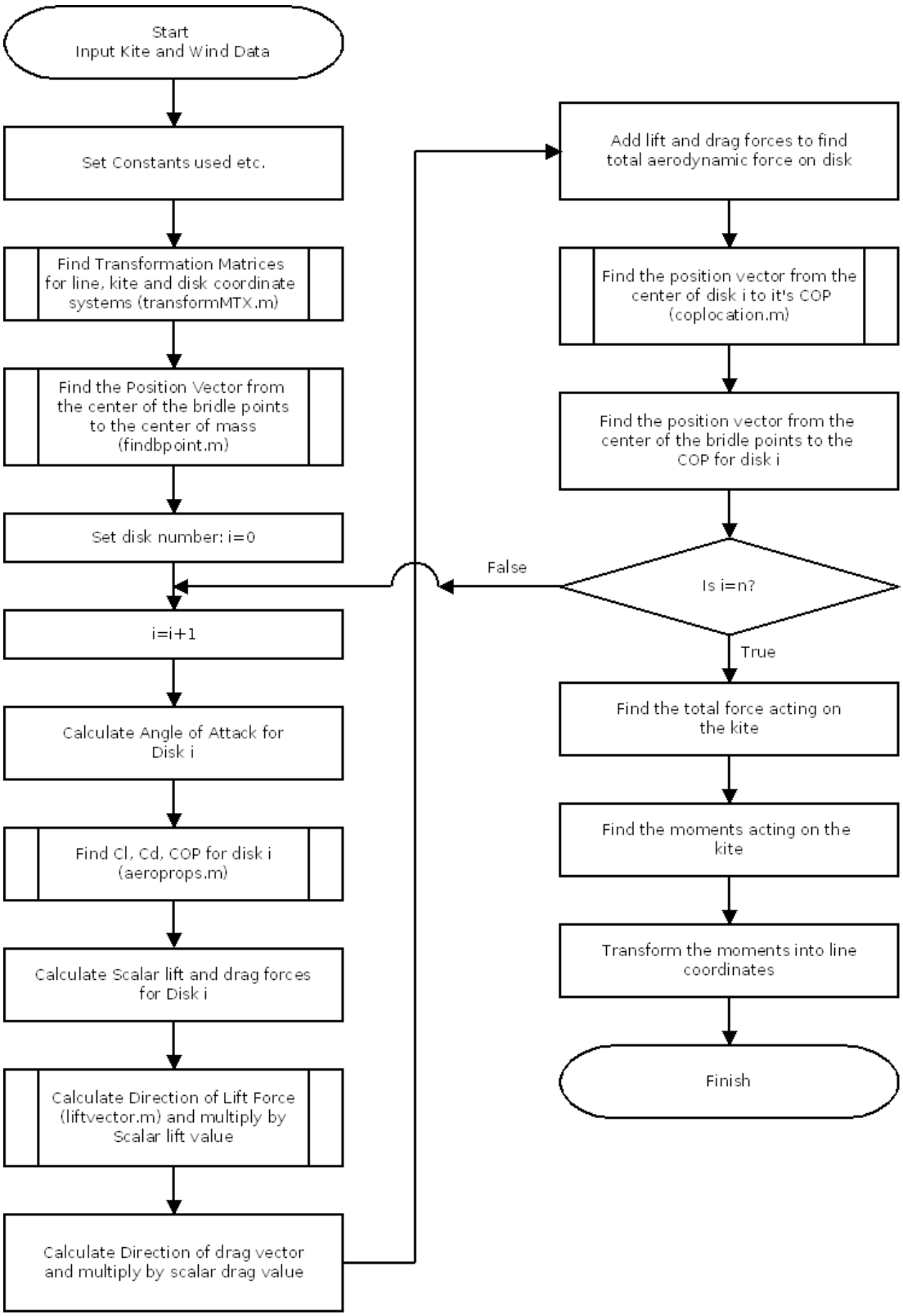

Figure 3.11 Schematic of ndisk.m

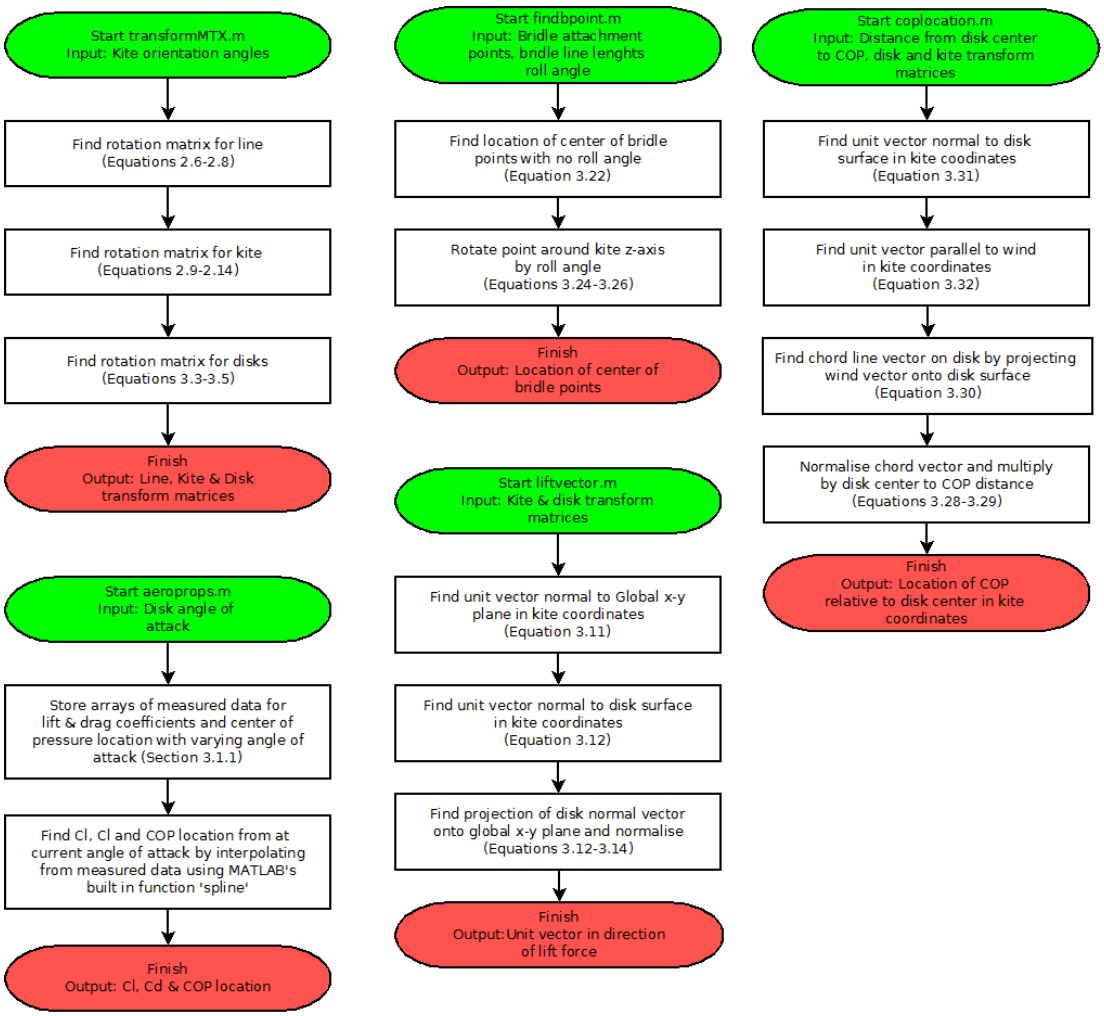

Figure 3.12 Schematic of sub-functions called by ndisk.m

3.3.2 Static Equilibrium

To find the equilibrium position of a kite, two angles must be found: the equilibrium line elevation angle and the equilibrium kite pitch angle[4]. The equilibrium pitch angle is found using the built in MATLAB function 'fzero', which finds a root of a given single variable function near a given guess value. This function is used to find a value of kite pitch that leads to a zero being returned for the x-component (pitch) of the moments about the bridle points, as calculated by the 'ndisk.m' function. Once the equilibrium kite pitch is known, the equilibrium line angle can be calculated by a summation of the forces acting on the kite – the line is in equilibrium when it is aligned with the vector sum of all the forces acting on the kite.

Some kite configurations may have more than one equilibrium pitch angle. When comparing different kite configurations, it is important that equivalent equilibrium points are used, otherwise any comparisons made will be invalid. For example, fig-

ure 3.13 shows the pitch moment of one particular kite as the pitch angle is varied. The moment crosses zero at three different pitch angles. The aerodynamic properties of the disks, and the relationship between the kite and line, will differ between these points, leading to different turning behaviour.

Additionally, some equilibrium pitch angles may not be statically stable. For example, figure 3.13 shows an example of a kite configuration that has three equilibrium pitch angles for the wind speed used. However, the second of these equilibrium points, at about -32° pitch, is not statically stable, as any perturbation to the pitch angle will cause a destabilising pitching moment. A perturbation from the first and third pitch angles will lead to a restorative moment – these are the stable equilibrium points. A schematic of code to find the first (closest to zero pitch) stable equilibrium point is shown in figure 3.14.

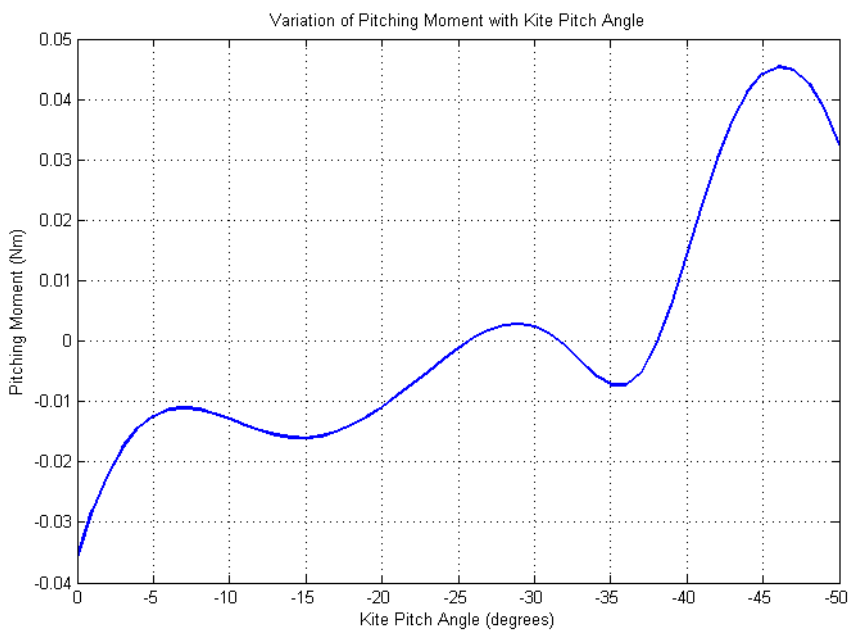

Figure 3.13 Chart of pitching moment about the bridle points vs. kite pitch angle, showing an example of a kite/wind combination with three equilibrium pitch angles

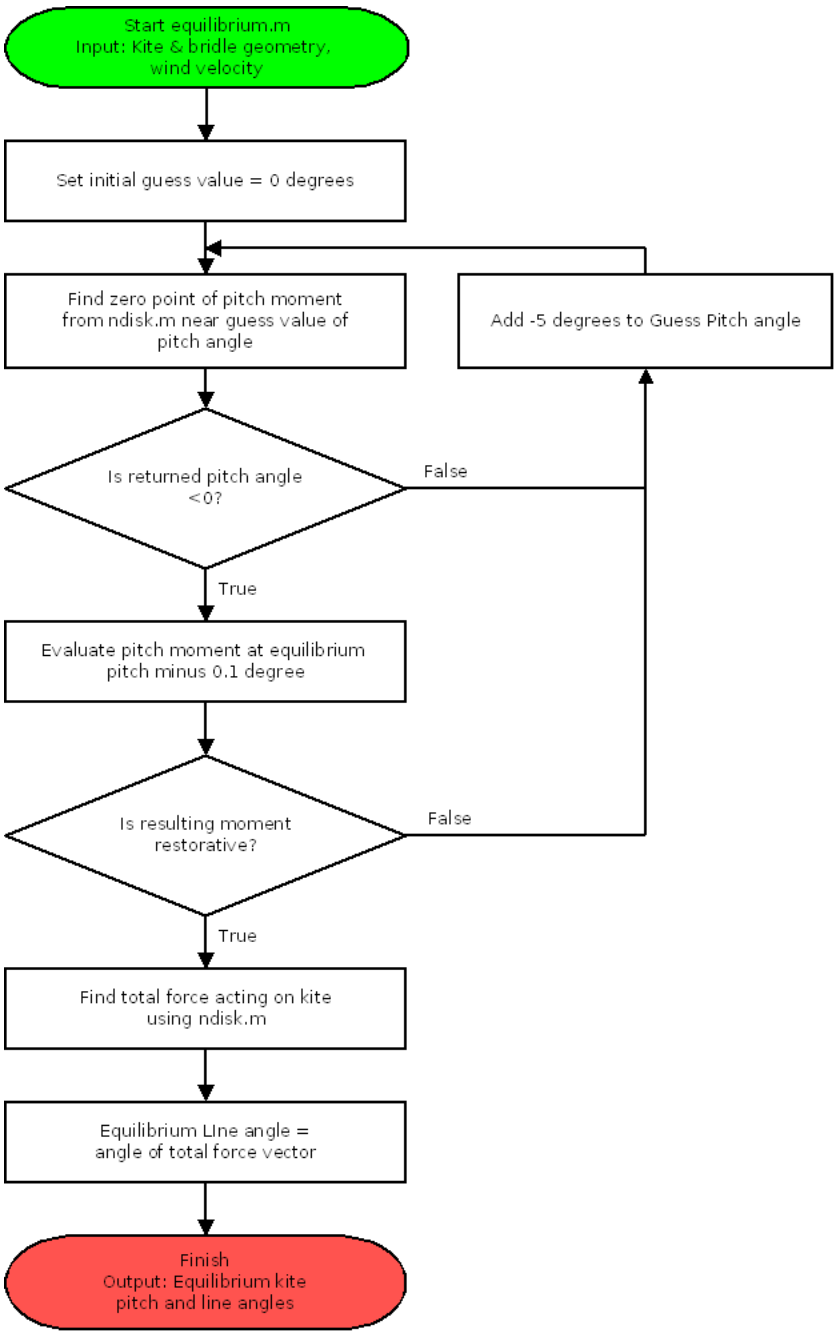

Figure 3.14 Schematic of code used to find the first stable equilibrium pitch angle and corresponding equilibrium line angle for a kite

Chapter 4

Verification of Mathematical Model

In order to validate the calculations outlined in the previous chapter, both wind tunnel testing and Computational Fluid Dynamics (CFD) analysis were used. Although CFD simulation was not initially thought necessary, the results of wind tunnel testing were unsatisfactory. The initial tests of a rigid kite using the open-circuit wind tunnel to find the yaw moment resulting from a bank angle seem to match results obtained from calculation. However, obtaining precise readings using the apparatus proved problematic, and the scatter of the results obtained was such that the accuracy of the calculated predictions could not be verified.

More precise measurements were obtained using disks held by an electronic force balance in the closed-circuit wind tunnel. However, the accuracy of these results is questionable, particularly for the case of measurements made for an anhedral kite. Results for the cases of dihedral to slightly anhedral kites matched those obtained by both calculation and the previous test rig, while those for a strongly anhedral kite deviated markedly. The reason for this deviation was not clear, but was likely caused by the test rig's support members interacting with the flow behind the disks. To supplement the results obtained from wind tunnel testing, CFD simulations were performed using ANSYS CFX. The results of these simulations closely matched the predictions made by calculation.

4.1 Open-Circuit Wind Tunnel Testing

A rigid model of a kite was constructed of steel to measure the yaw moment resulting from a roll angle applied to a two-disk kite. This was tested in the open-circuit wind tunnel with varying dihedral angles. Five identical test runs were performed to minimise experimental error.

4.1.1 Apparatus

A structure was designed to simulate a rigid two-disk kite with all degrees of freedom fixed except for yaw angle. The structure, shown in figure 4.1, held two 240mm diameter

disks at a centre width of 500mm, and allowed line elevation, kite pitch, dihedral, and roll angles to be adjusted. The steel bar acting as the kite line was mounted on rolling bearings to allow the yaw moment to be measured using a spring balance attached to a lever arm. Since any yaw rotation would affect the measured yaw moment, care was taken to ensure the structure maintained alignment to the original settings. This was achieved by using a laser level to point at the rear of the test rig.

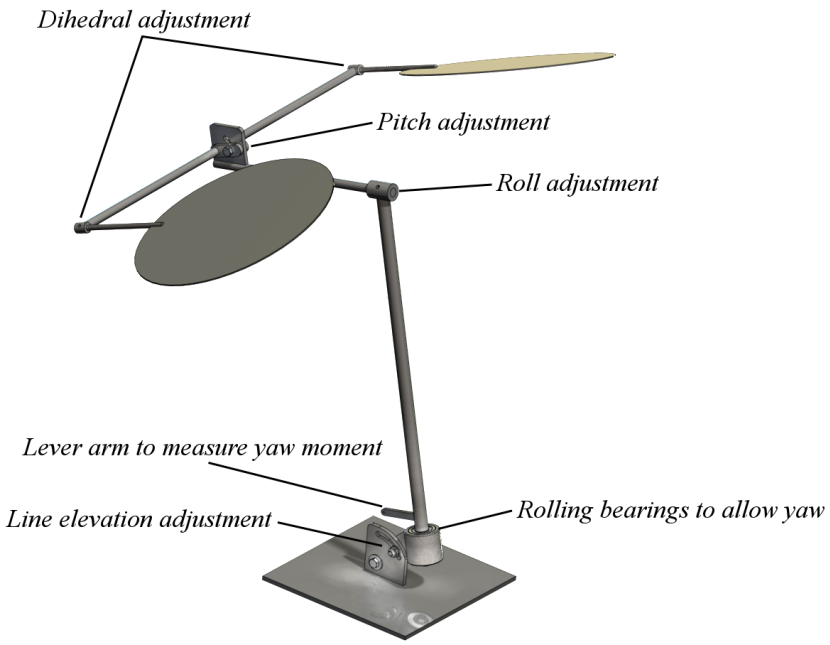

Figure 4.1 Diagram showing the test rig used for measuring yaw moment in the open circuit wind tunnel

Obtaining precise measurements with the test rig proved problematic, as the measured yaw moment was very sensitive to small variations in yaw angle and minor disturbances in the flow stream. Flex in the test rig also posed a problem, since some geometry parameters varied as the flow velocity increased, and flow disturbances also caused these parameters to oscillate. The values of the parameters most affected by flow velocity were indirectly measured by taking photographs of the rig at various angles while in the flow stream. Table 4.1 shows the geometry parameters as they were set, and as measured from photographs.

Table 4.1 Geometry parameters used for testing in the Open Circuit Wind Tunnel. Values as set and as measured at full flow velocity are shown.

Parameter	Set (Zero Flow)	Measured (8m/s Flow)
Disk diameter	240mm	240mm
Span between disk centres	500mm	500mm
Front bridle length	325mm	325mm
Rear bridle length	266mm	263mm ±4mm
Line elevation angle	81º	80º ±1º
Kite pitch angle	18º	20º ±2º
Kite roll angle	20º	20º ±1º
Kite yaw angle	0º	0º ±1º
Kite dihedral angle	-40º–40º	-40º–40º

4.1.2 Results

A comparison of the measured yaw moments with calculated yaw moments is shown in figure 4.2. The mean of the five sets of measured yaw moments was taken, and the standard error of the mean (SEM) was calculated to quantify the uncertainty caused by measurement error and fluctuations in the flow stream. Error bars shown in figure 4.2 represent 95% confidence intervals. Since considerable uncertainty existed in some of the test rig parameters, the method described in the previous chapter was used to calculate yaw moments for the range of measured values shown in table 4.1. The maximum and minimum yaw moment magnitudes resulting from calculations with combinations of these parameters were found, and these are shown dotted in figure 4.2. These lines give bounds within which the theoretical model indicates the experimental results are expected to lie.

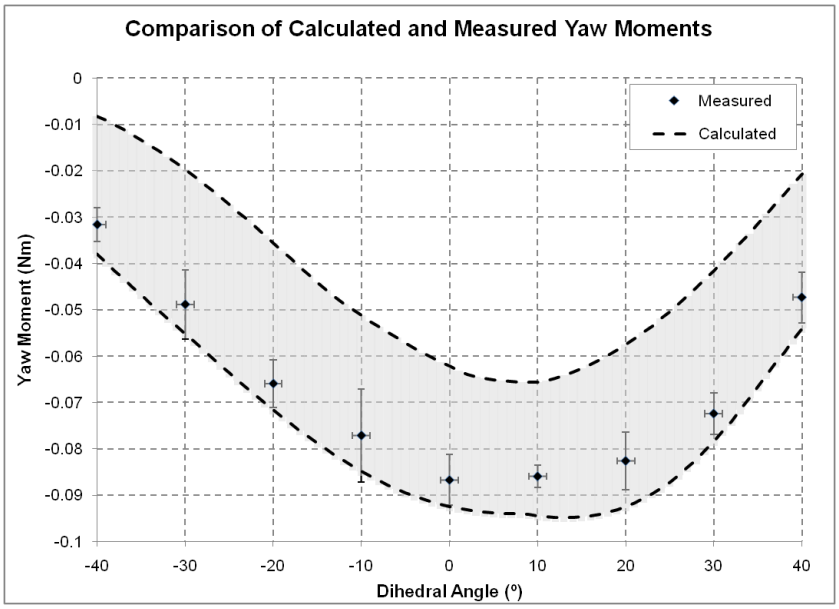

Figure 4.2 Chart showing a comparison of data obtained from the open circuit wind tunnel tests and calculation

The comparison shown in figure 4.2 highlights the margin of error present. While the experimental results do overlap the region of expected yaw moments, the magnitude of the uncertainty is very large. A significant variation in behaviour between the measured and calculated results could be masked by this uncertainty. Additionally, the measured yaw moments are all near the bottom of the expected region in figure 4.2. For these two reasons, this testing seemed inadequate to verify the calculated yaw moments.

The problems encountered with the use of the test rig described in section 4.1.1 arose due to the sensitivity of the measured yaw moment to variations in geometry. Small variations in disk angles of attack, dihedral angles, line elevation angle, and kite yaw angle caused significant variations in the yaw moment. Variations in these parameters arose both due to the flexibility of the test rig, and the difficulty of accurately setting the disk pitch and dihedral angles. Increasing the rigidity of the rig by using larger sections for the connecting members or adding mechanisms to accurately set angles would have introduced additional errors, as the flow immediately downstream of the disks would have been further disturbed. For this reason, this rig was abandoned in favour of a modified rig designed to interface with an electronic three-axis balance in the closed-circuit wind tunnel.

4.2 Closed-Circuit Wind Tunnel Testing

To obtain more precise measurements of yaw moment, the rig used in the previous section was modified to be attached to a three-axis balance in the closed circuit wind tunnel. The balance allows forces in two axes and a moment about one axis to be measured. It was hoped that this would remove the fluctuating flow conditions and yaw angles responsible for the scatter present in the results from the open circuit wind tunnel. However, results were still not completely consistent with predictions, with an unknown source still leading to discrepancies between calculated and measured yaw moments for anhedral kites.

4.2.1 Apparatus

In this instance the bar acting as the kite line was fixed rigidly to the three axis balance such that the moment measured would be equivalent to the yaw moment. The balance was fixed at an angle to the wind tunnel wall to simulate the line elevation angle, as shown in figure 4.3. The supporting members were rearranged to project the disks well forward of the bar acting as the kite line. This was done to minimise the disturbance to the flow over the disks. Moving the disks forward in such a manner results in a representation of a kite that could not fly, since the entire kite surface is upwind of the line. However, for the purposes of checking calculations this does not pose a problem.

Figure 4.3 Image showing the test rig used in the closed-circuit wind tunnel set up with with a positive dihedral angle, looking down wind

Tests were performed with a variety of different pitch, roll, and dihedral angles, and with two different disk sizes. For each disk size, two different flow stream velocities were tested. These were 12m/s and 13.9m/s for the 120mm disks, and 8.9m/s and 12m/s for the 240mm disks. These velocities were chosen to minimise vibrations in the test rig. The values of other parameters used are shown in tables 4.2 and 4.3, both as set and as measured under maximum flow velocity.

Table 4.2 Geometry parameters used for testing in the closed-circuit wind tunnel with 120mm disks. Values as set and as measured at full flow velocity are shown.

Parameter	**Set (Zero Flow)**	**Measured (13.9m/s Flow)**
Disk diameter	120mm	120mm
Span between disk centres	500mm	500mm
Front bridle length	565mm	565mm
Rear bridle length	452mm	452mm±1mm
Line elevation angle	85.2º	85º ±0.5º
Kite pitch angle	24.8º	25º ±0.5º
Kite roll angle	45º	45º ±0.5º
Kite yaw angle	0º	0º ±0.5º
Kite dihedral angle	-30º–30º	-30º–30º

Table 4.3 Geometry parameters used for testing in the closed-circuit wind tunnel with 240mm disks. Values as set and as measured at full flow velocity are shown.

Parameter	**Set (Zero Flow)**	**Measured (12m/s Flow)**
Disk diameter	240mm	240mm
Span between disk centres	500mm	500mm
Front bridle length	657mm	657mm
Rear bridle length	422mm	422mm±1mm
Line elevation angle	85.2º	85º ±0.5º
Kite pitch angle	34.8º	35º ±0.5º
Kite roll angle	45º	45º ±0.5º
Kite yaw angle	0º	0º ±0.5º
Kite dihedral angle	-30º–30º	-30º–30º

4.2.2 Results

Data obtained from the three axis balance showed significantly better precision than that obtained with the spring balance in the open circuit wind tunnel. Repeated runs

with the same parameters showed a variation in measured yaw moment of less than ±2%. However, figures 4.4 and 4.5 show that the measured results differ somewhat from the calculated yaw moments. Both show a significant deviation for anhedral kites, while the measurements performed using large disks show a deviation for dihedral kites as well. The calculated yaw moments are shown as shaded regions, representing the range of expected yaw moments resulting from uncertainties in the parameters used for measurement, as shown in tables 4.2 and 4.3.

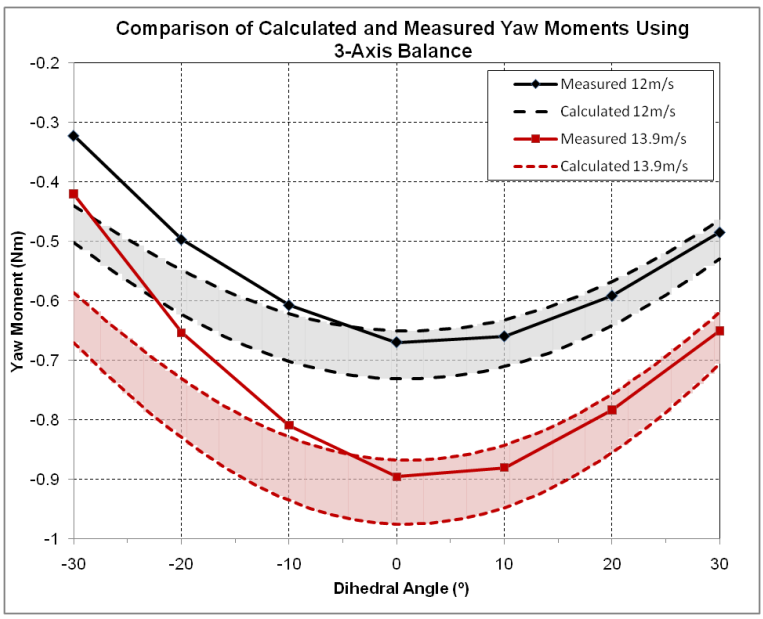

Figure 4.4 Chart showing a comparison of data obtained from tests in the closed-circuit wind tunnel and calculation for a disk with diameter=120mm

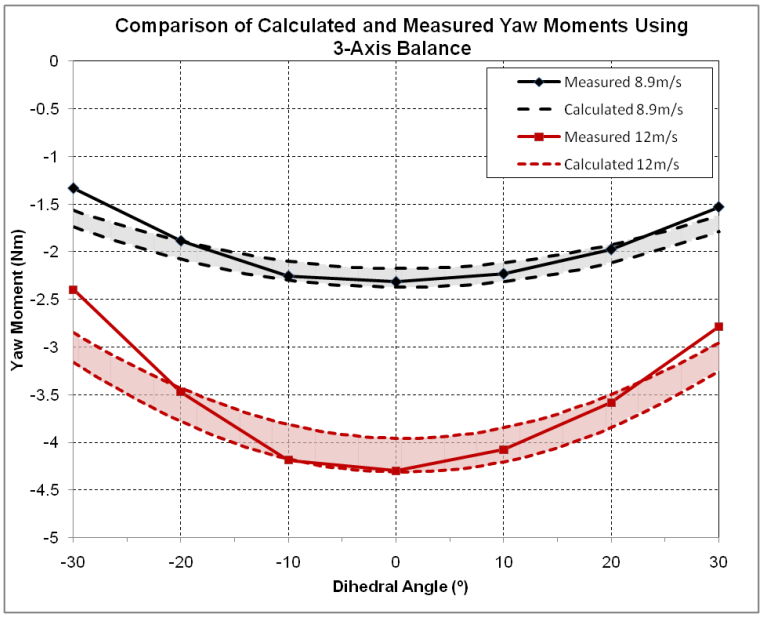

Figure 4.5 Chart showing a comparison of data obtained from tests in the closed-circuit wind tunnel and calculation for a disk with diameter=240mm

Various other combinations of geometry parameters were tried (see appendix C) with similar results – yaw moments showed a larger variation with dihedral angle than predicted, especially for anhedral kites. It is likely that this discrepancy is caused by the test rig support members disturbing the flow behind the disks to a varying degree as the disks are rotated to simulate different dihedral angles. This is difficult to verify, but is supported by the apparent variation of the error magnitude with disk size. Results from smaller disks (figure 4.4) differ from those predicted by a greater amount than results from larger disks (figure 4.5), presumably due to the same support structure causing a more significant disturbance with the smaller disks due to its relative size.

While there are still discrepancies between measured and predicted yaw moments, the general similarity of the curves indicates that the calculations are likely correct. The yaw moment resulting from a roll angle is very sensitive to variations in most parameters, and any calculation error would likely result in a completely different response. Further improvements to the test rig were unlikely to significantly reduce the problem of support member interference, since making the members more slender or further away from the disks would increase oscillations in the structure. Instead, the results above will be compared to a CFD simulation of disks in the same arrangement in the next section.

4.3 CFD Simulation

While both tests in the open and closed circuit wind tunnels indicate that calculated yaw moments largely match those found for a real kite, discrepancies in the data mean that the result is not conclusive. To further supplement this experimental data, some basic CFD simulations were performed for a small number of different dihedral kites. ANSYS Workbench and CFX were used for geometry meshing and analysis. Geometry and wind parameters used were chosen to match the 12m/s wind speed case shown in figure 4.4. The yaw moment found from these simulations matched those predicted by calculation with an offset error of around seven percent. The shape of the curves was a better match than with the experimental results. The 7% offset was thought to be caused by simplifications used in the CFD simulation.

Table 4.4 Geometry parameters used for CFD simulation

Parameter	Value
Disk diameter	120mm
Span between disk centres	500mm
Front bridle length	565mm
Rear bridle length	452mm
Line elevation angle	85.2º
Kite pitch angle	25.8º
Kite roll angle	45º
Kite yaw angle	0º
Kite dihedral angle	-30º–30º
Wind speed	12m/s

4.3.1 Geometry & Meshing

The geometry modelled for the CFD simulations was two flat disks, arranged to match the configuration used for 120mm disks in section 4.2. Simulations were performed both with and without the presence of supporting members behind the disk, to investigate the assumption that these members were the cause of the discrepancy between the results obtained in section 4.2 and those calculated as described in Chapter 4. The domain volume was chosen to match the closed circuit wind tunnel to provide a direct comparison of results, as shown in figure 4.6.

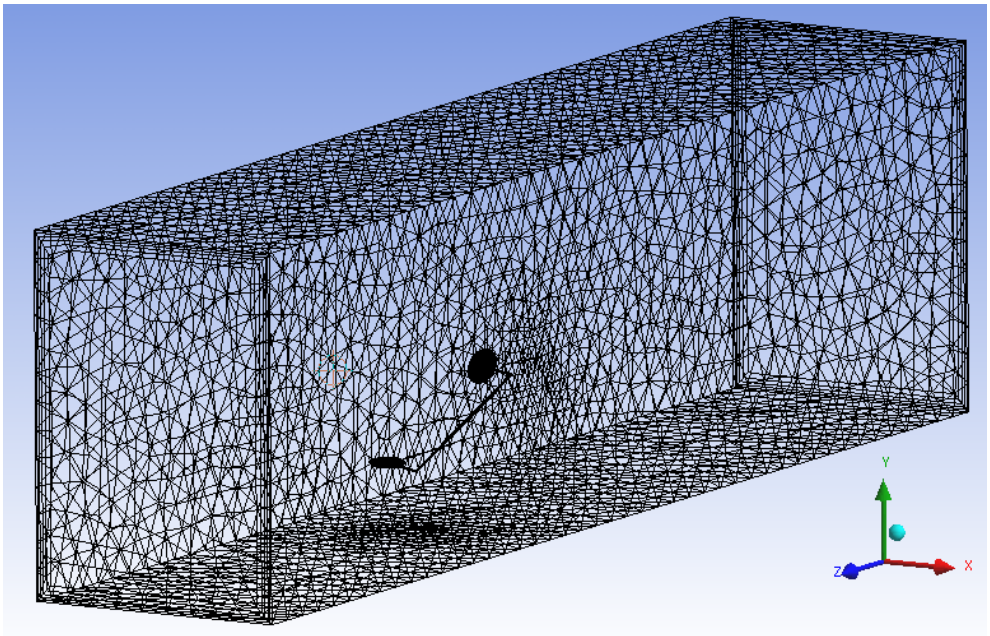

Figure 4.6 Image showing an example of the geometry and mesh used for simulation. This example includes the support members behind the disks, while other simulations were performed without these.

Meshing was performed using Meshing 12.1, incorporated within the ANSYS Workbench software suite. This generates an unstructured mesh. Inflation layers were used on both the wind tunnel walls and the disk surfaces to better model the boundary layers. Advanced mesh settings were mostly left as default, with some important exceptions. Because the geometry contains a large volume of fluid with a small area of interest (i.e. the disks), it was important to ensure fine enough detail around the kite to provide an accurate estimate of yaw moment, while minimising the total number of meshing elements used. To ensure accurate modelling of the flow at the edge of the disks, a rule was set to ensure that the two millimetre thickness of the disks was always at least three cells across. This prevented the edge of the disk being represented as a sharp point, rather than the square edge that was used in wind tunnel testing.

Further alterations to the default meshing parameters were found to be unnecessary. The mesh resulting from the above settings gave a mesh of acceptable quality, with Jacobian ratios ranging between 1 and 1.86 – a maximum Jacobian of less than 40 is generally regarded as acceptable [26]. Aspect ratios were also well within acceptable limits, with a maximum of 26.5. A low aspect ratio is desirable, but values of up to around 1000 can provide reasonable results [26].

4.3.2 Simulation Setup

Simulation setup was performed using ANSYS CFX-Pre. One normal-speed inlet and one average static pressure outlet were used. All other boundaries were defined as

smooth, no slip walls. Default solver parameters were used. Mesh adaption was utilised to refine the mesh in areas with large velocity gradients – this was important since the initial mesh created did not have any controls added to ensure a fine mesh downstream of the kite structure. Up to five refinement steps were allowed with a node factor of two.

4.3.3 Validation

4.3.3.1 Grid Independence

For a CFD simulation to give reliable results, the geometry must be divided into a sufficiently fine mesh. More complicated flow patterns require a finer mesh to accurately calculate flow conditions. To determine whether a mesh is adequate to give reliable measurements of some parameter, multiple simulations can be performed with increasing mesh resolution. The variation of the parameter of interest is monitored, and the mesh can be considered adequate when additional mesh resolution leads to an insignificant change in the parameter value.

In the case of this simulation, the yaw moment acting on the two disks was the parameter of interest. Starting with a coarse mesh of around 700,000 elements, mesh resolution was increased (or element size decreased) and automatic refinement levels added until the yaw moment varied less than 5%. For the case of the simulation without disk support members, this occurred for an initial mesh with around 1.4 million elements, with three refinement levels increasing the number of elements to around 3 million.

The simulation performed on geometry with disk support members did not reach grid Independence with initial mesh sizes of around 2.4 million elements and five refinement levels, leading to a final mesh size of over 5 million elements. At this stage the resources required to run the simulation were becoming excessive. Because the support members were of small diameter but had a long length, they introduced a large area of flow with small scale variations, causing this area to be preferentially treated by the refinement algorithm over the wake of the disks. As such, a large number of new elements were introduced to the mesh, with little improvement in the reliability of the yaw moments obtained from the results. While this problem could have been remedied by manually adding fine areas of mesh in the expected vicinity of the disk wakes, this was not thought necessary, as explained in section 4.3.4.

4.3.3.2 Turbulence Models

Another variable that can affect the reliability of results obtained from CFD is the turbulence model used. For a relatively simple flow stream such as the one being modelled, the k-ϵ or Shear Stress Transport models are usually adequate [26, 27]. To determine if

the turbulence model used had a significant effect on the resulting yaw moment, identical simulations were performed with both of the aforementioned turbulence models. The yaw moments found were within 1% of each other, indicating that both models worked equally well for this case. The simpler, widely used k-ϵ model was used for the remainder of the simulations performed.

4.3.4 Results

Using ANSYS CFD-Post, a coordinate frame was added to simulate the line coordinate system. The resultant yaw moment created from the aerodynamic forces on the disk faces could then be measured and compared with the results obtained from the closed-circuit wind tunnel and calculated directly. The results from CFD simulations of the disks with no support members showed a similar variation of yaw moment with dihedral angle to that obtained by calculation, as shown in figure 4.7. The magnitude of all the yaw moments found from the CFD simulations were slightly (7%) smaller than that calculated. Some difference was expected since the CFD simulation used perfect disks, whereas the lift and drag coefficients used for calculation were measured using a disk with protrusions to attach it to the wind tunnel. Additionally, the CFD simulation assumed the disk surfaces were perfectly smooth.

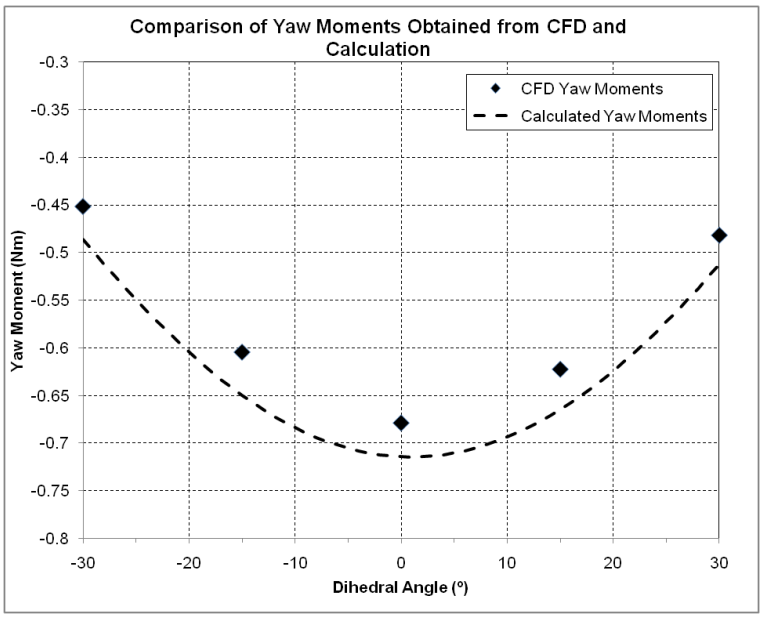

Figure 4.7 Chart showing a comparison of yaw moments found using CFD simulation of two disks with no supporting members and those calculated

The results from the CFD simulations performed with connecting members included did not closely match either calculated yaw moments or those obtained through experiment, as shown in figure 4.8. This may be due to a number of reasons. Firstly, only

representations of the members directly downstream of the disks were modelled – these were considered to be the members most likely to influence the flow. The other members not modelled may have had a more significant effect on the flow than was assumed, or the detail of the members (pivoting clamps etc. were not modelled) may have caused significant flow disruptions. Additionally, grid independence was not achieved to such a convincing degree as it was with the simulation with no support members (see section 4.3.3.1).

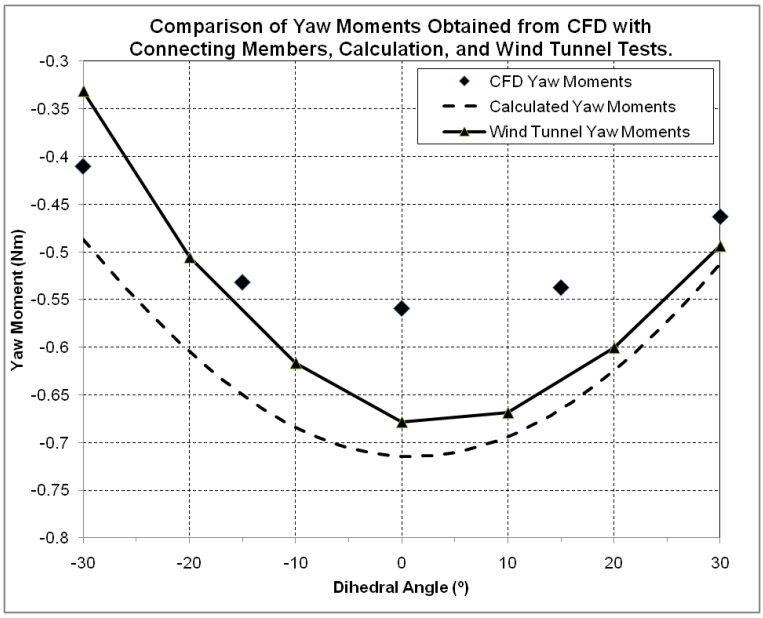

Figure 4.8 Chart showing a comparison of yaw moments found using CFD simulation of two disks with supporting members and those calculated and measured in the closed-circuit wind tunnel

The primary purpose of performing this CFD simulation was to add credibility to the indications from sections 5.1 and 5.2 that the yaw moment calculations were correct. The comparison shown in figure 4.7 largely achieves this, since it shows a very close similarity of curve shape between yaw moments found through CFD simulation and the calculation method outlined in Chapter 3, which in turn shows the same curve shape found from testing in the open circuit wind tunnel (see figure 4.2). This supports the notion in section 4.2.2 that the discrepancies found during testing in the closed circuit wind tunnel at large anhedral angles (see figures 4.4 and 4.5) are artefacts of the testing process.

The secondary purpose of performing the CFD simulation, to identify and quantify the source of error encountered in section 5.2, has not been completely fulfilled. This would likely require a more in-depth CFD simulation, with more detailed geometry and a finer mesh. This was not performed, since it was deemed to be less important than the main focus of this chapter – verifying the method of calculating yaw moments.

Chapter 5

Turning Response of a Kite Represented by Two Disks

While a two disk kite does not accurately represent any kite configuration in use, it does allow the effect of basic kite geometry parameters such as dihedral angle and bridle lengths to be investigated independently of other factors. For many of the parameters investigated in this section, calculating a dimensionless turning response was not practical. The effect one parameter has on turning response is often dependent on many other parameters, some of whose values are interdependent with others. Additionally, a dimensionless analysis would render the results less accessible. Due to the large number of parameters involved, a dimensionless analysis of turning response would become very abstract, and the actual behaviour of a kite would not be immediately apparent.

Determining how different parameters affect the turning response of a kite is complicated by the fact that most affect the kite's behaviour in two ways. Firstly, most parameters have a direct affect on the turning response of a kite that is held at a given pitch and line elevation angle, varying the parameter will vary the kite's turning response. Secondly, varying each parameter also affects the equilibrium pitch and line elevation angles, which in turn further varies the turning response.

Figure 5.1 shows how varying the dihedral angle changes the turning response of the kite, with both fixed and varying pitch and elevation angles. Ideally, the effect of varying each parameter on the turning response of a kite would be investigated in isolation from any other change. However, for most parameters this is not possible. Restricting the change in equilibrium position caused by modifying a parameter induces a pitching moment on the kite, which affects the yaw moment about the line axis when the kite is rolled. This introduces an artificial change in turning response that would not occur in a real kite. Similarly, there are no parameters which can be modified to adjust the equilibrium position without affecting the turning response.

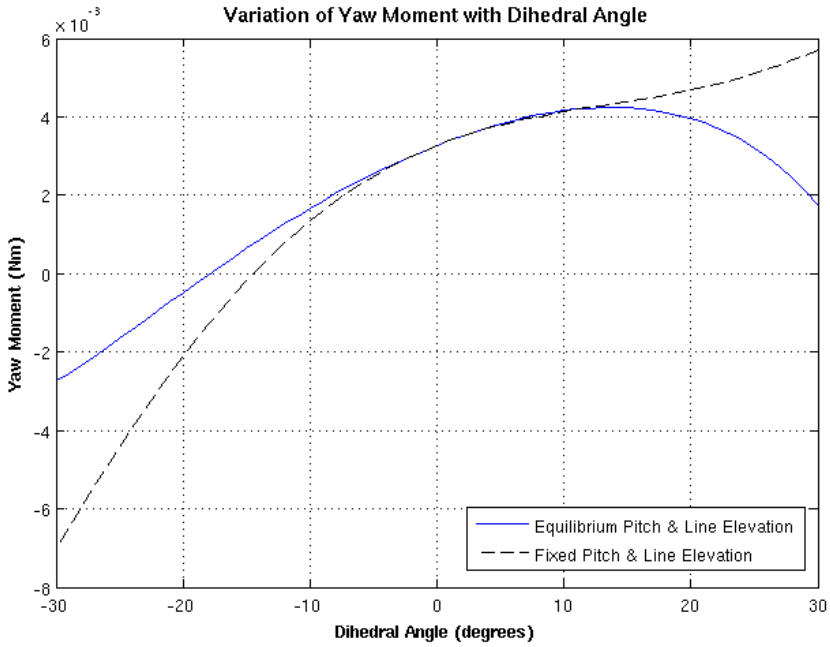

Figure 5.1 Chart showing the effect of dihedral angle on the yaw moment resulting from a roll angle, with and without the effect of changing equilibrium angles. For the case of fixed equilibrium angles, the pitch and line elevation angles are held at the equilibrium point for dihedral=0°.

The most meaningful method of calculating the change in turning response due to the variation of some parameter is to adjust the kite pitch and line elevation angles to maintain equilibrium. This represents the effect the adjustment would have on a real kite. When varying most parameters, the changes in equilibrium angles are small, and their effects on the turning response of a much smaller magnitude than the direct effects. Other parameters have little direct effect on turning response, but a large effect on equilibrium angles – for example the bridle lengths and kite mass. In cases where varying a parameter results in both significant direct changes to turning response and equilibrium angles, it is necessary to investigate both the equilibrium and non equilibrium cases.

5.1 Turning Response for a Simplified Zero Mass Kite

Initially, the special case of a kite with zero-mass where the bridle geometry is tuned such that the kite can fly with its y-axis aligned with the kite lines is considered. This is a special case since it leads to the roll axis, or line z-axis, aligning with the kite z-axis. This alignment means that when a roll angle is applied, the kite only rotates about its own z-axis, rather than about both its z- and y-axes. To achieve this condition, the kite parameters listed in table 5.1 are used throughout this section unless otherwise stated. This kite is in equilibrium with the kite z-axis aligned with the line z-axis only at the

Table 5.1 Table of kite parameters used for the baseline kite in this section

Parameter	Standard Value
Disk diameter	240mm
Kite span (between Disk centres)	500mm
Front bridle length	200mm
Rear bridle length	250.9mm
Kite pitch angle	-14.7º
Line elevation angle	75.3º
Dihedral/anhedral angle	20º
Roll angle	0º or 5º
Wind velocity	10m/s

values stated – where one or more parameters are varied, the rear bridle length and kite pitch and line elevation angles are modified to maintain equilibrium.

Many kite variables cannot be varied for the simplified kite used in this section because they are controlled by the simplifying assumption. These variables are rear bridle length, kite pitch, line elevation – these are all fine tuned to allow the kite to fly perpendicular to the line – and the mass has been assumed to be zero. The effects of these parameters must be investigated using a more general definition of a kite in later sections. The remaining parameters that can be varied in this simplified case will be investigated in the following subsections.

5.1.1 Turning Response with Varying Dihedral Angle

For a two-disk kite, the dihedral angle is the main variable that can be used to modify turning behaviour. While other variables, in particular bridle geometry, can be used to modify the turning response, they modify the equilibrium pitch and line elevation angles to a large extent. As such, bridle geometry would usually be tuned to give a good lift/drag ratio, rather than good turning response.

Since varying the dihedral angle also varies the equilibrium values for the kite pitch and line elevation angles, the pitch and elevation angles used on the base kite described above cannot be used for a kite with a dihedral angle of other than -20º or 20º. If new pitch and elevation equilibrium angles are found without any other modification, the kite and line will no longer be perpendicular. To enable equilibrium angles to be found that put the kite and line perpendicular to each other, the length of the rear bridle lines can be adjusted. This results in the kite flying with equal disk angles of attack for each dihedral angle with the kite perpendicular to the line. The variation of the Yaw moment with dihedral angle resulting from a roll angle of 5° for this kite is shown in Figure 5.2.

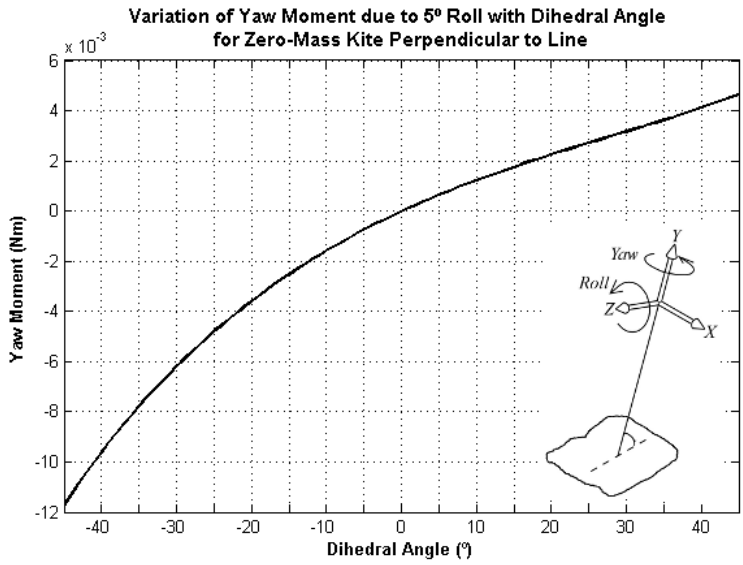

Figure 5.2 Chart showing the variation of yaw moment with dihedral angle for a zero-mass kite flying with kite perpendicular to lines

To explain the shape of the lines shown in figure 5.2, it is useful to consider the forces acting on the kite in line coordinates. For the kite system to be in equilibrium, the resultant force vector obtained by summing the aerodynamic forces acting on the disks (and generally the gravity force, which is zero in this case) must be co-linear to the kite line(s). This implies that when the zero-mass kite is flying at equilibrium, with no roll or yaw angles, the line and centre of pressure are aligned, as shown in figure 5.3. Because of this alignment of the position and direction of the aerodynamic force with the line and its corresponding coordinate system, there are no out of balance moments arising from the configuration.

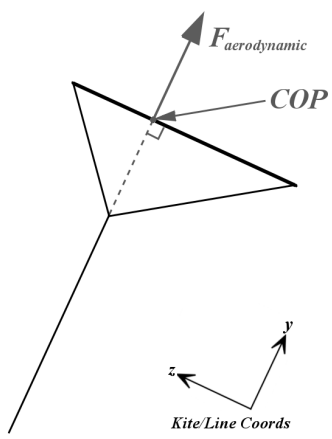

Figure 5.3 Two-dimensional diagram of a zero mass kite in an equilibrium condition with the kite perpendicular to the line

When a roll angle is applied to a kite with an anhedral or dihedral angle, the angles of attack for the two disks vary such that they are no longer equal, as shown in figure 5.4. This causes the direction, magnitude and point of action for their respective aerodynamic forces to change. The exact nature of these changes depends on the angles involved, but for the range of angles of attack where Cl, Cd and COP locations vary reasonably linearly some generalisations can be made. Firstly, when the angle of attack of a disk is increased, the magnitude of both the lift and drag forces increases. Secondly, the lift and drag forces vary at different rates (i.e. the lift to drag ratio changes), changing the angle of the resultant total aerodynamic force. Additionally, the location of the centre of pressure moves back towards the centre of the disk. These changes will now be examined in detail.

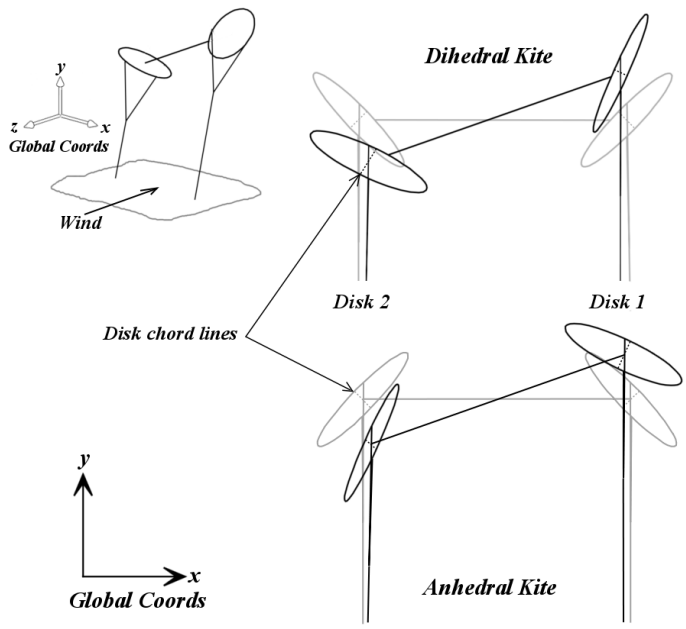

Figure 5.4 Diagram showing how a roll angle affects the angles of attack for each disk of a two-disk kite

For the special case being considered, the disk angles of attack resulting from a five degree roll angle are shown in figure 5.5. The chart shows that the disk on the positive x-side of the kite (referred to as disk number one) has an angle of attack equal to the kite pitch when the kite has a dihedral angle equal to the negative of the induced roll angle. This is as expected, since the kite has been rolled about an axis parallel to the kite z-axis. The chart also shows that rolling a kite with no dihedral angle does not result in different angles of attack for the two disks – both angles of attack have decreased.

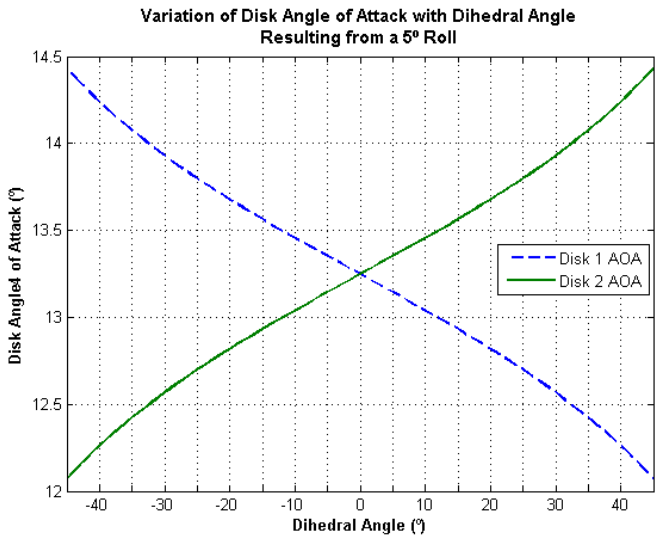

Figure 5.5 Chart showing the variation of disk angles of attack with dihedral angle for a two disk kite with an initial angle of attack of 13.3º and a roll angle of 5º

The variation of disk angles of attack with roll angle and dihedral angle for the kite in question is shown in figure 5.6. It shows that for a given dihedral angle, increasing the roll angle of a kite increases the difference in disk angles of attack roughly linearly. The chart also confirms that rolling this simplified kite with no dihedral angle does not result in a difference in disk angles of attack – both disk angles of attack decrease by the same amount as the roll angle is increased.

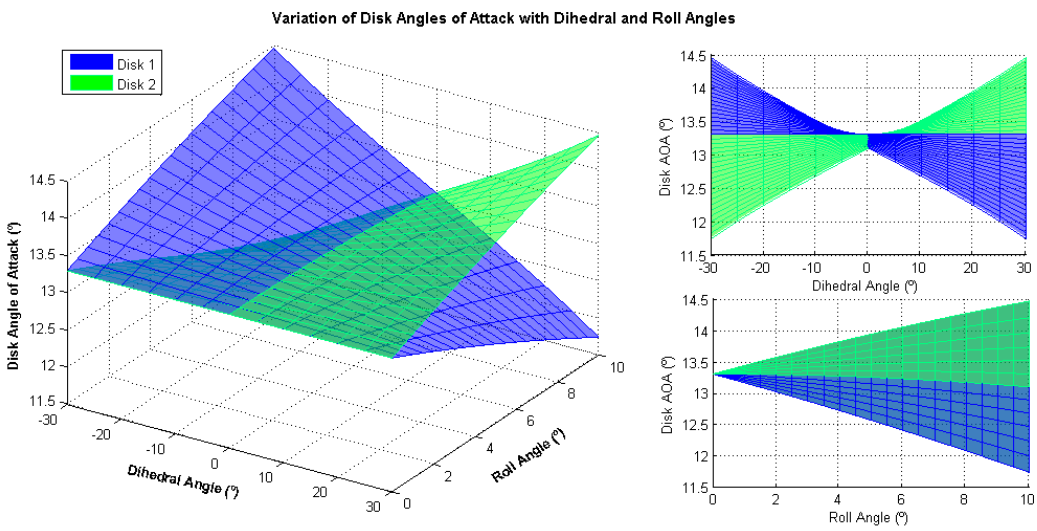

Figure 5.6 Chart showing the variation of disk angles of attack with varying roll and dihedral angles for a two disk kite with an initial angle of attack of 13.3º

The changing angles of attack cause the magnitude, direction, and point of action of the aerodynamic forces to change. Figure 5.7 shows that over the small range of angles of attack caused by a 5 º roll angle (between about ten and fifteen degrees for this kite), the force coefficient (combination of lift and drag coefficients) and centre of pressure location vary approximately linearly. The force angle, defined as the angle between the chord line and the aerodynamic force, first crosses 90º at the angle of attack of the disks before the kite is rolled, at 13.3º – this is the condition necessary for the kite to fly perpendicular to the line, as was required for this simplified case. Over the range of angles of attack of ten to fifteen degrees experienced by this kite when rolled up to ten degrees, the resultant force angle increases with angle of attack (or angles forward with respect to the disk). As such, when a roll angle is applied, the force angle of one disk increases while the force angle of the other disk decreases due to their corresponding changes in angle of attack.

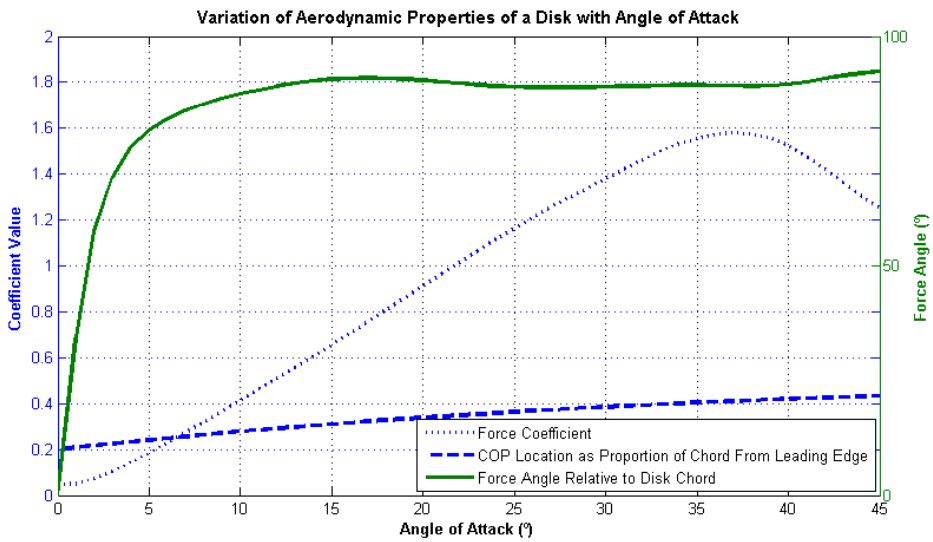

Figure 5.7 Chart showing the variation of disk aerodynamic properties with angle of attack

To determine the effect that the changing aerodynamic forces have on the out of balance moments acting on the kite structure, a kite with a positive dihedral angle will be considered. If a positive roll angle is applied, the angle of attack of disk one (positive x-side of the kite) decreases, while the angle of attack of disk two increases (the reverse of this applies for a kite with a negative dihedral angle). In isolation, the change in the magnitudes of the aerodynamic forces this leads to does not affect the yaw moment. However, the change in the angles and points of action for the forces leads to an out of balance moment about the yaw axis.

The yaw moment can be split into two components. The first of these arises from a force in the X-direction acting at a distance in the Z-direction from the yaw axis (in line coordinates). The second arises from a force in the Z direction acting at a distance

in the X-direction from the yaw axis. The force and distance components for a kite with a positive dihedral and roll angle are shown in figure 5.8, and the yaw moment components resulting from these are shown in figure 5.9.

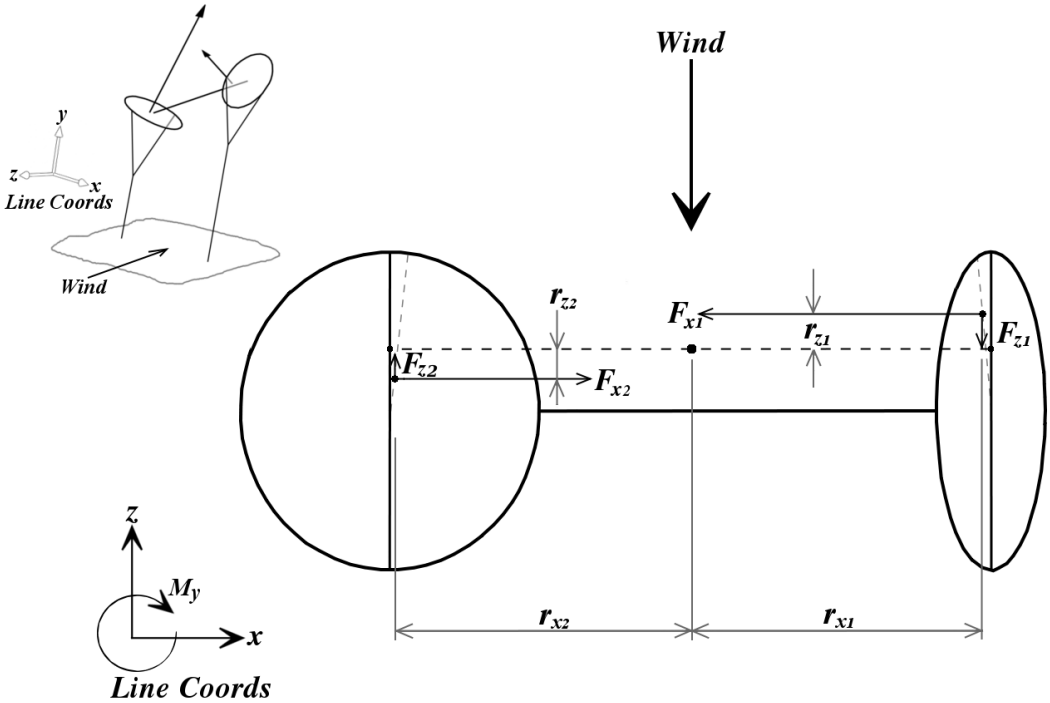

Figure 5.8 Diagram showing components of the disk aerodynamic forces affecting yaw moment, and their locations, viewed from below the kite looking up the lines

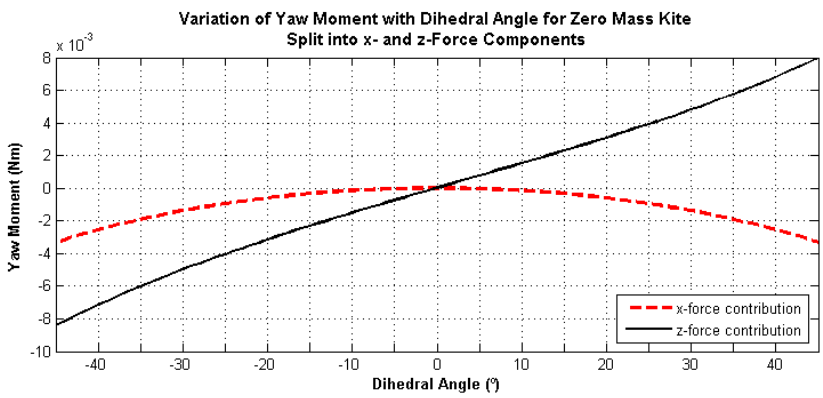

Figure 5.9 Chart showing the components of the yaw moment acting on a zero mass kite arising from forces in the x- and z-directions in line coordinates with varying dihedral angle

The yaw moment caused by the force in the line x-direction is always in the negative (anti-clockwise, when looking in the Y-direction as in figure 5.8) direction for a positive roll angle, and the magnitude of the moment increases with increasing dihedral or

anhedral angle. This is caused by the centres of pressure moving with the changing disk angles of attack – for a positive roll applied to a dihedral kite, the centre of pressure of the disk on the positive X-side of the kite moves forward, while that of the disk on the negative X-side of the kite moves rearwards. This, combined with the forces in the X-direction resulting from the dihedral angle causes a yaw moment.

The yaw moment caused by the force in the Z-direction increases with increasing dihedral angle, and passes through zero when there is no dihedral angle. While the lengths of the moment arms for the forces in the Z-direction do change as the centres of pressure move, the effect of this is very small compared to that of the changing Z-components of the resultant aerodynamic forces. For this special case of a zero mass kite, at equilibrium with the kite surface perpendicular to the line, when the kite has no roll angle the line (or kite, since the coordinate systems are aligned in this case) Z-component of the aerodynamic forces is zero, as was shown in figure 5.3. However, figure 5.10 shows that the angle between the resultant aerodynamic force and the disk chord line changes with angle of attack – the angle is 90 degrees at six different angles of attack. For this case, the equilibrium point being considered is where the disk angle of attack is about 13.3 degrees. When the angle of attack for each disk is varied by applying a roll angle to the kite, the Z-component of the aerodynamic force (in the line coordinate system) becomes non-zero.

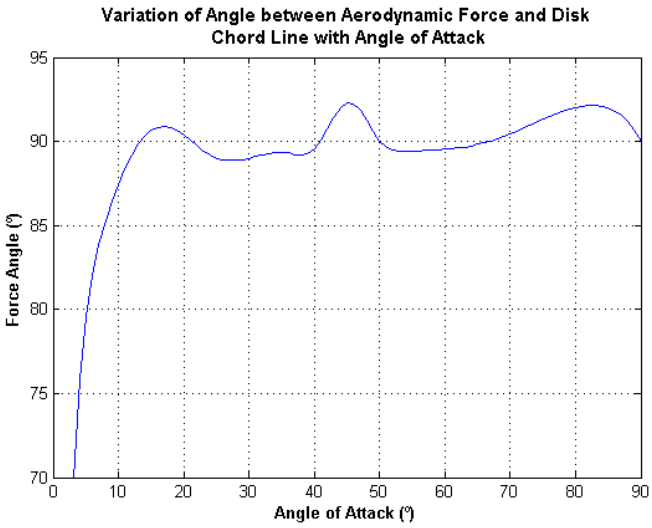

Figure 5.10 Chart showing the variation of the angle between the aerodynamic force and the disk chord line with angle of attack, scaled to highlight the variation at angles of attack greater than 10º

For a positive roll angle applied to a kite with a positive dihedral angle, the angle of attack for the disk on the positive X-side of the kite decreases, while the angle of attack for the other disk increases. Figure 5.10 shows that these changes in angles of attack lead to the resultant aerodynamic force for the positive X disk angling backwards,

and that of the negative X- disk angling forwards. The resulting negative and positive Z-force components on the positive X and negative X disks, respectively, result in a positive yaw moment. The reverse is true for the same kite with a negative roll angle, or an anhedral kite with a positive roll angle.

5.1.2 Effect of Bridle Length on Turning Response on a Zero Mass Kite

In setting parameters to allow a kite to fly at equilibrium with the kite and line z-axes aligned, the rear bridle line length is adjusted relative to the front bridle line length. If the front bridle length is varied, a new rear bridle line length can be calculated to maintain the kite and line alignment condition – the bridle point must retain the same location in the kite X-direction, but can be moved in the kite y-direction, as shown in figure 5.11. Changing the length of the bridles in such a manner does not change the angle of attack of a kite with no mass, nor does it change the roll axis. As such, it has no effect on the turning response.

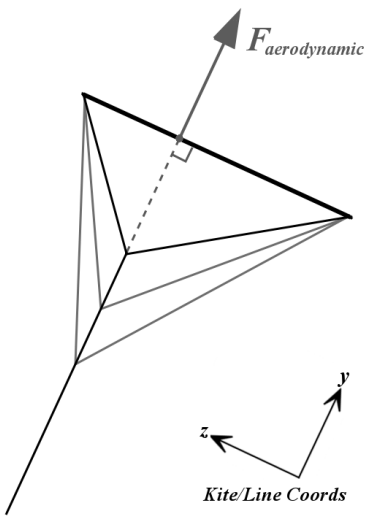

Figure 5.11 Diagram showing adjustments possible to bridle geometry while maintaining kite/line perpendicularity

5.1.3 Effect of Wind Velocity on Turning Response

For a zero mass kite, wind velocity does not vary the equilibrium kite pitch or line equilibrium angles, since disk aerodynamic properties are assumed to be independent of flow velocity. However, the magnitudes of the aerodynamic forces are affected. This causes a change in the yaw moment caused by a bank angle. Figure 5.12 shows that the yaw moment caused by a roll angle increases in magnitude with wind velocity.

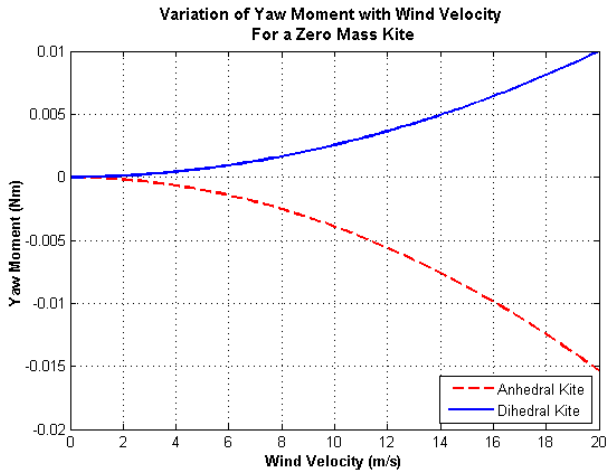

Figure 5.12 Chart showing the variation of yaw moment resulting from a 5° roll with wind velocity for an anhedral and dihedral kite

While the aerodynamic forces increase in magnitude with the square of the wind velocity equally for both anhedral and dihedral cases, the yaw moment does not. This is because the X-force component of the yaw moment always acts in the same direction, as shown in section 5.13. As such, it adds to the yaw moment of a kite with a negative dihedral angle (anhedral kite) and subtracts from that of a kite with a positive dihedral angle. These components all increase in magnitude with increasing wind velocity, but remain in proportion to each other, as shown in figure 5.13.

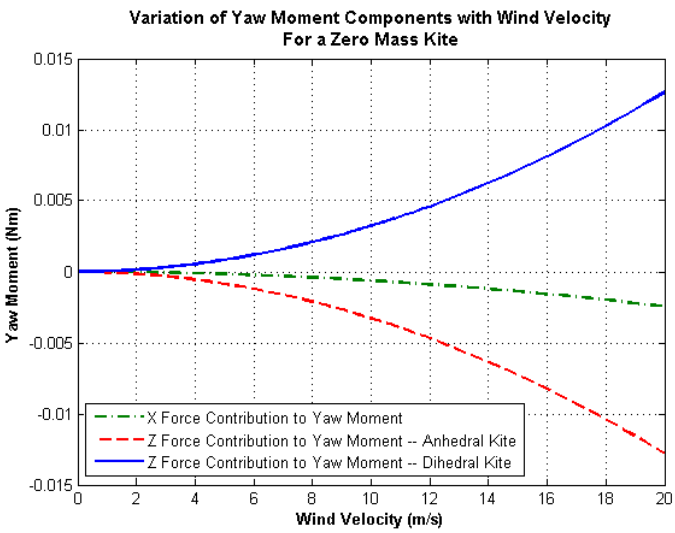

Figure 5.13 Chart showing the components of yaw moment caused by x- and z-components of disk aerodynamic forces for an anhedral and dihedral kite

5.1.4 Effect of Kite Width on Turning Response

Varying the width of a kite, defined as the distance between the centres of the two disks, has no effect on the equilibrium kite pitch or line elevation angles, nor does it vary the changes in disk angles of attack caused by a roll angle. However, modifying the kite width does change the position vectors for the Z-force components of the aerodynamic forces acting on the disks. Since the X-component of the force position vectors is increased with increasing width, the yaw moment caused by a roll angle increases linearly with kite width. The rate of increase in yaw moment with kite width is the same for a dihedral and anhedral kite. However, the magnitudes are different due to the yaw moment caused by the X-component of the aerodynamic force, which is unaffected by kite width.

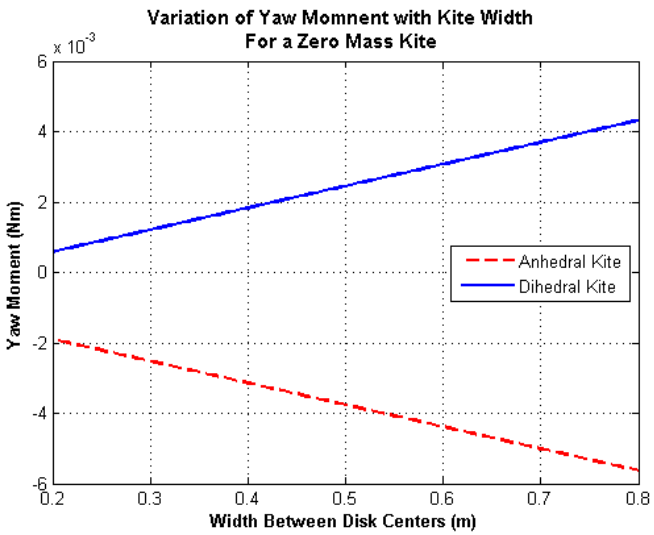

Figure 5.14 Chart showing the variation of yaw moment resulting from a 5° roll with the width between disk centres for an anhedral and dihedral kite

5.2 Turning Response of a General Two-Disk Kite

The previous section utilised a simplified kite model to demonstrate the effects (or lack thereof) of some kite parameters on kite turning response. Other parameters cannot be modified within the restrictions of the simplified kite, and will be investigated in this section. The effect of the variation of bridle geometry and wind velocity will also be revisited. The investigation of the effects of varying bridle geometry in the previous section was restricted to the variation of the bridle point location in the kite y-direction only, while the wind velocity has a significantly different effect on turning response of a kite with mass. Table 5.2 shows the parameter values used for kite models in this section unless otherwise stated.

Table 5.2 Table of kite parameters used for the baseline kite in this section

Parameter	Standard Value
Disk diameter	240mm
Kite span (between disk centres)	500mm
Front bridle length	200mm
Rear bridle length	250mm
Kite pitch angle	Equilibrium
Line elevation angle	Equilibrium
Dihedral angle	20°
Roll angle	0° or 5°
Wind velocity	10m/s
Kite mass	0 or 0.1kg

5.2.1 Turning Response with Varying Bridle Geometry

The effect of varying both front and rear bridle line lengths simultaneously so as to maintain the position of the bridle point in the kite y-direction has already been covered, and was found to have no effect on the turning response. This section examines the effect of varying the rear bridle line length while holding the front line length constant, as shown in figure 5.15. The kite investigated in the previous section had its bridle line lengths tuned to allow it to fly at equilibrium with the kite and line coordinate systems aligned. At equilibrium, the aerodynamic force of a zero-mass kite must align with the bridle point and line, as shown in section 5.15. This leads to the line and kite no longer being perpendicular to each other in cases where the force angle is not 90 degrees. In this case, the kite no longer rolls about its own Z-axis – rather, it rolls around the line Z-axis, as explained in section 2.3.2. The yaw axis is also modified, since it is aligned with the line Y-axis.

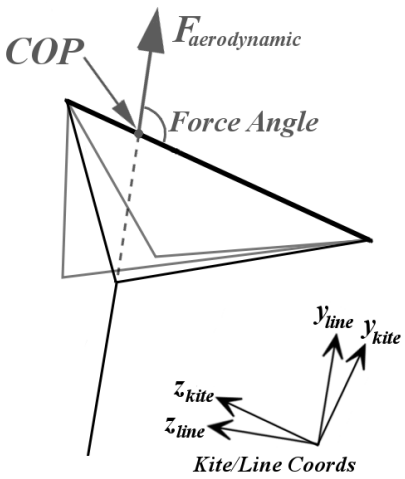

Figure 5.15 Diagram showing the equilibrium condition for a general zero-mass kite

Changing the length of the rear bridle line affects the flight of a kite in two ways. Firstly, it alters the equilibrium pitch angle of the kite, since the line on which the aerodynamic force acts on must pass through the bridle point (for a zero mass kite). This change in pitch angle also causes a change in equilibrium line elevation angle since it results in a change in the aerodynamic force – the line assumes the same orientation as the total force acting on the kite at equilibrium. The variation of both equilibrium kite pitch and line elevation with rear bridle length is shown in figure 5.16.

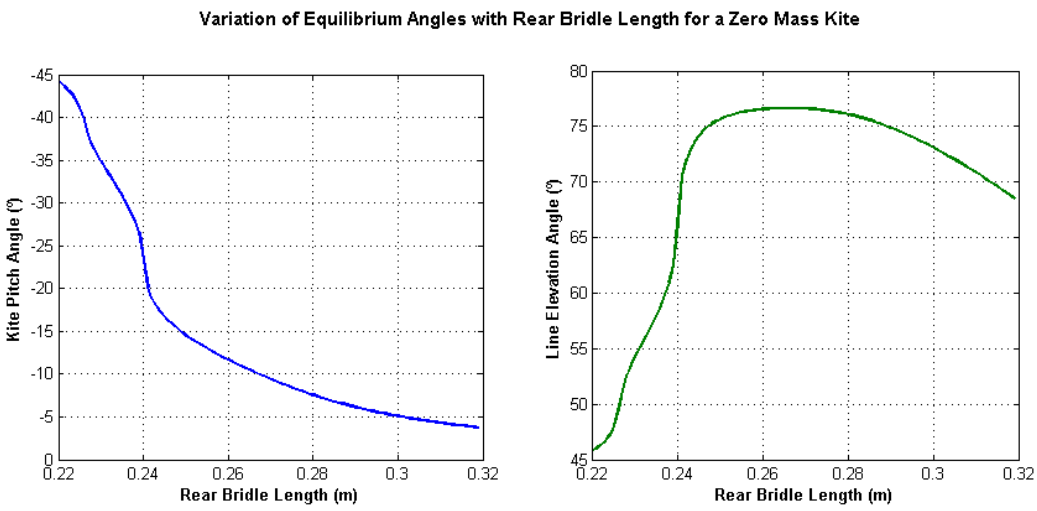

Figure 5.16 Charts showing the variation of equilibrium kite pitch and line elevation angles with rear bridle line length for a zero-mass kite

The effect that the changes in kite pitch and line elevation angles caused by varying bridle geometry have on turning performance cannot be investigated independently. If

either parameter is held constant, yaw moments are created that would never occur in a real kite, making the results meaningless. As such, an exact analysis of the factors causing the yaw moment as was performed in the previous sections is impractical. However, the causes of changes to the yaw moment and their relative significance can be determined.

Figure 5.17 shows that as the rear bridle length is modified, the yaw moment resulting from a roll angle changes in a more complicated manner than the cases dealt with previously. There are two points on the chart where the variation of the yaw moment changes abruptly. These points correspond to values of rear bridle length where the equilibrium kite pitch and line elevation angles change rapidly, as shown in figure 5.16. The rapid variation of equilibrium behaviour at these points means that such a kite would be very unstable in flight – small variations in the angle of the apparent wind would cause large fluctuations in kite position and turning behaviour.

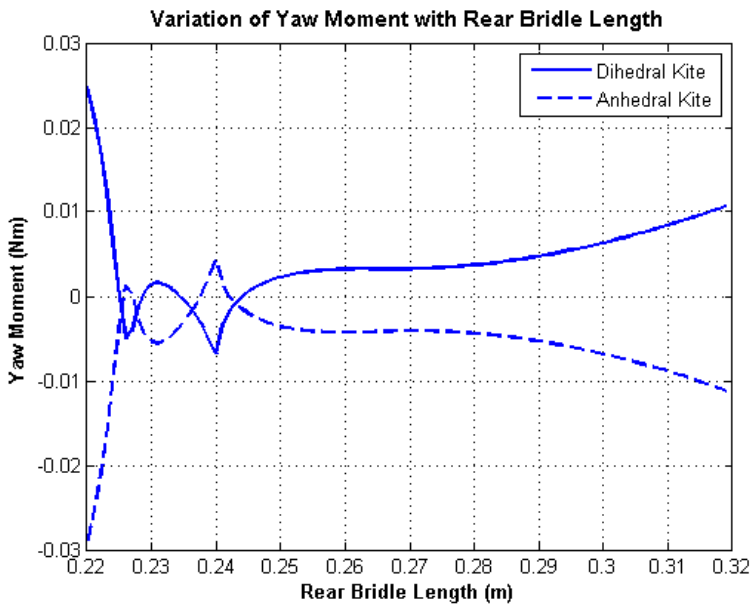

Figure 5.17 Chart showing the variation of yaw moment resulting from a 5° roll with varying rear bridle line length

When the yaw moment is split into components caused by X- and Z-force components, the reason for the erratic changes in turning behaviour becomes clear. The yaw moment resulting from the X-force is always negative for a positive roll, as explained in section 5.1.1. However, the component resulting from the Z-force varies significantly to both sides of zero, and often has a magnitude much greater than the X-force component. This variation is due to the change in the force angle – the angle the resultant aerodynamic force makes with the disk surface – as the disk angle of attack changes, as explained in section 5.1.1 and Figure 5.8.

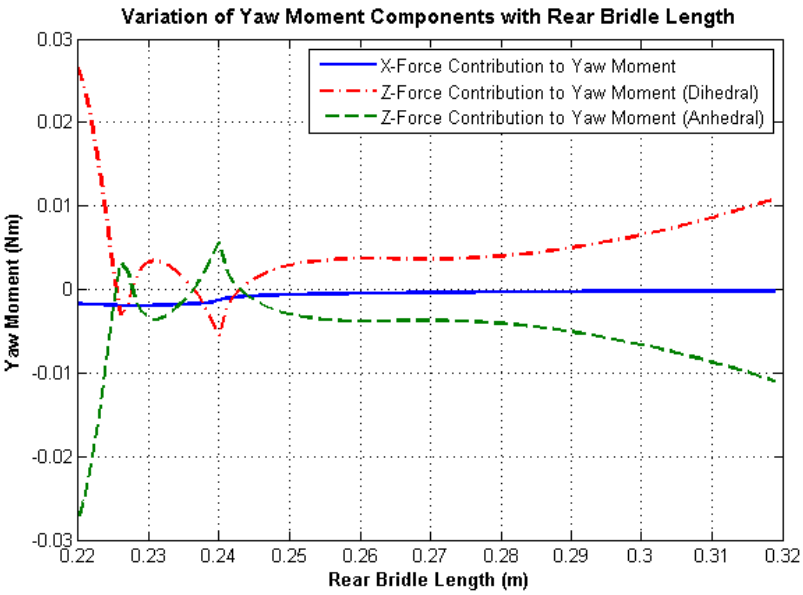

Figure 5.18 Chart showing the variation of the X- and Z-force components of the yaw moment resulting from a 5° roll with varying rear bridle length

The force angle only changes very slightly with the small changes in disk angle of attack caused by rolling the kite. However, the lever arm length for the Z-Force is much larger than that for the X-force, resulting in a significant yaw moment. Because such small changes in force angle have such a great effect on yaw moment, turning response is very sensitive to variations in disk geometry (flatness, thickness etc.). Figure 5.10 shows that with angles of attack greater than around 15°, the force angle varies a few degrees above and below 90° in a seemingly erratic manner. Subtle differences in disks will cause the exact variation in this region to differ, thereby causing significantly different turning behaviour.

Since stability of equilibrium and turning behaviour is important when designing a kite, bridle lengths need to be chosen to give equilibrium positions where the turning behaviour is not sensitive to slight changes in parameters that occur in normal flight. In the case of the kite examined here, the turning behaviour and equilibrium angles are well behaved with the bridle lines tuned to give the highest elevation angle (or maximum lift to drag ratio). This elevation angle is about 76° for this kite, as indicated in figure 5.16. This is in part due to the fact that the kite and line are close to perpendicular at this point, as well as the variation of the force angle being more consistent at disk angles of attack below around 15° (see figure 5.10).

5.2.2 Turning Response with Varying Mass and Wind Velocity

To this point, all kites used for analysis have been assumed mass-less. As such, the aerodynamic forces acting on the disks have been taken to be the only forces acting on the kite system. Adding mass to the kite alters the equilibrium kite pitch and line elevation angles. Since kites are usually quite lightweight, the magnitude of this change is small, but is nonetheless significant especially for heavier kites or where the wind velocity is low. For a kite with mass, it is useful to investigate the effect of varying wind speed and kite mass together using a dimensionless analysis, since an increase in mass or a decrease in wind velocity are equivalent.

Figure 5.19 shows the aerodynamic and gravity forces acting on a kite. For a two-disk kite, the centre of mass is aligned with the mid-point of the chord, while the centre of pressure is always forward of this point – it approaches the mid-point of the chord as the angle of attack approaches 90°. To maintain equilibrium, the aerodynamic force must act behind the bridle point to offset the moment created by the gravity force. For this to happen, the magnitude of the kite pitch increases, resulting in the centre of pressure moving rearwards and the magnitude of the aerodynamic force increasing.

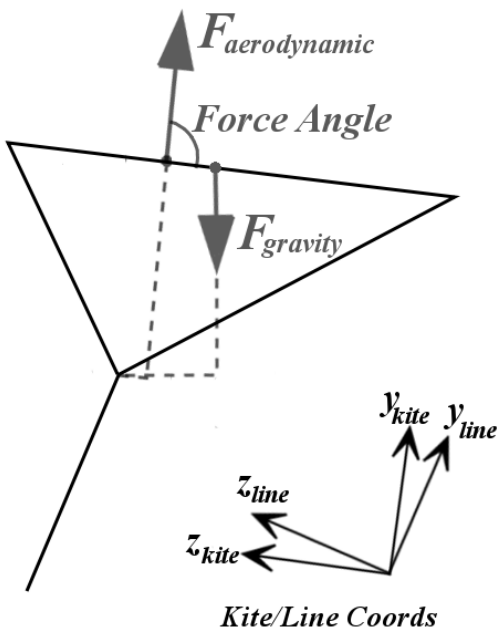

Figure 5.19 Diagram showing forces acting on a kite with mass

The line elevation angle is also changed, since it is aligned with the resultant of the aerodynamic and gravity forces. The magnitude of the change in line elevation angle is larger than the change in kite pitch, as shown in figure 5.20. Small changes in kite pitch offset the moment created by the gravity force, since the change causes both an

increase in magnitude and location of the aerodynamic force. However, the change in the direction of the resultant force directly alters the line elevation angle.

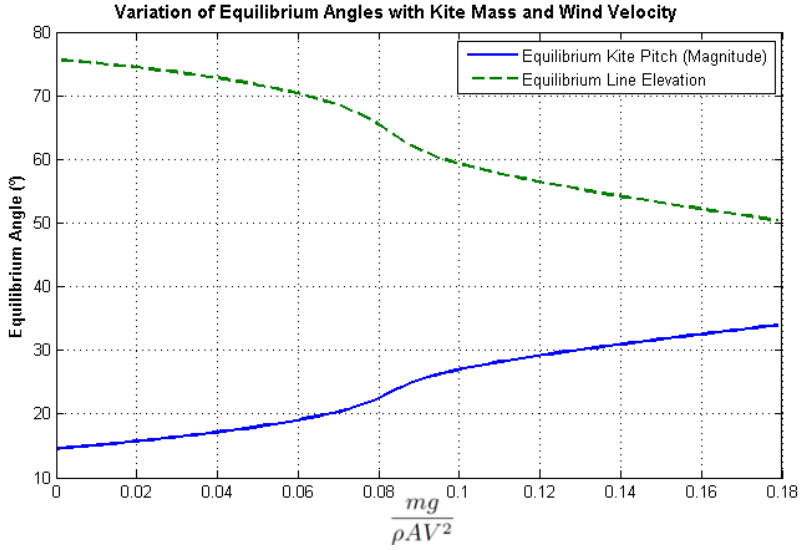

Figure 5.20 Chart showing the variation of kite pitch and line elevation equilibrium angles with kite mass and wind velocity

The changes in equilibrium kite pitch and line elevation angles cause a change in turning behaviour, as shown in Figure 5.21. As was the case with varying bridle geometry, the effects on the turning response due to kite pitch and line elevation angles cannot be investigated separately, since holding either constant would induce additional yaw moments.

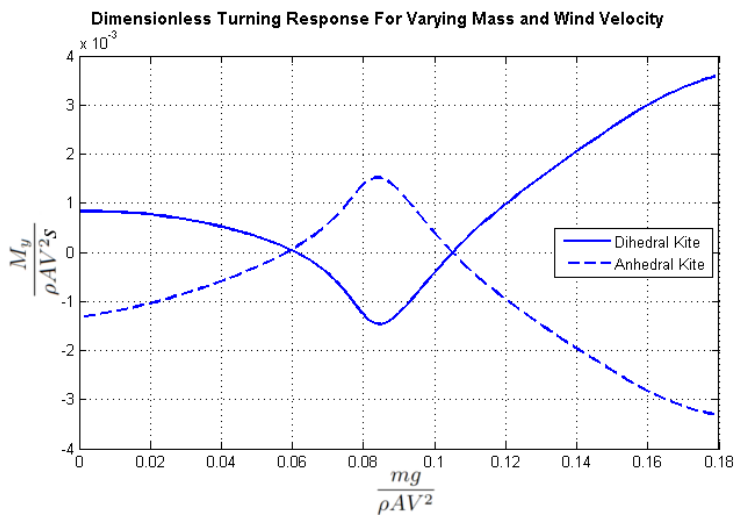

Figure 5.21 Chart showing the variation of the yaw moment resulting from a 5° roll applied to a kite with varying kite mass

Figure 5.22 shows the dimensionless turning response for a dihedral kite from figure 5.21 split into components arising from X- and Z-forces. As with varying bridle geometry, the X- force component of the yaw is small and always negative, while the Z-force component varies significantly to both sides of zero. As described in the previous section, this is caused by the variation of the angle the aerodynamic forces make to the disks, which vary with angle of attack.

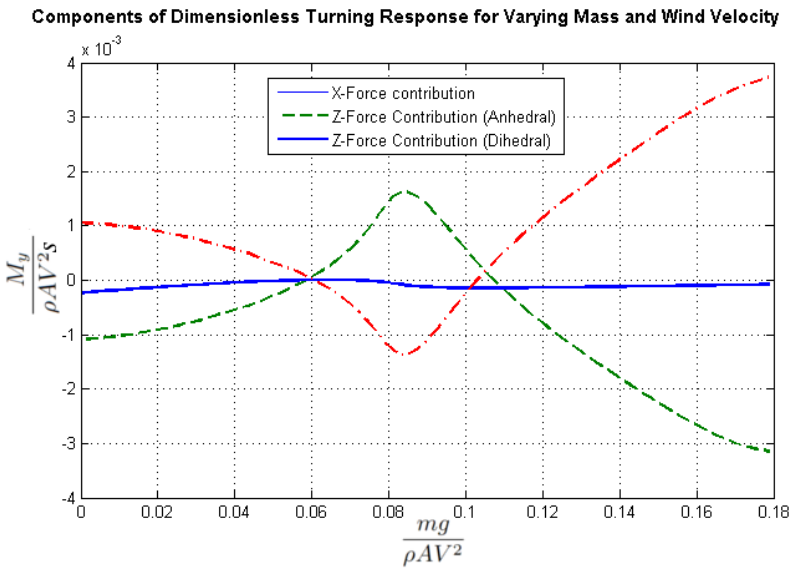

Figure 5.22 Chart showing the variation of the yaw moment resulting from a $5^{\underline{o}}$ roll split into X- and Z-force components with varying kite mass

As with the bridle lengths, mass is not a parameter that would normally be used to vary turning response. Rather, a kite is usually constructed to be as light as possible to enable it to perform in light winds. Additionally, it does not directly affect turning response, only indirectly through changing the kite pitch and line elevation equilibrium angles. However, the change in turning response due to wind velocity is an important factor to consider when designing a kite. Figure 5.22 shows that a kite constructed with the geometry used in this section can turn in different directions for a given roll angle, depending on the wind speed. Consequently, this may not be a suitable kite for general use, depending on the exact kite area and mass and the expected range of wind speeds.

5.2.3 Turning Response with Varying Dihedral Angle for a Kite with Mass

As was shown in the previous section, the addition of mass to a kite has a significant effect on turning response. This is primarily due to the gravity force acting at a different position to the resultant aerodynamic force. This means that the line is no longer aligned with the aerodynamic force in the Z-direction when at equilibrium, as shown in

figure 5.19. Additionally, the mass changes the angle between the line and kite, further altering turning response.

As was discussed in section 5.1.1, when a kite with a dihedral angle is rolled, the location of the centre of pressure for each disk moves in opposite directions. For the mass-less kite, these locations were initially aligned with the line in the Z-direction, and the roll resulted in a negative Z-location for one disk and a positive Z-location for the other, as was shown in figure 5.8. Coupled with the X-component of the aerodynamic forces, this resulted in a yaw moment of varying magnitude but constant direction for a roll angle applied to a kite with any dihedral angle – specifically, a negative yaw moment for a positive roll angle and vice-versa (This is only the component of yaw moment caused by forces in the X-direction)..

A kite with mass has a negative z-location for both aerodynamic forces at equilibrium. As with the mass-less kite, one of these locations will move forward, and the other will move backwards when a roll angle is applied. However, for some kite configurations, both disks may still have negative Z-locations. In this case, the direction of the resulting component of yaw moment is determined by the relative magnitudes of the Z-locations and the X-components of the aerodynamic forces, and may be negative or positive for a given roll angle.

Figure 5.23 shows the components of the yaw moment resulting from a 5° roll applied to the kite described in table 5.2 with varying dihedral angle. As described above, the X-force component of the yaw moment is no longer always in the negative direction for the positive roll angle applied, as was the case for simplified kites with no mass. For dihedral angles between -20° and 20°, the change in the magnitudes of the X-Forces outweighs the change in the Z-locations of the aerodynamic forces, leading to a positive yaw moment. For dihedral angles outside this range, the difference in the location of the aerodynamic forces again becomes more significant.

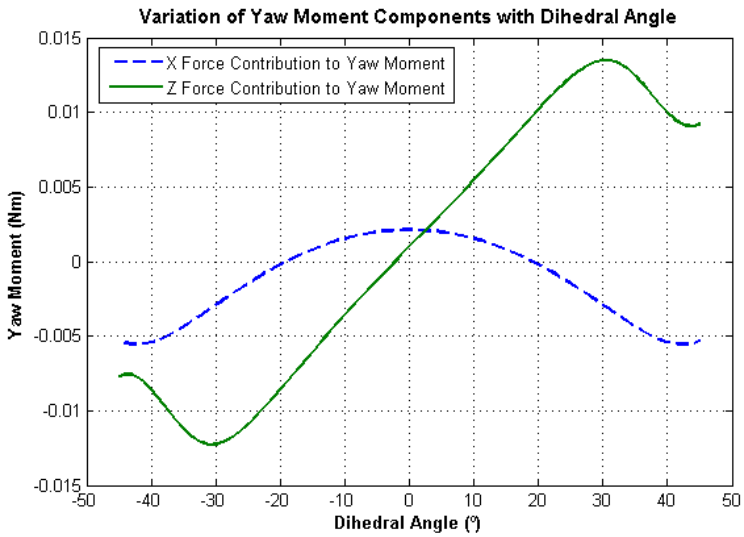

Figure 5.23 Chart showing the variation of yaw moment components caused by X- and Z- forces with dihedral angle for a kite with mass

Figure 5.24 shows the total yaw moment resulting from the components shown in figure 5.23. The addition of mass to the kite results in the yaw moment crossing zero at a negative dihedral angle, rather than at zero dihedral as was the case with a mass-less kite. This shows that a real kite requires a certain anhedral angle (in this case, at least 6° anhedral) for a roll angle to result in a yaw moment in the correct direction – i.e. a negative yaw moment for a positive roll angle.

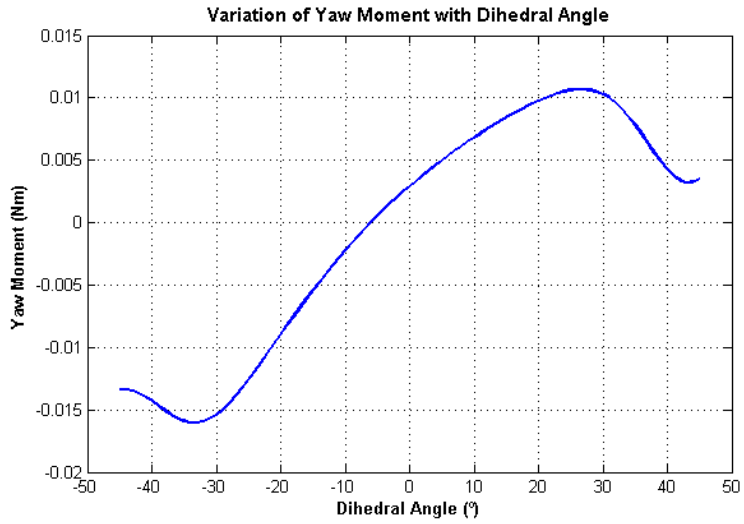

Figure 5.24 Chart showing the variation of yaw moment with dihedral angle for a kite with mass

5.2.4 Effect of Other Parameters on Turning Response

Parameters such as disk diameter and kite width also affect the turning response of a disk kite. However, the ways in which these affect the yaw moment resulting from a roll angle are simple and predictable. Increasing the size of the disk simply causes in increase in the magnitude of the aerodynamic forces in proportion to the increase in surface area. The yaw moment caused by a given roll angle increases correspondingly. Increasing the width of the kite (the distance between the centres of the two disks) increases the lever arm of the Z-force component of the yaw moment. This leads to the yaw moment varying more as other parameters are varied, since the previous sections showed that the Z-force component of the yaw moment is more variable than the X-force component.

5.3 Turning Mechanisms Not Considered Here

While the static model used here provides insight into the mechanisms that can lead to a yaw movement of a kite when a roll angle is initially applied, there are other effects that can occur and these require a dynamic model to simulate. The first of these is particularly important for kites whose dihedral angles are such that little or no yaw moment is directly caused by a roll angle. When such a kite is rolled, it will not immediately yaw, as has been shown. However, the imbalance in the aerodynamic forces in the X-direction will cause the kite to move sideways. This, in turn, effectively modifies the direction of the apparent wind as seen by the kite, and leads to unequal angles of attack between the two disks. As has been shown, this will lead to a yaw moment.

The second scenario where a static model is inadequate to explain yaw moments occurs if a roll angle is applied quickly. In this case, the apparent wind direction experienced by each disk becomes unequal, again leading to a yaw moment. The exact behaviour this causes cannot be determined by a static model. An indication of the relative magnitude of the yaw moments caused by a rapidly applied roll rotation was found by direct manipulation of the apparent wind vectors for each disk. The magnitude of the yaw moment due to the rotation rate was found to be comparable to that caused by the final roll angle. However, factors such as added mass and the finite time period required for a change in apparent wind to affect aerodynamic forces mean that this indication is of little practical use.

Another factor not considered in this static analysis is what happens as the kite proceeds to yaw under the influence of the yaw moment. Clearly, as this happens the apparent wind direction for each disk changes, further affecting the yaw moment acting on the kite. As with the effect of roll rotation rate, this is left for a future dynamic analysis of the kite system.

Chapter 6

Summary and Conclusions

6.1 Rotations Axes for a Two-Line Kite

Investigating how a two-line kite turns necessitated first defining how exactly a kite can rotate in the sky, as it was realised that previous studies had made simplifications that would modify turning behaviour. Definitions of pitch, roll, and yaw angles were proposed that differ from those of the convention used for aircraft. This new definition changes the definition of roll and yaw axes to reflect how a kite is controlled and how it is free to move.

The pitch axis for a kite is defined by the imaginary line running between the two points where the lines attach to the bridles. This is the axis about which the kite-bridle system can pivot in order to reach an equilibrium angle of attack. The kite-bridle system acts as an inverted pendulum about this axis.

The new roll axis is defined as a line running through the centre of the bridle points aligned perpendicular to two imaginary lines: One running between the two bridle points (where the kite lines attach to the bridles), and the other running between the midpoint of the line between the bridle points and the midpoint of an imaginary line between the two kite line ends (where the kite lines are held at the ground). This is simply the result of the fact that this is the only axis about which the lines can influence the orientation of the kite, assuming that their length is much greater than their distance apart from each other at either end. This assumption is valid for any standard two-line kite arrangement flying at a good altitude.

The new yaw axis is defined by the line running between the middle of the bridle points and the middle of the points where the kite lines are attached at the ground, as was used in defining the roll axis. The kite is free to rotate about this axis due to any imbalance of forces and moments.

6.2 Static Model of a Kite

The static model of a kite outlined in this thesis provides a starting point for an analysis of kite turning. Flat disks were used to represent a kite to enable aerodynamic forces to be calculated. While the examples given use two disks to represent a kite's structure, the method can easily be scaled to any number of disks, provided that they are far enough apart to prevent a disk interfering with the flow over a neighbouring disk. The shape of the kites that can be represented by disks is also somewhat limited by the restriction that disks cannot be placed in front of or behind each other.

By defining rotation matrices that convert vectors between coordinate systems relative to the ground/wind, lines, kite, and individual disks, the forces acting on each disk can be calculated with relative ease. Using the rotation matrices, these forces can be transformed into any coordinate system that is convenient, allowing the out of balance forces and moments to be found relative to the pitch, roll, and yaw axes that were defined for a two-line kite. This process allows a force and moment balance to be found for a kite in any given position in the sky.

While the above procedure used to model a static kite can be represented quite simply, it is nonetheless quite a tedious procedure to calculate out numerically. A series of programs were written for MATLAB to automate the process. This also allowed equilibrium conditions for a kite configuration to be found by trial and error based methods. This is important, since a static analysis of a kite not initially at an equilibrium condition (i.e. before any perturbation is applied) does not provide useful information about turning response – The line elevation and kite pitch angles have a significant influence on how a kite turns.

6.3 Result of Applying a Roll Angle to a Disk Kite

6.3.1 Kite Flying Perpendicular to Lines

When a roll angle is applied to a kite by manipulating the lines, the disk angles of attack can change so that they are no longer equal. The exact direction and magnitude of this change depends on the dihedral angle of the kite and the angle between the kite and lines. If the kite happens to be able to fly at equilibrium perpendicular to the line, the dihedral angle and the kite pitch angle are the primary parameters influencing turning response.

A kite flying perpendicular to the lines with no dihedral angle will not yaw in response to a static roll angle. A kite with a dihedral angle may turn in either direction for a given roll angle, depending on the initial disk angles of attack, which are set by the kite pitch angle. For low angles of attack, below about 15° for a disk, the angle between a plate and the aerodynamic force acting on it, measured from the rear of the

plate, increases with increasing angle of attack. This angle increases to a maximum of around 91° for a disk, then decreases again down to about 89° as the angle of attack is increased to about 25°. This angle crosses the 90° mark three more times as the angle of attack is further increased, before settling on 90° when the plate is perpendicular to the flow stream (see figure 5.10).

If the initial angle of attack is such that an increase in angle of attack causes an increase in the angle between the force and plate surface, an anhedral (i.e. negative dihedral angle) disk kite will yaw in a counter-clockwise direction, as viewed from the ground, when a positive roll angle (i.e. a roll resulting from a kite flyer pulling on the line in their left hand) is applied. A disk kite with a positive dihedral angle will yaw in the opposite direction for the same roll angle. However, the same kites will respond in the opposite manner if the initial angle of attack is such that an increase in angle of attack causes a decrease in the angle between the aerodynamic force and disk surface.

The change in the angle of the aerodynamic force is not the only cause for a kite to yaw when a roll angle has been applied. When the angle of attack of a disk changes, the centre of pressure, the point at which the aerodynamic force can be assumed to act, moves. This movement is always to the rearward of the disk as angle of attack is increased. When a roll angle is applied to a kite with a nonzero dihedral angle, the disk on one side of the centre line experience in increase in angle of attack, while the disk on the other side experiences a decrease – which disk is which depends on whether the kite is anhedral or dihedral, and what direction the roll angle is. The corresponding changes in centres of pressure, combined with the sideways components of the aerodynamic forces caused by the presence of a dihedral angle, cause a yaw moment. This moment is always in the negative direction for a positive roll, and vice-versa, since while changing from an anhedral to dihedral kite changes the directions of the centre of pressure movements resulting from a roll angle, the directions of the sideways aerodynamic force components are also reversed.

6.3.2 General Kite

Under most circumstances, a kite will not fly aligned perpendicular to the lines. In this case, the roll rotation also influences the angles of attack for each disk differently irrespective of dihedral angle, since the roll axis is aligned with the lines rather than the kite. The angle between the kite and line depends on kite and bridle geometry, kite mass and wind speed – almost every variable. The angle may be less than or greater than 90° (measured between the line and the kite surface forward of the line), although only by small amounts in the latter case.

In addition to the aerodynamic forces discussed already, a kite also has a force due to gravity acting on it. This force causes the kite to require a larger pitch angle to maintain equilibrium, and decreases the lift to drag ratio resulting in a lower line elevation. As

has been discussed, these angles have a significant influence on the turning behaviour of the kite. For a given kite, the relative magnitude of the gravity force compared to the aerodynamic force dictates how significant the change in pitch angle and line elevation caused by this gravity force is.

6.4 Observations on Designing a Kite for Proper Turning Response

Although the kites investigated in this thesis are very simple representations of basic, rigid kites, some observations have been made that could be useful in designing real kites. These observations could also provide a starting point for further analysis using the method outlined in this thesis with more than two disks.

Firstly, it is clear that for a kite with only two flat surfaces, the dihedral angle is the most important parameter for designing for turning performance. Dihedral angle has the largest effect on turning response, as it is the primary factor determining the changes in angles of attack of the two sides of the kite when a roll angle is applied. It is also one of the few parameters that have little detrimental effect on other flight parameters. The analysis presented here shows that some anhedral angle is required for a kite to turn in the expected direction when a roll angle is applied. The exact amount of anhedral angle varies with other factors, but is generally between 8° and 20° (an anhedral angle is a negative dihedral angle).

Secondly, wind velocity can have a significant effect on both the direction and magnitude of the yaw moment resulting from a roll angle. Consequently, a poorly designed kite may turn in opposite directions under different wind conditions for the same roll angle. This would pose a significant problem if these changes in behaviour occurred at wind speeds that could be encountered by the kite. This means that the dihedral angle (and to a lesser extent bridle geometry) must be tuned for turning performance over a range of expected wind velocities.

Finally, the large dependence of turning response on kite pitch and line elevation angles means that a kite must maintain a relatively consistent equilibrium position under changing wind conditions. Otherwise, a small change in wind velocity could cause a large change in turning behaviour. Additionally, some kites may have multiple equilibrium positions at a given wind speed. This is not desirable, since the kite may respond differently to control inputs for each of these positions.

Chapter 7

Future Work

The calculations outlined in Chapters 2 and 3 can easily be used to model more complicated kites by introducing additional disks. The main complication arising from this is the large number of interacting geometry parameters that such a kite has, since each pair of disks has dihedral and twist angles that can be varied independently, as well as their relative position in the kite structure. This will make presenting the results in a meaningful way challenging. One possible method of producing meaningful results would be to concentrate on configurations similar to existing kites and make incremental changes to their geometry.

For a complete understanding of the behaviour of two-lined kites, a dynamic simulation may be required to show what happens when a yaw rotation occurs under the influence of the yaw moment, and the effects of different rates of application for control inputs, as well as investigating the dynamic stability of the system. Such a simulation could be performed for disk kites using the work in this thesis, which only finds the yaw moment, as a starting point.

Performing a dynamic simulation of a disk kite would incur a number of added complexities over the static simulation presented in this thesis. Firstly, the line and kite coordinate systems can no longer be assumed to be at rest with respect to the global coordinate system. The motion of these coordinate systems would need to be taken into account when calculating the apparent wind vector, which is used to find the disk angles of attack and aerodynamic force magnitudes.

Secondly, the aerodynamic properties of the disks cannot be assumed to act the same as they do for a static analysis. Since kites are very light, the mass of air that must be accelerated around an object as it moves (known as added mass) must be included in any calculations. Additionally, the aerodynamic forces likely cannot be assumed to change at the same instant as a change in the apparent wind, which may be important when modelling the effect of a quickly applied roll angle.

It will be apparent that gaining a full understanding of how kites turn is a significant task, and this thesis is a first step towards this goal.

Bibliography

[1] B. White. (2008) Kite history. [Online]. Available: http://best-breezes.squarespace.com/

[2] T. Sugimoto, "Mechanics of classical kite buggying or how mr. pocock gained 9m/s by his charvolant," in *The Seventh Asia-Pacific Conference on Wind Engineering*, 2009.

[3] C. F. Marvin, *A Monograph on the Mechanics and Equilibrium of Kites*, W. L. Moore, Ed. United States Department of Agriculture Weather Bureau, 1897.

[4] K. Alexander and J. Stevenson, "Kite equilibrium and bridle length," *Aeronautical Journal*, vol. 105, pp. 535–541, 2001.

[5] R. A. Adomaitis, "Kites and birfurcation theory," *SIAM Review*, vol. 31, no. 3, pp. 478–483, 1989.

[6] K. Alexander and J. Stevenson, "A test rig for kite performance measurement," *Proceedings of the Institution of Mechanical Engineers*, vol. 215, pp. 595–598, 2001.

[7] J. Stevenson, K. Alexander, and P. Lynn, "Kite performance testing by flying in a circle," *The Aeronautical Journal*, vol. 109, pp. 269–276, June 2005.

[8] J. Stevenson and K. Alexander, "Circular flight kite tests: Converting to standard results," *The Aeronautical Journal*, vol. 110, pp. 605–614, September 2006.

[9] J. Stevenson, "Traction kite testing and aerodynamics," Ph.D. dissertation, University of Canterbury, 2003.

[10] G. Sánchez, "Dynamics and control of single-line kites," *The Aeronautical Journal*, vol. 110, pp. 615–621, September 2006.

[11] S. E. Hobbs, "A quantitative study of kite performance in natural wind with application to kite anemometry," Ph.D. dissertation, Cranfield Institute of Technology, 1986.

[12] P. Williams, B. Lansdorp, and W. Ockels, "Modeling and control of a kite on a variable length flexible inelastic tether," in *AIAA Modeling and Simulation Technologies Conference and Exhibit*, no. 2007-6705, August 2007.

[13] J. Breukels and W. J. Ockels, "Tethered "kiteplane" design for the laddermill project," in *World Wind Energy Conference*, 2005.

[14] P. Naaijen and V. Koster, "Performance of auxiliary wind propusion for merchant ships using a kite," in *2nd International Conference on Marine Research and Transportation*, 2007.

[15] A. R. Podgaets and W. J. Ockels, "Three-dimensional simulation of a laddermill," in *Proceedings of the 3rd Asian Wind Power Conference*, 2006, pp. 116–121.

[16] P. Williams, B. Lansdorp, R. Ruiterkamp, and W. Ockels, "Modeling, simulation, and testing of surf kites for power generation," in *AIAA Modeling and Simulation Technologies Conference and Exhibit*, no. 2008-6693, August 2008.

[17] P. S. Jackson, "Optimum loading of a tension kite," *AIAA Journal*, vol. 43, no. 11, pp. 2273–2278, 2005.

[18] H. de Haven, "Kite," U.S. Patent 1 744 529, January 21, 1930.

[19] ——, "Kite," U.S. Patent 1 908 325, May 9, 1933.

[20] A. Grahame, "Target kite imitates plane's flight," *Popular Science*, vol. 146, no. 5, pp. 65–70, May 1945.

[21] P. Powell, "Kites," U.S. Patent 3 954 235, May 4, 1976.

[22] G. Lafortune, "Fundamental kite motion," research project for 5th Year of Mechanical Engineering at INSA of Rouen, France, carried out at the University of Canterbury.

[23] B. Pamadi, *Performance, Stability, Dynamics, and Control of Airplanes*, 2nd ed. American Institute of Aeronautics and Astronautics Inc., 2004.

[24] R. Murray, Z. Li, and S. S. Sastry, *A Mathematical Introduction to Robotic Manipulation*. CRC Press, 1994.

[25] "Fluid forces and moments on flat plates," Engineering Sciences Data Unit, Tech. Rep. ESDU 70015, 1970.

[26] *ANSYS 12.1 Help Manual.*

[27] J. H. Ferziger and M. Periæ, *Computational Methods for Fluid Mechanics*, 3rd ed. Springer, 2002.

[28] D. J. Olinger and J. S. Goela, "Performance characteristics of a one-kilowatt scale kite power system," in *Proceedings of Energy Sustainability*, 2008.

[29] W. P. Reid, "Stability of a towed object," *SIAM Journal on Applied Mathematics*, vol. 15, no. 1, pp. 1–12, January 1967.

[30] P. Williams, B. Lansdorp, and W. Ockels, "Flexible tethered kite with moveable attachment points, part i: Dynamics and control," in *AIAA Atmospheric Flight Mechanics Conference and Exhibit*, 2007.

Appendix A

Example Calculation of Yaw Moment

A.1 Example Case

This section has been added to aid those not familiar with vector and matrix notation. The calculations presented in Chapters 2 and 3 will be briefly run through for the kite described below.

Table A.1 Parameters used for example calculation

Parameter	Symbol	Value
Disk diameter	$\emptyset$	0.24m
Wind velocity	V	10m/s
Line azimuth angle	Θ	180° or πradians
Line elevation angle	Φ	75° or 1.31 radians
Kite pitch angle	θ	15° or 0.262 radians
Kite roll angle	φ	10° or 0.175 radians
Kite yaw angle	ψ	2° or 0.035 radians
Kite dihedral angle	γ	-25° or -0.436 radians
Kite mass	m	0.1kg
Distance between bridle attachment points	l_a	0.24m
Front bridle length	l_f	0.2m
Rear bridle length	l_r	0.23m
Kite span	s	0.5m

A.2 Rotation Matrices

A.2.1 Rotation Matrix for the Line Coordinate System

The rotation matrices for the line elevation and azimuth angles are given by equations 2.6 and 2.7:

$$R_{azimuth} = \begin{bmatrix} \cos(\pi\text{-}\Theta) & 0 & \sin(\pi\text{-}\Theta) \\ 0 & 1 & 0 \\ -\sin(\pi\text{-}\Theta) & 0 & \cos(\pi\text{-}\Theta) \end{bmatrix}$$

$$R_{elevation} = \begin{bmatrix} 1 & 0 & 0 \\ 0 & \cos\left(\frac{\pi}{2} - \Phi\right) & -\sin\left(\frac{\pi}{2} - \Phi\right) \\ 0 & \sin\left(\frac{\pi}{2} - \Phi\right) & \cos\left(\frac{\pi}{2} - \Phi\right) \end{bmatrix}$$

The rotation matrices can then be calculated using the angles in radians given in table A.1:

$$\begin{aligned} R_{azimuth} &= \begin{bmatrix} \cos(0) & 0 & \sin(0) \\ 0 & 1 & 0 \\ -\sin(0) & 0 & \cos(0) \end{bmatrix} \\ &= \begin{bmatrix} 1 & 0 & 0 \\ 0 & 1 & 0 \\ 0 & 0 & 1 \end{bmatrix} \end{aligned}$$

$$\begin{aligned} R_{elevation} &= \begin{bmatrix} 1 & 0 & 0 \\ 0 & \cos(0.261) & -\sin(0.261) \\ 0 & \sin(0.261) & \cos(0.261) \end{bmatrix} \\ &= \begin{bmatrix} 1 & 0 & 0 \\ 0 & 0.966 & -0.258 \\ 0 & 0.258 & 0.966 \end{bmatrix} \end{aligned}$$

Note that the rotation matrix for the azimuth angle is the 3x3 identity matrix, since no rotation is required due to the azimuth angle being 180°.

The rotation matrix to change a vector defined in the global (wind-ground based) coordinate system into its equivalent in the line coordinate system can now be found:

$$\begin{aligned} R_{line} =& R_{elevation} \times R_{azimuth} \\ &= \begin{bmatrix} 1 & 0 & 0 \\ 0 & 0.966 & -0.258 \\ 0 & 0.258 & 0.966 \end{bmatrix} \times \begin{bmatrix} 1 & 0 & 0 \\ 0 & 1 & 0 \\ 0 & 0 & 1 \end{bmatrix} \\ &= \begin{bmatrix} 1 & 0 & 0 \\ 0 & 0.966 & -0.258 \\ 0 & 0.258 & 0.966 \end{bmatrix} \end{aligned}$$

A.2.2 Rotation Matrix for the Kite Coordinate System

The rotation matrix for the pitch rotation is given by equation 2.9:

$$R_{Pitch} = \begin{bmatrix} 1 & 0 & 0 \\ 0 & \cos(-\theta) & -\sin(-\theta) \\ 0 & \sin(-\theta) & \cos(-\theta) \end{bmatrix}$$

Using the value for pitch given in table A.1 in radians:

$$\begin{aligned} R_{Pitch} &= \begin{bmatrix} 1 & 0 & 0 \\ 0 & \cos(-0.262) & -\sin(-0.262) \\ 0 & \sin(-0.262) & \cos(-0.262) \end{bmatrix} \\ &= \begin{bmatrix} 1 & 0 & 0 \\ 0 & 0.966 & 0.259 \\ 0 & -0.259 & 0.966 \end{bmatrix} \end{aligned}$$

Equation 2.10 finds a vector defining the roll axis, which is the line Z-axis expressed in kite coordinates. At this stage only a pitch angle has been applied, so the kite rotation matrix is simply the pitch rotation matrix R_{Pitch}. Since line and kite coordinates are defined relative to the global coordinate system, the line Z-axis must first be transformed into its equivalent in global coordinates by applying the inverse of the line rotation matrix, then transformed into kite coordinates:

$$\begin{aligned} u_{roll} =& R_{Pitch} \cdot R_{line}^{-1} \cdot \begin{bmatrix} 0 \\ 0 \\ 1 \end{bmatrix} \\ =& \begin{bmatrix} 1 & 0 & 0 \\ 0 & 0.966 & 0.259 \\ 0 & -0.259 & 0.966 \end{bmatrix} \cdot \begin{bmatrix} 1 & 0 & 0 \\ 0 & 0.966 & -0.258 \\ 0 & 0.258 & 0.966 \end{bmatrix}^{-1} \cdot \begin{bmatrix} 0 \\ 0 \\ 1 \end{bmatrix} \\ =& \begin{bmatrix} 1 & 0 & 0 \\ 0 & 0.966 & 0.259 \\ 0 & -0.259 & 0.966 \end{bmatrix} \cdot \begin{bmatrix} 1 & 0 & 0 \\ 0 & 0.966 & 0.258 \\ 0 & -0.258 & 0.966 \end{bmatrix} \cdot \begin{bmatrix} 0 \\ 0 \\ 1 \end{bmatrix} \\ =& \begin{bmatrix} 1 & 0 & 0 \\ 0 & 0.966 & 0.259 \\ 0 & -0.259 & 0.966 \end{bmatrix} \cdot \begin{bmatrix} 0 \\ 0.258 \\ 0.966 \end{bmatrix} \\ =& \begin{bmatrix} 0 \\ 0.5 \\ 0.867 \end{bmatrix} \end{aligned}$$

Using this rotation axis, equation 2.11 uses Rodrigue's rotation formula to find the roll rotation matrix:

$$R_{roll} = I + \tilde{u}_{roll} \sin(-\varphi) + \tilde{u}_{roll}^2 (1 - \cos(-\varphi))$$

Which first requires the cross product matrix of u_{roll}, $\tilde{u}_{roll}$to be found:

$$\begin{aligned}\tilde{u}_{roll} &= \begin{bmatrix} 0 & -u_z & u_y \\ u_z & 0 & -u_x \\ -u_y & u_x & 0 \end{bmatrix} \\ &= \begin{bmatrix} 0 & -0.867 & 0.5 \\ 0.867 & 0 & 0 \\ -0.5 & 0 & 0 \end{bmatrix}\end{aligned}$$

So the rotation matrix is:

$$\begin{aligned}R_{roll} =& I + \tilde{u}_{roll} \sin(-\varphi) + \tilde{u}_{roll}^2 (1 - \cos(-\varphi)) \\ =& \begin{bmatrix} 1 & 0 & 0 \\ 0 & 1 & 0 \\ 0 & 0 & 1 \end{bmatrix} + \begin{bmatrix} 0 & -0.867 & 0.5 \\ 0.867 & 0 & 0 \\ -0.5 & 0 & 0 \end{bmatrix} \cdot \sin(-0.175) + \ldots \\ & \begin{bmatrix} 0 & -0.867 & 0.5 \\ 0.867 & 0 & 0 \\ -0.5 & 0 & 0 \end{bmatrix}^2 \cdot (1 - \cos(-0.175)) \\ =& \begin{bmatrix} 1 & 0 & 0 \\ 0 & 1 & 0 \\ 0 & 0 & 1 \end{bmatrix} + \begin{bmatrix} 0 & 0.151 & -0.087 \\ -0.151 & 0 & 0 \\ 0.087 & 0 & 0 \end{bmatrix} + \begin{bmatrix} -1 & 0 & 0 \\ 0 & -0.752 & 0.434 \\ 0 & 0.434 & -0.25 \end{bmatrix} \cdot 0.0153 \\ =& \begin{bmatrix} 1 & 0 & 0 \\ 0 & 1 & 0 \\ 0 & 0 & 1 \end{bmatrix} + \begin{bmatrix} 0 & 0.151 & -0.087 \\ -0.151 & 0 & 0 \\ 0.087 & 0 & 0 \end{bmatrix} + \begin{bmatrix} -0.0153 & 0 & 0 \\ 0 & -0.0115 & 0.0066 \\ 0 & 0.0066 & -0.0038 \end{bmatrix} \\ =& \begin{bmatrix} 0.985 & 0.151 & -0.087 \\ -0.151 & 0.989 & 0.007 \\ 0.087 & 0.007 & 0.996 \end{bmatrix}\end{aligned}$$

As with the roll rotation, the yaw rotation requires a rotation axis to be found and Rodrigue's rotation formula to be used to find the rotation matrix. Equation 2.12 finds a vector representing the yaw axis, which is defined as the line Y-axis expressed in kite coordinates. This is found by first finding the line Y-axis in global coordinates by applying the inverse of the line rotation matrix, then applying the roll and pitch

rotations found above:

$$
\begin{aligned}
u_{yaw} =& R_{roll} \cdot R_{Pitch} \cdot R_{line}^{-1} \cdot \begin{bmatrix} 0 \\ 1 \\ 0 \end{bmatrix} \\
=& \begin{bmatrix} 0.985 & 0.151 & -0.087 \\ -0.151 & 0.989 & 0.007 \\ 0.087 & 0.007 & 0.996 \end{bmatrix} \cdot \begin{bmatrix} 1 & 0 & 0 \\ 0 & 0.966 & 0.259 \\ 0 & -0.259 & 0.966 \end{bmatrix} \cdot \ldots \\
& \begin{bmatrix} 1 & 0 & 0 \\ 0 & 0.966 & -0.258 \\ 0 & 0.258 & 0.966 \end{bmatrix}^{-1} \cdot \begin{bmatrix} 0 \\ 1 \\ 0 \end{bmatrix} \\
=& \begin{bmatrix} 0.985 & 0.151 & -0.087 \\ -0.151 & 0.989 & 0.007 \\ 0.087 & 0.007 & 0.996 \end{bmatrix} \cdot \begin{bmatrix} 1 & 0 & 0 \\ 0 & 0.966 & 0.259 \\ 0 & -0.259 & 0.966 \end{bmatrix} \cdot \ldots \\
& \begin{bmatrix} 1 & 0 & 0 \\ 0 & 0.966 & 0.258 \\ 0 & -0.258 & 0.966 \end{bmatrix} \cdot \begin{bmatrix} 0 \\ 1 \\ 0 \end{bmatrix} \\
=& \begin{bmatrix} 0.985 & 0.151 & -0.087 \\ -0.151 & 0.989 & 0.007 \\ 0.087 & 0.007 & 0.996 \end{bmatrix} \cdot \begin{bmatrix} 1 & 0 & 0 \\ 0 & 0.966 & 0.259 \\ 0 & -0.259 & 0.966 \end{bmatrix} \cdot \begin{bmatrix} 0 \\ 0.966 \\ -0.258 \end{bmatrix} \\
=& \begin{bmatrix} 0.985 & 0.151 & -0.087 \\ -0.151 & 0.989 & 0.007 \\ 0.087 & 0.007 & 0.996 \end{bmatrix} \cdot \begin{bmatrix} 0 \\ 0.867 \\ -0.5 \end{bmatrix} \\
=& \begin{bmatrix} 0.174 \\ 0.854 \\ -0.495 \end{bmatrix}
\end{aligned}
$$

The cross product matrix of this vector must be found for use in Rodrigue's rotation formula:

$$
\begin{aligned}
\tilde{u}_{yaw} =& \begin{bmatrix} 0 & -u_z & u_y \\ u_z & 0 & -u_x \\ -u_y & u_x & 0 \end{bmatrix} \\
=& \begin{bmatrix} 0 & 0.495 & 0.854 \\ -0.495 & 0 & -0.174 \\ -0.854 & 0.174 & 0 \end{bmatrix}
\end{aligned}
$$

The rotation matrix for the yaw rotation can now be determined:

$$
\begin{aligned}
R_{yaw} =& I + \tilde{u}_{yaw} \sin(-\psi) + \tilde{u}_{yaw}^2 (1 - \cos(-\psi)) \\
=& \begin{bmatrix} 1 & 0 & 0 \\ 0 & 1 & 0 \\ 0 & 0 & 1 \end{bmatrix} + \begin{bmatrix} 0 & 0.495 & 0.854 \\ -0.495 & 0 & -0.174 \\ -0.854 & 0.174 & 0 \end{bmatrix} \cdot \sin(-0.035) + \ldots \\
& \begin{bmatrix} 0 & 0.495 & 0.854 \\ -0.495 & 0 & -0.174 \\ -0.854 & 0.174 & 0 \end{bmatrix}^2 \cdot (1 - \cos(-0.035)) \\
=& \begin{bmatrix} 1 & 0 & 0 \\ 0 & 1 & 0 \\ 0 & 0 & 1 \end{bmatrix} + \begin{bmatrix} 0 & -0.017 & -0.03 \\ 0.017 & 0 & 0.006 \\ 0.03 & -0.006 & 0 \end{bmatrix} + \ldots \\
& \begin{bmatrix} -0.974 & 0.149 & -0.086 \\ 0.149 & -0.275 & -0.423 \\ -0.086 & -0.423 & -0.76 \end{bmatrix} \cdot 6 \times 10^{-4} \\
=& \begin{bmatrix} 0.999 & -0.017 & -0.03 \\ 0.017 & 1 & 0.006 \\ 0.03 & -0.06 & 1 \end{bmatrix}
\end{aligned}
$$

Now that all three of the rotations used to define the position of the kite have been found, the rotation matrix to change a vector given in the global coordinate system into its equivalent in the kite coordinate system can be found:

$$
\begin{aligned}
R_{kite} =& R_{yaw} \cdot R_{roll} \cdot R_{pitch} \\
=& \begin{bmatrix} 0.999 & -0.017 & -0.03 \\ 0.017 & 1 & 0.006 \\ 0.03 & -0.06 & 1 \end{bmatrix} \cdot \begin{bmatrix} 0.985 & 0.151 & -0.087 \\ -0.151 & 0.989 & 0.007 \\ 0.087 & 0.007 & 0.996 \end{bmatrix} \cdot \begin{bmatrix} 1 & 0 & 0 \\ 0 & 0.966 & 0.259 \\ 0 & -0.259 & 0.966 \end{bmatrix} \\
=& \begin{bmatrix} 0.999 & -0.017 & -0.03 \\ 0.017 & 1 & 0.006 \\ 0.03 & -0.06 & 1 \end{bmatrix} \cdot \begin{bmatrix} 0.985 & 0.168 & -0.045 \\ -0.151 & 0.954 & 0.263 \\ 0.087 & -0.251 & 0.964 \end{bmatrix} \\
=& \begin{bmatrix} 0.984 & 0.159 & -0.078 \\ -0.133 & 0.955 & 0.268 \\ 0.117 & -0.252 & 0.961 \end{bmatrix}
\end{aligned}
$$

A.2.3 Rotation Matrix for the Disk Coordinate system

For this example case, no twist angle will be applied, therefore the disk coordinate system differs from the kite coordinate system by one rotation representing the dihedral angle, given by equation 3.3:

$$R_{Dihedral(i)} = \begin{bmatrix} \cos\left(-1^i \cdot \gamma\right) & -\sin\left(-1^i \cdot \gamma\right) & 0 \\ \sin\left(-1^i \cdot \gamma\right) & \cos\left(-1^i \cdot \gamma\right) & 0 \\ 0 & 0 & 1 \end{bmatrix}$$

The rotation matrix for the disk on the positive X-side of the coordinate system, disk one, is:

$$\begin{aligned} R_{Dihedral(1)} &= \begin{bmatrix} \cos\left(-0.436 \cdot \left(-1^1\right)\right) & -\sin\left(-0.436 \cdot \left(-1^1\right)\right) & 0 \\ \sin\left(-0.436 \cdot \left(-1^1\right)\right) & \cos\left(-0.436 \cdot \left(-1^1\right)\right) & 0 \\ 0 & 0 & 1 \end{bmatrix} \\ &= \begin{bmatrix} \cos\left(0.436\right) & -\sin\left(0.436\right) & 0 \\ \sin\left(0.436\right) & \cos\left(0.436\right) & 0 \\ 0 & 0 & 1 \end{bmatrix} \\ &= \begin{bmatrix} 0.906 & -0.422 & 0 \\ 0.422 & 0.906 & 0 \\ 0 & 0 & 1 \end{bmatrix} \end{aligned}$$

And the rotation matrix for the disk on the negative X-side of the kite coordinate system, disk two, is:

$$\begin{aligned} R_{Dihedral(2)} &= \begin{bmatrix} \cos\left(-0.436 \cdot \left(-1^2\right)\right) & -\sin\left(-0.436 \cdot \left(-1^2\right)\right) & 0 \\ \sin\left(-0.436 \cdot \left(-1^2\right)\right) & \cos\left(-0.436 \cdot \left(-1^2\right)\right) & 0 \\ 0 & 0 & 1 \end{bmatrix} \\ &= \begin{bmatrix} \cos\left(-0.436\right) & -\sin\left(-0.436\right) & 0 \\ \sin\left(-0.436\right) & \cos\left(-0.436\right) & 0 \\ 0 & 0 & 1 \end{bmatrix} \\ &= \begin{bmatrix} 0.906 & 0.422 & 0 \\ -0.422 & 0.906 & 0 \\ 0 & 0 & 1 \end{bmatrix} \end{aligned}$$

The rotation matrices to change a vector defined in the global coordinate system to its equivalents in the disk coordinate systems are given by equation 3.5:

$$R_{Disk(i)} = R_{Twist(i)} \cdot R_{Dihedral(i)} \cdot R_{Kite}$$

Since there are no twist angles for this kite, the disk rotation matrices are:

$$
\begin{aligned}
R_{Disk(1)} =& R_{Dihedral(1)} \cdot R_{Kite} \\
=& \begin{bmatrix} 0.906 & -0.422 & 0 \\ 0.422 & 0.906 & 0 \\ 0 & 0 & 1 \end{bmatrix} \cdot \begin{bmatrix} 0.984 & 0.159 & -0.078 \\ -0.133 & 0.955 & 0.268 \\ 0.117 & -0.252 & 0.961 \end{bmatrix} \\
=& \begin{bmatrix} 0.948 & -0.259 & -0.184 \\ 0.295 & 0.932 & 0.210 \\ 0.117 & -0.252 & 0.961 \end{bmatrix} \\
R_{Disk(2)} =& R_{Dihedral(2)} \cdot R_{Kite} \\
=& \begin{bmatrix} 0.906 & 0.422 & 0 \\ -0.422 & 0.906 & 0 \\ 0 & 0 & 1 \end{bmatrix} \cdot \begin{bmatrix} 0.984 & 0.159 & -0.078 \\ -0.133 & 0.955 & 0.268 \\ 0.117 & -0.252 & 0.961 \end{bmatrix} \\
=& \begin{bmatrix} 0.835 & 0.547 & 0.042 \\ -0.536 & 0.798 & 0.276 \\ 0.117 & -0.252 & 0.961 \end{bmatrix}
\end{aligned}
$$

A.3 Calculating Forces and Moments

A.3.1 Angle of Attack

Equation 3.7 gives the formula to calculate the angle of attack for each disk:

$$\alpha_i = \arcsin\left(W_i \bullet \begin{bmatrix} 0 \\ 1 \\ 0 \end{bmatrix} \right)$$

Where:

$$W_i = R_{Disk(i)} \cdot \begin{bmatrix} 0 \\ 0 \\ 1 \end{bmatrix}$$

For disk one, the wind vector in disk coordinates, W_1, is:

$$\begin{aligned} W_1 =& R_{Disk(1)} \cdot \begin{bmatrix} 0 \\ 0 \\ 1 \end{bmatrix} \\ =& \begin{bmatrix} 0.948 & -0.259 & -0.184 \\ 0.295 & 0.932 & 0.210 \\ 0.117 & -0.252 & 0.961 \end{bmatrix} \cdot \begin{bmatrix} 0 \\ 0 \\ 1 \end{bmatrix} \\ =& \begin{bmatrix} -0.184 \\ 0.210 \\ 0.961 \end{bmatrix} \end{aligned}$$

And the angle of attack, α_1, is:

$$\begin{aligned} \alpha_1 =& \arcsin\left(W_1 \bullet \begin{bmatrix} 0 \\ 1 \\ 0 \end{bmatrix} \right) \\ =& \arcsin\left(\begin{bmatrix} -0.184 \\ 0.210 \\ 0.961 \end{bmatrix} \bullet \begin{bmatrix} 0 \\ 1 \\ 0 \end{bmatrix} \right) \\ =& \arcsin(0.210) \\ =& 0.212 \text{ radians} \\ =& 12.15^{\text{o}} \end{aligned}$$

Similarly for disk two:

$$\begin{aligned} W_2 =& R_{Disk(2)} \cdot \begin{bmatrix} 0 \\ 0 \\ 1 \end{bmatrix} \\ =& \begin{bmatrix} 0.835 & 0.547 & 0.042 \\ -0.536 & 0.798 & 0.276 \\ 0.117 & -0.252 & 0.961 \end{bmatrix} \cdot \begin{bmatrix} 0 \\ 0 \\ 1 \end{bmatrix} \\ =& \begin{bmatrix} 0.042 \\ 0.276 \\ 0.961 \end{bmatrix} \end{aligned}$$

$$
\begin{aligned}
\alpha_2 &= \arcsin\left(W_2 \bullet \begin{bmatrix} 0 \\ 1 \\ 0 \end{bmatrix}\right) \\
&= \arcsin\left(\begin{bmatrix} 0.042 \\ 0.276 \\ 0.961 \end{bmatrix} \bullet \begin{bmatrix} 0 \\ 1 \\ 0 \end{bmatrix}\right) \\
&= \arcsin(0.276) \\
&= 0.279 \text{ radians} \\
&= 15.99^{\text{o}}
\end{aligned}
$$

A.3.2 Aerodynamic Properties of disks

Using the interpolated data shown in figures 3.3 and 3.4, the aerodynamic properties of the disks at the above angles of attack are found to be:

$$
\begin{aligned}
Cl_1 &= 0.505 \\
Cd_1 &= 0.115 \\
COP_1 &= 0.292
\end{aligned}
$$

$$
\begin{aligned}
Cl_2 &= 0.681 \\
Cd_2 &= 0.185 \\
COP_2 &= 0.316
\end{aligned}
$$

A.3.3 Lift Force

The magnitude of the lift force acting on each disk is given by equation 3.9:

$$
|L| = \frac{\rho \cdot A \cdot Cl(\alpha) \cdot V^2}{2}
$$

For disk one, the lift force magnitude is:

$$
\begin{aligned}
|L|_1 &= \frac{\rho \cdot \left(\frac{\pi \cdot \emptyset^2}{4}\right) \cdot Cl_1 \cdot V^2}{2} \\
&= \frac{1.2 \cdot \left(\frac{\pi \cdot 0.24^2}{4}\right) \cdot 0.505 \cdot 10^2}{2} \\
&= 1.371N
\end{aligned}
$$

And for disk two:

$$
\begin{aligned}
|L|_2 =& \frac{\rho \cdot \left(\frac{\pi \cdot \emptyset^2}{4}\right) \cdot Cl_2 \cdot V^2}{2} \\
=& \frac{1.2 \cdot \left(\frac{\pi \cdot 0.24^2}{4}\right) \cdot 0.505 \cdot 10^2}{2} \\
=& 1.849N
\end{aligned}
$$

Equation 3.11 finds a vector in the Z-direction of the global coordinate system in disk coordinates, which is required before the direction of the lift force can be found:

$$
N^D = R_{Disk} \cdot \begin{bmatrix} 0 \\ 0 \\ 1 \end{bmatrix}
$$

For disk one:

$$
\begin{aligned}
N_1^D =& R_{Disk(1)} \cdot \begin{bmatrix} 0 \\ 0 \\ 1 \end{bmatrix} \\
=& \begin{bmatrix} 0.948 & -0.259 & -0.184 \\ 0.295 & 0.932 & 0.210 \\ 0.117 & -0.252 & 0.961 \end{bmatrix} \cdot \begin{bmatrix} 0 \\ 0 \\ 1 \end{bmatrix} \\
=& \begin{bmatrix} -0.184 \\ 0.210 \\ 0.961 \end{bmatrix}
\end{aligned}
$$

And for disk two:

$$
\begin{aligned}
N_2^D =& R_{Disk(2)} \cdot \begin{bmatrix} 0 \\ 0 \\ 1 \end{bmatrix} \\
=& \begin{bmatrix} 0.835 & 0.547 & 0.042 \\ -0.536 & 0.798 & 0.276 \\ 0.117 & -0.252 & 0.961 \end{bmatrix} \cdot \begin{bmatrix} 0 \\ 0 \\ 1 \end{bmatrix} \\
=& \begin{bmatrix} 0.042 \\ 0.276 \\ 0.961 \end{bmatrix}
\end{aligned}
$$

The direction that the lift force acts in can now be found in disk coordinates, as given

in equation 3.12:

$$\overrightarrow{L^D} = \begin{bmatrix} 0 \\ 1 \\ 0 \end{bmatrix} - \left(\begin{bmatrix} 0 \\ 1 \\ 0 \end{bmatrix} \bullet N^D \right) \cdot N^D$$

For disk one:

$$\begin{aligned}
\overrightarrow{L_1^D} &= \begin{bmatrix} 0 \\ 1 \\ 0 \end{bmatrix} - \left(\begin{bmatrix} 0 \\ 1 \\ 0 \end{bmatrix} \bullet N_1^D \right) \cdot N_1^D \\
&= \begin{bmatrix} 0 \\ 1 \\ 0 \end{bmatrix} - \left(\begin{bmatrix} 0 \\ 1 \\ 0 \end{bmatrix} \bullet \begin{bmatrix} -0.184 \\ 0.210 \\ 0.961 \end{bmatrix} \right) \cdot \begin{bmatrix} -0.184 \\ 0.210 \\ 0.961 \end{bmatrix} \\
&= \begin{bmatrix} 0 \\ 1 \\ 0 \end{bmatrix} - 0.21 \cdot \begin{bmatrix} -0.184 \\ 0.210 \\ 0.961 \end{bmatrix} \\
&= \begin{bmatrix} 0 \\ 1 \\ 0 \end{bmatrix} - \begin{bmatrix} -0.039 \\ 0.044 \\ 0.202 \end{bmatrix} \\
&= \begin{bmatrix} 0.039 \\ 0.956 \\ -0.202 \end{bmatrix}
\end{aligned}$$

And for disk two:

$$\begin{aligned}
\overrightarrow{L_2^D} &= \begin{bmatrix} 0 \\ 1 \\ 0 \end{bmatrix} - \left(\begin{bmatrix} 0 \\ 1 \\ 0 \end{bmatrix} \bullet N_2^D \right) \cdot N_2^D \\
&= \begin{bmatrix} 0 \\ 1 \\ 0 \end{bmatrix} - 0.276 \cdot \begin{bmatrix} 0.042 \\ 0.276 \\ 0.961 \end{bmatrix} \\
&= \begin{bmatrix} -0.012 \\ 0.924 \\ -0.265 \end{bmatrix}
\end{aligned}$$

To find the vector describing the lift forces acting on each disk, equation 3.13 multiplies the normalised lift force direction vector (the vectors found above no longer have a length of 1 since they have been projected onto a plane) by the lift force magnitude:

$$L^D = |L| \cdot \frac{\overrightarrow{L}}{\left|\overrightarrow{L}\right|}$$

For disk one:

$$
\begin{aligned}
L_1^D =& |L|_1 \cdot \frac{\overrightarrow{L_1}}{\left|\overrightarrow{L_1}\right|} \\
=& 1.371 \cdot \frac{\begin{bmatrix} 0.039 \\ 0.956 \\ -0.202 \end{bmatrix}}{\sqrt{0.039^2 + 0.956^2 + 0.202^2}} \\
=& \begin{bmatrix} 0.055 \\ 1.340 \\ -0.283 \end{bmatrix} N
\end{aligned}
$$

And for disk two:

$$
\begin{aligned}
L_2^D =& |L|_2 \cdot \frac{\overrightarrow{L_2}}{\left|\overrightarrow{L_2}\right|} \\
=& 1.849 \cdot \frac{\begin{bmatrix} -0.012 \\ 0.924 \\ -0.265 \end{bmatrix}}{\sqrt{0.012^2 + 0.924^2 + 0.265^2}} \\
=& \begin{bmatrix} -0.023 \\ 1.777 \\ -0.510 \end{bmatrix} N
\end{aligned}
$$

The lift force vectors will be more useful in later calculations if expressed in kite coordinates, as shown in equation 3.14:

$$
L^K = R_{Kite} \cdot R_{Disk}^{-1} \cdot L^D
$$

For disk one:

$$
\begin{aligned}
L_1^K =& R_{Kite} \cdot R_{Disk(1)}^{-1} \cdot L_1^D \\
=& \begin{bmatrix} 0.984 & 0.159 & -0.078 \\ -0.133 & 0.955 & 0.268 \\ 0.117 & -0.252 & 0.961 \end{bmatrix} \cdot \begin{bmatrix} 0.948 & -0.259 & -0.184 \\ 0.295 & 0.932 & 0.210 \\ 0.117 & -0.252 & 0.961 \end{bmatrix}^{-1} \cdot \begin{bmatrix} 0.055 \\ 1.340 \\ -0.283 \end{bmatrix} \\
=& \begin{bmatrix} 0.616 \\ 1.193 \\ -0.283 \end{bmatrix} N
\end{aligned}
$$

And for disk two:

$$
\begin{aligned}
L_2^K =& R_{Kite} \cdot R_{Disk(2)}^{-1} \cdot L_2^D \\
=& \begin{bmatrix} 0.984 & 0.159 & -0.078 \\ -0.133 & 0.955 & 0.268 \\ 0.117 & -0.252 & 0.961 \end{bmatrix} \cdot \begin{bmatrix} 0.835 & 0.547 & 0.042 \\ -0.536 & 0.798 & 0.276 \\ 0.117 & -0.252 & 0.961 \end{bmatrix}^{-1} \cdot \begin{bmatrix} -0.023 \\ 1.777 \\ -0.510 \end{bmatrix} \\
=& \begin{bmatrix} -0.773 \\ 1.601 \\ -0.510 \end{bmatrix} N
\end{aligned}
$$

A.3.4 Drag Force

The magnitude of the drag force acting on a disk is given by equation 3.15:

$$|D| = \frac{\rho \cdot A \cdot Cd\,(\alpha) \cdot V^2}{2}$$

The drag force acting on disk one of this kite is:

$$
\begin{aligned}
|D|_1 =& \frac{\rho \cdot \left(\frac{\pi \cdot \emptyset^2}{4}\right) \cdot Cd_1 \cdot V^2}{2} \\
=& \frac{1.2 \cdot \left(\frac{\pi \cdot 0.24^2}{4}\right) \cdot 0.115 \cdot 10^2}{2} \\
=& 0.312N
\end{aligned}
$$

And for disk two:

$$
\begin{aligned}
|D|_2 =& \frac{\rho \cdot \left(\frac{\pi \cdot \emptyset^2}{4}\right) \cdot Cd_2 \cdot V^2}{2} \\
=& \frac{1.2 \cdot \left(\frac{\pi \cdot 0.24^2}{4}\right) \cdot 0.185 \cdot 10^2}{2} \\
=& 0.502N
\end{aligned}
$$

The drag force acts in the same direction as the wind (the global Z-axis). Equitation 3.16 gives this in kite coordinates:

$$\begin{aligned}\overrightarrow{D^K} =& R_{Kite} \cdot \begin{bmatrix} 0 \\ 0 \\ -1 \end{bmatrix} \\ =& \begin{bmatrix} 0.984 & 0.159 & -0.078 \\ -0.133 & 0.955 & 0.268 \\ 0.117 & -0.252 & 0.961 \end{bmatrix} \cdot \begin{bmatrix} 0 \\ 0 \\ -1 \end{bmatrix} \\ =& \begin{bmatrix} 0.078 \\ -0.268 \\ -0.961 \end{bmatrix}\end{aligned}$$

The drag force vectors for each disk can now be found using equation 3.17:

$$D_i^K = |D|_i \cdot \overrightarrow{D^K}$$

For disk one:

$$\begin{aligned}D_1^K =& |D|_1 \cdot \overrightarrow{D^K} \\ =& 0.312 \cdot \begin{bmatrix} 0.078 \\ -0.268 \\ -0.961 \end{bmatrix} \\ =& \begin{bmatrix} 0.024 \\ -0.084 \\ -0.300 \end{bmatrix} N\end{aligned}$$

And for disk two:

$$\begin{aligned}D_2^K =& |D|_2 \cdot \overrightarrow{D^K} \\ =& 0.502 \cdot \begin{bmatrix} 0.078 \\ -0.268 \\ -0.961 \end{bmatrix} \\ =& \begin{bmatrix} 0.039 \\ -0.135 \\ -0.482 \end{bmatrix} N\end{aligned}$$

A.3.5 Combined Forces Acting on the Kite Structure

In addition to the aerodynamic forces, the force due to gravity acting on the kite must be taken into account. This is given by equation 3.19:

$$
\begin{aligned}
F^K_{Gravity} =& R_{Kite} \cdot \begin{bmatrix} 0 \\ -mg \\ 0 \end{bmatrix} \\
=& \begin{bmatrix} 0.984 & 0.159 & -0.078 \\ -0.133 & 0.955 & 0.268 \\ 0.117 & -0.252 & 0.961 \end{bmatrix} \cdot \begin{bmatrix} 0 \\ -0.1 \cdot 9.81 \\ 0 \end{bmatrix} \\
=& \begin{bmatrix} -0.156 \\ -0.937 \\ 0.247 \end{bmatrix} N
\end{aligned}
$$

The combined force is either resisted by the lines and/or causes the kite to accelerate, depending on its direction. This force is given by equation 3.18:

$$
\begin{aligned}
F^K_T =& \sum_{i=1}^{n} L^K_i + \sum_{i=1}^{n} D^K_i + F^K_{Gravity} \\
=& L^K_1 + L^K_2 + D^K_1 + D^K_2 + F^K_{Gravity} \\
=& \begin{bmatrix} 0.616 \\ 1.193 \\ -0.283 \end{bmatrix} + \begin{bmatrix} -0.773 \\ 1.601 \\ -0.510 \end{bmatrix} + \begin{bmatrix} 0.024 \\ -0.084 \\ -0.300 \end{bmatrix} + \begin{bmatrix} 0.039 \\ -0.135 \\ -0.482 \end{bmatrix} + \begin{bmatrix} -0.156 \\ -0.937 \\ 0.247 \end{bmatrix} \\
=& \begin{bmatrix} -0.250 \\ 1.638 \\ -1.328 \end{bmatrix} N
\end{aligned}
$$

To determine whether this kite is in positional equilibrium (the moments found next are needed to determine whether it is in angular equilibrium) this force can be converted

into line coordinates:

$$
\begin{aligned}
F_T^L =& R_{Line} \cdot R_{Kite}^{-1} \cdot F_T^K \\
=& \begin{bmatrix} 1 & 0 & 0 \\ 0 & 0.966 & -0.258 \\ 0 & 0.258 & 0.966 \end{bmatrix} \cdot \begin{bmatrix} 0.984 & 0.159 & -0.078 \\ -0.133 & 0.955 & 0.268 \\ 0.117 & -0.252 & 0.961 \end{bmatrix}^{-1} \cdot \begin{bmatrix} -0.250 \\ 1.638 \\ -1.328 \end{bmatrix} \\
=& \begin{bmatrix} 1 & 0 & 0 \\ 0 & 0.966 & -0.258 \\ 0 & 0.258 & 0.966 \end{bmatrix} \cdot \begin{bmatrix} 0.984 & -0.133 & 0.117 \\ 0.159 & 0.954 & -0.253 \\ -0.078 & 0.266 & 0.960 \end{bmatrix} \cdot \begin{bmatrix} -0.250 \\ 1.638 \\ -1.328 \end{bmatrix} \\
=& \begin{bmatrix} 0.984 & -0.133 & 0.117 \\ 0.174 & 0.853 & -0.492 \\ -0.035 & 0.503 & 0.862 \end{bmatrix} \cdot \begin{bmatrix} -0.250 \\ 1.638 \\ -1.328 \end{bmatrix} \\
=& \begin{bmatrix} -0.619 \\ 2.007 \\ -0.312 \end{bmatrix} N
\end{aligned}
$$

The line can only resist forces aligned with its Y-axis, so this kite is not in positional equilibrium.

A.3.6 Moments about the Bridle Point

To find the moments acting about the central bridle point, position vectors between this point and each force are required. This first requires that the bridle point location with respect to the kite centre is found from the bridle geometry. Equation 3.22 finds the Y- and Z-coordinates of the bridle point with respect to the centre of the kite in kite coordinates:

$$
\begin{aligned}
d_y =& -\sqrt{l_f^2 - \left(\frac{l_f^2 - l_r^2 + l_a^2}{2 \cdot l_a}\right)^2} \\
=& -\sqrt{0.2^2 - \left(\frac{0.2^2 - 0.23^2 + 0.24^2}{2 \cdot 0.24}\right)^2} \\
=& -0.177m
\end{aligned}
$$

$$
\begin{aligned}
d_z =& \frac{l_a}{2} - \frac{l_f^2 - l_r^2 + l_a^2}{2 \cdot l_a} \\
=& \frac{0.24}{2} - \frac{0.2^2 - 0.23^2 + 0.24^2}{2 \cdot 0.24} \\
=& 0.027m
\end{aligned}
$$

Next, the angle through which the bridles rotate due to the kite roll angle must be found, as given by equation 3.24:

$$
\begin{aligned}
\beta &= -\arcsin\left(\begin{bmatrix}1\\0\\0\end{bmatrix}\bullet\left(R_{Kite}\cdot R_{line}^{-1}\cdot\begin{bmatrix}0\\1\\0\end{bmatrix}\right)\right)\\
&= -\arcsin\left(\begin{bmatrix}1\\0\\0\end{bmatrix}\bullet\left(\begin{bmatrix}0.984 & 0.159 & -0.078\\-0.133 & 0.955 & 0.268\\0.117 & -0.252 & 0.961\end{bmatrix}\cdot\begin{bmatrix}1 & 0 & 0\\0 & 0.966 & -0.258\\0 & 0.258 & 0.966\end{bmatrix}^{-1}\cdot\begin{bmatrix}0\\1\\0\end{bmatrix}\right)\right)\\
&= -\arcsin\left(\begin{bmatrix}1\\0\\0\end{bmatrix}\bullet\left(\begin{bmatrix}0.984 & 0.174 & -0.034\\-0.133 & 0.854 & 0.505\\0.117 & -0.492 & 0.864\end{bmatrix}\cdot\begin{bmatrix}0\\1\\0\end{bmatrix}\right)\right)\\
&= -\arcsin\left(\begin{bmatrix}1\\0\\0\end{bmatrix}\bullet\begin{bmatrix}0.174\\0.854\\-0.492\end{bmatrix}\right)\\
&= -\arcsin(0.174)\\
&= -0.175rad\\
&= -10^{\circ}
\end{aligned}
$$

In this case, the angle is identical to the roll angle due to rounding. However, in some cases, the angle may differ from the roll angle sufficiently to make substituting in the roll angle incorrect.

The position vector between the bridle point and kite centre can now be found by rotating the Y- and Z-bridle coordinates (reversed, since they express the distance from the kite centre to the bridle point, rather than from the bridle point to the kite centre) by this angle:

$$
\begin{aligned}
\mathbf{r}_{BP-CK}^{K} &= \begin{bmatrix}\cos\beta & -\sin\beta & 0\\\sin\beta & \cos\beta & 0\\0 & 0 & 1\end{bmatrix}\cdot\begin{bmatrix}0\\-d_y\\-d_z\end{bmatrix}\\
&= \begin{bmatrix}0.985 & 0.174 & 0\\-0.174 & 0.985 & 0\\0 & 0 & 1\end{bmatrix}\cdot\begin{bmatrix}0\\0.177\\-0.027\end{bmatrix}\\
&= \begin{bmatrix}0.031\\0.174\\-0.027\end{bmatrix}m
\end{aligned}
$$

For a two disk kite, the centre of mass is assumed to be at the kite centre:

$$\mathbf{r}_{BP-CM} = \mathbf{r}_{BP-CK}$$

To calculate the moments caused by the lift and drag forces, a vector describing the positions of the centres of pressure relative to the bridle point is required. This can be split into three components which are added together: the position vector of the centre of the kite (found above), the position vector for the disk centre relative to the centre of the kite, and the position vector of the centre of pressure relative to the disk centre. The position vectors for the disk centres relative to the kite centre are described by equation 3.27:

$$\mathbf{r}^K_{CK-CDi} = \begin{bmatrix} -1^{i+1} \cdot s/2 \\ 0 \\ 0 \end{bmatrix}$$

$$\mathbf{r}^K_{CK-CD1} = \begin{bmatrix} 0.25 \\ 0 \\ 0 \end{bmatrix} m$$

$$\mathbf{r}^K_{CK-CD2} = \begin{bmatrix} -0.25 \\ 0 \\ 0 \end{bmatrix} m$$

The position vectors for the centres of pressure relative to the disk centres are found by calculating the magnitude and direction separately. Equation 3.29 gives the magnitudes:

$$\begin{aligned}
|CPi - CDi| =& \frac{\emptyset_i}{2} - COP_i(\alpha) \cdot \emptyset_i \\
|CP1 - CD1| =& \frac{\emptyset}{2} - COP_1 \cdot \emptyset \\
=& \frac{0.24}{2} - 0.292 \cdot 0.24 \\
=& 49.9mm \\
|CP2 - CD2| =& \frac{\emptyset}{2} - COP_2 \cdot \emptyset \\
=& \frac{0.24}{2} - 0.316 \cdot 0.24 \\
=& 44.2mm
\end{aligned}$$

To find the direction of the line on which the centre of pressure lies in kite coordinates, vectors normal to the disk surfaces and parallel to the wind are required. Disk normal

vectors are given by equation 3.31:

$$N_i^K = R_{Kite} \cdot R_{diski}^{-1} \cdot \begin{bmatrix} 0 \\ 1 \\ 0 \end{bmatrix}$$

So the normal vector for disk one is:

$$\begin{aligned}
N_1^K =& R_{Kite} \cdot R_{disk1}^{-1} \cdot \begin{bmatrix} 0 \\ 1 \\ 0 \end{bmatrix} \\
=& \begin{bmatrix} 0.984 & 0.159 & -0.078 \\ -0.133 & 0.955 & 0.268 \\ 0.117 & -0.252 & 0.961 \end{bmatrix} \cdot \begin{bmatrix} 0.948 & -0.259 & -0.184 \\ 0.295 & 0.932 & 0.210 \\ 0.117 & -0.252 & 0.961 \end{bmatrix}^{-1} \cdot \begin{bmatrix} 0 \\ 1 \\ 0 \end{bmatrix} \\
=& \begin{bmatrix} 0.906 & 0.422 & 0 \\ -0.422 & 0.906 & 0 \\ 0 & 0 & 1 \end{bmatrix} \cdot \begin{bmatrix} 0 \\ 1 \\ 0 \end{bmatrix} \\
=& \begin{bmatrix} 0.422 \\ 0.906 \\ 0 \end{bmatrix}
\end{aligned}$$

And the vector for disk two is:

$$\begin{aligned}
N_2^K =& R_{Kite} \cdot R_{disk2}^{-1} \cdot \begin{bmatrix} 0 \\ 1 \\ 0 \end{bmatrix} \\
=& \begin{bmatrix} 0.984 & 0.159 & -0.078 \\ -0.133 & 0.955 & 0.268 \\ 0.117 & -0.252 & 0.961 \end{bmatrix} \cdot \begin{bmatrix} 0.835 & 0.547 & 0.042 \\ -0.536 & 0.798 & 0.276 \\ 0.117 & -0.252 & 0.961 \end{bmatrix}^{-1} \cdot \begin{bmatrix} 0 \\ 1 \\ 0 \end{bmatrix} \\
=& \begin{bmatrix} 0.906 & 0.422 & 0 \\ -0.422 & 0.906 & 0 \\ 0 & 0 & 1 \end{bmatrix} \cdot \begin{bmatrix} 0 \\ 1 \\ 0 \end{bmatrix} \\
=& \begin{bmatrix} -0.422 \\ 0.906 \\ 0 \end{bmatrix}
\end{aligned}$$

Equation 3.32 gives the wind vector in kite coordinates:

$$
\begin{aligned}
W^K =& R_{Kite} \cdot \begin{bmatrix} 0 \\ 0 \\ 1 \end{bmatrix} \\
=& \begin{bmatrix} 0.984 & 0.159 & -0.078 \\ -0.133 & 0.955 & 0.268 \\ 0.117 & -0.252 & 0.961 \end{bmatrix} \cdot \begin{bmatrix} 0 \\ 0 \\ 1 \end{bmatrix} \\
=& \begin{bmatrix} -0.078 \\ 0.268 \\ 0.961 \end{bmatrix}
\end{aligned}
$$

And equation 3.30 finds a vector in the direction of the disk chord:

$$
\overrightarrow{Chord}_i = W^K - \left(W^K \bullet N_i^K\right) \cdot N_i^K
$$

Which for disk one is:

$$
\begin{aligned}
\overrightarrow{Chord}_1 =& W^K - \left(W^K \bullet N_1^K\right) \cdot N_1^K \\
=& \begin{bmatrix} -0.078 \\ 0.268 \\ 0.961 \end{bmatrix} - \left(\begin{bmatrix} -0.078 \\ 0.268 \\ 0.961 \end{bmatrix} \bullet \begin{bmatrix} 0.422 \\ 0.906 \\ 0 \end{bmatrix} \right) \cdot \begin{bmatrix} 0.422 \\ 0.906 \\ 0 \end{bmatrix} \\
=& \begin{bmatrix} -0.078 \\ 0.268 \\ 0.961 \end{bmatrix} - 0.210 \cdot \begin{bmatrix} 0.422 \\ 0.906 \\ 0 \end{bmatrix} \\
=& \begin{bmatrix} -0.167 \\ 0.078 \\ 0.961 \end{bmatrix}
\end{aligned}
$$

And for disk two:

$$
\begin{aligned}
\overrightarrow{Chord}_2 =& W^K - \left(W^K \bullet N_2^K\right) \cdot N_2^K \\
=& \begin{bmatrix} -0.078 \\ 0.268 \\ 0.961 \end{bmatrix} - \left(\begin{bmatrix} -0.078 \\ 0.268 \\ 0.961 \end{bmatrix} \bullet \begin{bmatrix} -0.422 \\ 0.906 \\ 0 \end{bmatrix} \right) \cdot \begin{bmatrix} -0.422 \\ 0.906 \\ 0 \end{bmatrix} \\
=& \begin{bmatrix} -0.078 \\ 0.268 \\ 0.961 \end{bmatrix} - 0.276 \cdot \begin{bmatrix} -0.422 \\ 0.906 \\ 0 \end{bmatrix} \\
=& \begin{bmatrix} 0.039 \\ 0.018 \\ 0.961 \end{bmatrix}
\end{aligned}
$$

The position vectors for the centres of pressure relative to the disk centres can now be found using equation 3.28:

$$
\mathbf{r}^K_{CDi-CPi} = \frac{|CPi - CDi| \cdot \overrightarrow{Chord_i}}{\left|\overrightarrow{Chord_i}\right|}
$$

For disk one:

$$
\begin{aligned}
\mathbf{r}^K_{CD1-CP1} =& \frac{|CP1 - CD1| \cdot \overrightarrow{Chord_1}}{\left|\overrightarrow{Chord_1}\right|} \\
=& \frac{49.9 \times 10^{-3} \cdot \begin{bmatrix} -0.167 \\ 0.078 \\ 0.961 \end{bmatrix}}{\sqrt{0.167^2 + 0.078^2 + 0.961^2}} \\
=& \begin{bmatrix} -8.5 \times 10^{-3} \\ 4.0 \times 10^{-3} \\ 49.0 \times 10^{-3} \end{bmatrix} m
\end{aligned}
$$

And for disk two:

$$\begin{aligned}\mathbf{r}^K_{CD2-CP2} =& \frac{|CP2 - CD2| \cdot \overrightarrow{Chord_2}}{\left|\overrightarrow{Chord_2}\right|} \\ =& \frac{44.2 \times 10^{-3} \cdot \begin{bmatrix} 0.039 \\ 0.018 \\ 0.961 \end{bmatrix}}{\sqrt{0.039^2 + 0.018^2 + 0.961^2}} \\ =& \begin{bmatrix} 1.8 \times 10^{-3} \\ 0.8 \times 10^{-3} \\ 44.2 \times 10^{-3} \end{bmatrix} m\end{aligned}$$

The position vector for the centres of pressure relative to the central bridle point can now be found using equation 3.26:

$$\mathbf{r}^K_{BP-CPi} = \mathbf{r}^K_{BP-CK} + \mathbf{r}^K_{CK-CDi} + \mathbf{r}^K_{CDi-CPi}$$

For disk one:

$$\begin{aligned}\mathbf{r}^K_{BP-CP1} =& \mathbf{r}^K_{BP-CK} + \mathbf{r}^K_{CK-CD1} + \mathbf{r}^K_{CD1-CP1} \\ =& \begin{bmatrix} 0.031 \\ 0.174 \\ -0.027 \end{bmatrix} + \begin{bmatrix} 0.25 \\ 0 \\ 0 \end{bmatrix} + \begin{bmatrix} -8.5 \times 10^{-3} \\ 4.0 \times 10^{-3} \\ 49.0 \times 10^{-3} \end{bmatrix} \\ =& \begin{bmatrix} 0.273 \\ 0.178 \\ 0.022 \end{bmatrix} m\end{aligned}$$

For disk two:

$$\begin{aligned}\mathbf{r}^K_{BP-CP2} =& \mathbf{r}^K_{BP-CK} + \mathbf{r}^K_{CK-CD2} + \mathbf{r}^K_{CD2-CP2} \\ =& \begin{bmatrix} 0.031 \\ 0.174 \\ -0.027 \end{bmatrix} + \begin{bmatrix} -0.25 \\ 0 \\ 0 \end{bmatrix} + \begin{bmatrix} 1.8 \times 10^{-3} \\ 0.8 \times 10^{-3} \\ 44.2 \times 10^{-3} \end{bmatrix} \\ =& \begin{bmatrix} -0.217 \\ 0.175 \\ 0.017 \end{bmatrix} m\end{aligned}$$

The moments about the bridle point caused by the aerodynamic and gravity forces

can now be found using equation 3.20:

$$
\begin{aligned}
M^K =& \sum_{i=1}^{n} \left(\mathbf{r}^K_{BP-CPi} \times L^K_i\right) + \sum_{i=1}^{n} \left(\mathbf{r}^K_{BP-CPi} \times D^K_i\right) + \mathbf{r}^K_{BP-CM} \times F^K_{Gravity} \\
=& \mathbf{r}^K_{BP-CP1} \times L^K_1 + \mathbf{r}^K_{BP-CP2} \times L^K_2 + \mathbf{r}^K_{BP-CP1} \times D^K_1 + \mathbf{r}^K_{BP-CP2} \times D^K_2 \ldots \\
& + \mathbf{r}^K_{BP-CM} \times F^K_{Gravity} \\
=& \mathbf{r}^K_{BP-CP1} \times \left(L^K_1 + D^K_1\right) + \mathbf{r}^K_{BP-CP2} \times \left(L^K_2 + D^K_2\right) + \mathbf{r}^K_{BP-CM} \times F^K_{Gravity} \\
=& \begin{bmatrix} 0.273 \\ 0.178 \\ 0.022 \end{bmatrix} \times \left(\begin{bmatrix} 0.616 \\ 1.193 \\ -0.283 \end{bmatrix} + \begin{bmatrix} 0.024 \\ -0.084 \\ -0.300 \end{bmatrix} \right) + \begin{bmatrix} -0.217 \\ 0.175 \\ 0.017 \end{bmatrix} \times \ldots \\
& \left(\begin{bmatrix} -0.773 \\ 1.601 \\ -0.510 \end{bmatrix} + \begin{bmatrix} 0.039 \\ -0.135 \\ -0.482 \end{bmatrix} \right) + \begin{bmatrix} 0.031 \\ 0.174 \\ -0.027 \end{bmatrix} \times \begin{bmatrix} -0.156 \\ -0.937 \\ 0.247 \end{bmatrix} \\
=& \begin{bmatrix} -0.128 \\ 0.173 \\ 0.189 \end{bmatrix} + \begin{bmatrix} -0.199 \\ -0.228 \\ -0.190 \end{bmatrix} + \begin{bmatrix} -0.068 \\ -0.003 \\ -0.056 \end{bmatrix} \\
=& \begin{bmatrix} -0.395 \\ -0.058 \\ -0.057 \end{bmatrix} Nm
\end{aligned}
$$

This moment is more usefully expressed in line coordinates:

$$
\begin{aligned}
M^L =& R_{Line} \cdot R^{-1}_{Kite} \cdot M^K \\
=& \begin{bmatrix} 1 & 0 & 0 \\ 0 & 0.966 & -0.258 \\ 0 & 0.258 & 0.966 \end{bmatrix} \cdot \begin{bmatrix} 0.984 & 0.159 & -0.078 \\ -0.133 & 0.955 & 0.268 \\ 0.117 & -0.252 & 0.961 \end{bmatrix}^{-1} \cdot \begin{bmatrix} -0.395 \\ -0.058 \\ -0.057 \end{bmatrix} \\
=& \begin{bmatrix} -0.388 \\ -0.090 \\ -0.065 \end{bmatrix} Nm
\end{aligned}
$$

This kite is not in rotational equilibrium about any axis. The negative X-moment indicates it will try to pitch back, increasing its angle of attack. The negative Y-moment indicates that it will try to yaw in an anti-clockwise direction from the flyer's point of view – the direction expected from the positive roll angle applied. The negative Z-moment is held by the lines, and indicates that the kite tries to return to a zero-roll configuration if the force in the two lines is equal.

Appendix B

MATLAB Code for Two-Disk Kite

Code to Find Forces and Moments Acting on a Two-Disk Kite

twodisk.m

```
function[Ml,Ft]=twodisk(pitch, roll, yaw, dihedral, elevation,lbr,lbf,...
                                                    DD,W,m,windV,DegUnits)

%Calculates the resultant forces and moments acting on a two disk kite.
%Forces (Ft) are given in the kite-based coordinate system, while the
%moments (Ml) is given in the line-based coordinate system.

%Input parameters:

%pitch           Pitch of the kite.  .

%roll            Roll angle.  Defined as rotation about line z-axis.

%yaw             Yaw angle.  Defined as rotaion about line y-axis.

%dihedral        Dihedral angle.  -ve values for anhedral.

%elevation       Line elevation angle -- measured as the acute angel the
%                line makes to the ground plane.

%lbr            Length of rear bridle line in m.

%lbf            Length of front bridle line in m.

%DD             Diameter of the kite disks in m.

%W              Width of the kite, measured as the distance between disk
%               centres.

%m              Mass of the kite in kg

```

```
%windV          Wind velocity in m/s

%DegUnits       Specifies the units (degrees or radians) in which the
%               input angles are given.  Use 'd' for degrees, 'r' for
%               radians.

if DegUnits=='d'
    pitch=pitch*2*pi/360;
    roll=roll*2*pi/360;             %Change the input angles to radians
    dihedral=dihedral*2*pi/360;     %if they have been given in degrees.
    elevation=elevation*2*pi/360;
    yaw=yaw*2*pi/360;
end


%% ==================Set Kite Parameters================================

n=2;                        % Number of disks.

P(:,1)=[W/2;0;0];           % Position of disk 1 in meters from
P(:,2)=[-W/2;0;0];          % reference point (COM).

Area=pi*DD^2/4;             % Area of each disk surface in m^2.


%% ==================Set Environment Parameters=========================

rho=1.2;                % Air density.

g=9.81;                 % Acceleration due to gravity.


%% ==================Find Transformation Matrices=======================

[Ak,Ad1,Ad2,Al]=transformMTX(pitch,elevation,roll,dihedral,yaw);
                                % Transform matrices to change from
                                % global coords to kite, disk and line
                                % coords.

%% ==================Find Aerodynamic Forces on Disks===================


Wind_Disk1=Ad1*[0;0;1];                 % Unit vector in direction of
Wind_Disk2=Ad2*[0;0;1];                 % wind in disk coordinates.


AOA(1)=-asin(dot(Wind_Disk1,[0;1;0])/(norm(Wind_Disk1)));
AOA(2)=-asin(dot(Wind_Disk2,[0;1;0])/(norm(Wind_Disk2)));
                                        % Angle of attack for each disk
```

```
for i=1:n                    % Loop for number of disks.

    [cl(i) cd(i) cop(i)]=aeroProps(AOA(i)); % Find lift,drag and center
                                            % of pressure coefficients.


    cop(i)=DD/2-cop(i)*DD;           % Find distance from center of disk
                                     % to center of pressure.

    L(i)=Area*cl(i)*rho*(windV^2)/2;     % Find Magnitude of lift force.

    D(i)=Area*cd(i)*rho*(windV^2)/2;     % Find Magnitude of drag force.

    if (cl(i)<0 || cd(i)<0 )            % Check for negative coefficients.
       [cl(i) cd(i) cop(i)]=aeroProps(-AOA(i));
       cop(i)=DD/2-cop(i)*DD;
       L(i)=Area*-cl(i)*rho*(windV^2)/2;
       D(i)=Area*-cd(i)*rho*(windV^2)/2;
    end

    if i==1
        Adisk=Ad1;               % Set the appropriate disk transfomation
    elseif i==2                  % matrix.
        Adisk=Ad2;
    end

    copl(:,i)=coplocation(cop(i),Adisk,Ak);     % Location of COP relative
                                                % to disk center in kite
                                                % coordinates.

    lift(:,i)=L(i)*liftvector(Adisk, Ak);    % Find the lift force vector.

    Drag(:,i)=(Ak)*(D(i)*[0;0;-1]);          % Find the drag force vector.

    F(:,i)=lift(:,i)+Drag(:,i);              % Find the total aerodynamic
                                             % force acting on the current
                                             % disk.
end


%% =================Find total forces and moments acting on kite=========

Ft=F(:,1)+F(:,2)+(Ak)*[0;-m*g;0];            % Find total force vector

[bpoint]=findbpoint(DD, lbf, lbr, DD,roll); % Find the distance between
                                             % the kite center of mass and
                                             % the center of  bridle
```

```
                                                % points in kite coords.

for j=1:n

    r(:,j)=copl(:,j)-bpoint+P(:,j);     % Find the position vector for the
                                        % aerodynamic force acting on each
end                                     % disk.


Mgravity=cross(-bpoint, Ak*[0;-m*g;0]);     % Find the moment about the
                                            % bridle point due to gravity.

MomentK=cross(r(:,1),F(:,1))+cross(r(:,2),F(:,2))+Mgravity;
                                                % Find the total moment about
                                                % the bridle point.


Ml=Al*inv(Ak)*MomentK;              % Transform moments into line coords.
```

Code to Find Transform Matrices for line, kite, and disk coordinate systems

transformMTX.m

```
function[Ak,Ad1,Ad2,Al]=transformMTX(pitch,elevation,roll,dihedral, yaw)

% Calculates the transformation matrices to change from global to kite,
% disk and line coordinates.

Al=[1 0 0;
    0 cos(pi/2-elevation) -sin(pi/2-elevation);
    0 sin(pi/2-elevation) cos(pi/2-elevation)]  ;
                                                % Transform matrix to change
                                                % from global to line coords.

Ap=[1 0 0;
    0 cos(-pitch) -sin(-pitch);                 % Rotation matrix for pitch
    0 sin(-pitch) cos(-pitch)];                 % rotation.

axisb=Ap*inv(Al)*[0;0;1];                       % Axis for Roll rotation

wb=[0 -axisb(3) axisb(2);                       % Cross-product matrix for
    axisb(3) 0 -axisb(1);                       % roll rotation axis.
    -axisb(2) axisb(1) 0];


```

```
Ab=eye(3)+wb*sin(-roll)+wb^2*(1-cos(-roll));
                                            % Rotation matrix for
                                            % roll rotation found using
                                            % Rodrigues rotation formula.

axisy=Ap*Ab*inv(Al)*[0;1;0];                % Axis for yaw rotation.

wy=[0 -axisy(3) axisy(2);                   % Cross-product matrix for
    axisy(3) 0 -axisy(1);                   % yaw rotation axis.
    -axisy(2) axisy(1) 0];

Ay=eye(3)+wy*sin(-yaw)+wy^2*(1-cos(-yaw));
                                            % Rotation matrix for
                                            % yaw rotation found using
                                            % Rodrigues rotation formula.

AD=[cos(-dihedral) -sin(-dihedral) 0;
    sin(-dihedral) cos(-dihedral) 0;        % Rotation matrix for
    0 0 1];                                 % dihedral rotation.


Ak=Ay*Ab*Ap;                        % Matrix to transform from global
                                    % to kite coordinates.

Ad1=(AD)*Ak;                        % Matrices to transform from global
Ad2=(AD)\Ak;                        % to disk coordinates
```

Code to Find Aerodynamic Properties of a Disk

aeroprops.m

```
function[cl cd cop]=aeroProps(AOAd)

% finds Cl, Cd and COP (Measured from front of disk, as a proportion of
% chord length) given the angle of atack in radians using data obtained
% from wind tunnel testing.


%% ============Results from wind tunnel tests============================

Ang=[0 5 10 15 20 25 30 35 40 45 50 55 60 90];

Cd_exp=[0.0468 0.0487 0.09 0.1624 0.3057 0.5101 0.7102 0.9069 0.9886...
                                        0.8488 0.8813 0.9314 0.9878 1];

```

```
Cl_exp=[0 0.1762 0.4044 0.6359 0.8581 1.0462 1.1818 1.2653 1.1603...
                                        0.9203 0.7406 0.638 0.5595 0];

Ang=Ang*2*pi/360;


cl=spline(Ang,Cl_exp,AOAd)  ;          % Find lift coefficient, drag
cd=spline(Ang,Cd_exp, AOAd)     ;      % coefficient, and location of
                                       % centre of pressure by
                                       % interpolation.

cop=0.0744*AOAd^3-0.3131*AOAd^2+0.4973*AOAd+0.2;
                                       % Find center of pressure loication
                                       % as proportion of chord length
                                       % from leading edge.
```

Code to Find Centre of Bridle Points

findbpoint.m

```
function[bpoint]=findbpoint(chordL, Lbf, Lbr, DD,roll)

%calculates position of bridle point relative to COM in a kite based
%coordinate system with origin at COM and x axis aligned with chord


% Need angle between line Y-axis and Kite Y axis

kiteY=[1 0 0;0 cos(pi/2-elevation) -sin(pi/2-elevation);0 sin(pi/2-...
            elevation)cos(pi/2-elevation)]/(Ak)*[0 1 0]';
angle=acos(dot(kiteY,[0 1 0]'));


% Find lower bridle point relative to kite center in kite
% coordinates before roll

BPK=[0; -((Lbf^2-((Lbf^2-Lbr^2+chordL^2)/(2*chordL))^2)^0.5) ;
    DD/2-(((Lbf^2)-(Lbr^2)+(chordL^2))/(2*chordL))];

% Rotate this around the kite Z axis

bpoint=[cos(-angle) -sin(-angle) 0;
    sin(-angle) cos(-angle) 0;
    0 0 1]                          * BPK;
```

Code to Find Unit Vector in Lift Force Direction

liftvector.m

```
function[Lk]=liftvector(Adisk, Akite)
% Finds a unit vector in the direction of the lift force for a disk in
% kite coordinates given transformation matrices for the disk and kite.

N=Akite*[0; 0; 1];          % A vector normal to the global
                    % x-y plane in kite coordinates

V=Akite*inv(Adisk)*[0; 1; 0];       % A vector normal to the disk
                    % x-z plane in kite coordinates

Lk = V - (dot(V,N))*N;          % The projection of the vector V
                    % onto the plane described by it's
                    % normal vector N.

Lk=Lk/norm(Lk);             % Normalise the projected vector to
                    % give a unit vector in the
                    % direction of the  lift force.
```

Code to Find Location of centre of Pressure

coplocation.m

```
function [CoPV]=coplocation(cop,Adisk,Akite)

% Finds a vector defining the location of the center of pressure

N=Akite*inv(Adisk)*[0 ;1 ;0];   % A vector normal to the disk surface
                % in kite coordinates.

V=Akite*[0 ;0; 1];              % A vector parallel to the wind in
                % kite coordinates.

chord = V - (dot(V,N))*N;   % The projection of V onto the disk
                % surface, giving a chord line.

CoPV=cop*(chord/norm(chord));   % The location of the CoP relative
                % to the disk center in kite coordinates
```

Appendix C

Results from Wind Tunnel Testing

Open-Circuit Wind Tunnel Results

Yaw moments were measured with a spring balance attached to the end of a 100mm lever arm. To aid stability, weights were used to create a constant 'base load' force opposing the spring balance. The means of the five sets of results were taken, and the standard error of the means was found. This was used to calculate the 95% confidence interval for the data. Parameters used for these sets of data are shown in table C.1.

Table C.1 Parameters used for testing in the open-circuit wind tunnel.

Parameter	Value
Disk diameter	240mm
Width between disk centres	500mm
Front bridle length	325mm
Rear bridle length	266mm
Line elevation angle	81º
Kite pitch angle	18º
Kite roll angle	20º
Kite yaw angle	0º
Kite dihedral angle	Varied

Table C.2 Results from open-circuit wind tunnel test run#1

Dihedral Angle (º)	Base (g)	Measured (g)	Total (g)	Moment (Nm)
-40	100	64	-36	-0.035
-30	100	40	-60	-0.059
-20	100	24	-76	-0.075
-10	100	10	-90	-0.088
0	100	16	-84	-0.082
10	100	13	-87	-0.085
20	100	5	-95	-0.093
30	100	23	-77	-0.076
40	100	47	-53	-0.052

Table C.3 Results from open-circuit wind tunnel test run#2

Dihedral Angle (º)	Base (g)	Measured (g)	Total (g)	Moment (Nm)
-30	110	72	-38	-0.037
-25	140	85	-55	-0.054
-20	140	80	-60	-0.059
-15	140	74	-66	-0.065
-10	160	96	-64	-0.063
-5	160	81	-79	-0.077
0	160	79	-81	-0.079
5	160	70	-90	-0.088
10	160	75	-85	-0.083
15	160	72	-88	-0.086
20	160	76	-84	-0.082
25	160	65	-75	-0.074
30	160	93	-67	-0.066

Table C.4 Results from open-circuit wind tunnel test run#3

Dihedral Angle (º)	Base (g)	Measured (g)	Total (g)	Moment (Nm)
-40	300	270	-30	-0.029
-30	300	250	-50	-0.049
-20	300	230	-70	-0.069
-10	300	210	-90	-0.088
0	300	205	-95	-0.093
10	300	210	-90	-0.088
20	300	215	-85	-0.083
30	300	220	-80	-0.078
40	300	250	-50	-0.049

Table C.5 Results from open-circuit wind tunnel test run#4

Dihedral Angle (º)	Base (g)	Measured (g)	Total (g)	Moment (Nm)
-40	120	92	-28	-0.027
-30	120	64	-56	-0.055
-20	120	55	-65	-0.064
-10	120	41	-79	-0.077
0	120	33	-87	-0.085
10	120	29	-91	-0.089
20	120	38	-82	-0.080
30	120	45	-75	-0.074
40	120	70	-50	-0.049

Table C.6 Results from open-circuit wind tunnel test run #5

Dihedral Angle (º)	Base (g)	Measured (g)	Total (g)	Moment (Nm)
-40	120	86	-34	-0.033
-30	120	75	-45	-0.044
-20	120	58	-62	-0.061
-10	120	52	-68	-0.067
0	120	25	-95	-0.093
10	120	37	-83	-0.081
20	120	44	-76	-0.075
30	120	50	-70	-0.069
40	120	80	-40	-0.039

Table C.7 Combined results from open-circuit wind tunnel tests

Dihedral Angle (º)	Mean Moment (Nm)	S.E.M. (Nm)	95% C.I. (±Nm)
-40	-0.0314	0.001791	0.00349
-30	-0.0489	0.00383	0.00747
-20	-0.0653	0.00284	0.00553
-10	-0.0767	0.00530	0.0103
0	-0.0867	0.00280	0.00546
10	-0.0855	0.00147	0.00286
20	-0.0828	0.00302	0.00588
30	-0.0724	0.00231	0.00450
40	-0.0473	0.00279	0.00543

Closed-Circuit Wind Tunnel Results

The following data was obtained using a three axis balance, using the geometry parameters given in tables 4.2 and 4.3. The measurements were repeated three times to minimise error. The data has been corrected for balance zero errors and the moment caused by the support structure alone in the flow stream. 95% confidence intervals are given, although these should be treated with caution since there are only three samples. The largest value for the confidence interval for each test is likely to apply to all data points.

Table C.8 Parameters used for testing in the closed-circuit wind tunnel

Parameter	Value
Disk diameter	Varied
Width between disk centres	500mm
Front bridle length	Varied
Rear bridle length	Varied
Line elevation angle	85.2º
Kite pitch angle	Varied
Kite roll angle	Varied
Kite yaw angle	0º
Kite dihedral angle	Varied

Table C.9 Closed circuit wind tunnel test 1: 120mm disks, 565mm front bridle, 452mm rear bridle, 12m/s flow, 24.8º pitch, 45º roll, varying dihedral.

Dihedral Angle (º)	M1 (Nm)	M2 (Nm)	M3 (Nm)	Avg. Moment (Nm)	95% C.I. (±Nm)
-30	-0.3327	-0.3312	-0.3289	-0.3309	0.0022
-20	-0.5066	-0.5076	-0.5030	-0.5057	0.0027
-10	-0.6190	-0.6166	-0.6138	-0.6165	0.0029
0	-0.6776	-0.6783	-0.6795	-0.6785	0.0011
10	-0.6689	-0.6699	-0.6670	-0.6686	0.0017
20	-0.6009	-0.6013	-0.5990	-0.6004	0.0014
30	-0.4940	-0.4925	-0.4946	-0.4937	0.0012

Table C.10 Closed circuit wind tunnel test 2: 120mm disks, 565mm front bridle, 452mm rear bridle, 13.9m/s flow, 24.8º pitch, 45º roll, varying dihedral.

Dihedral Angle (º)	M1 (Nm)	M2 (Nm)	M3 (Nm)	Avg. Moment (Nm)	95% C.I. (±Nm)
-30	-0.4310	-0.4351	-0.4341	-0.4334	0.0024
-20	-0.6705	-0.6625	-0.6667	-0.6665	0.0045
-10	-0.8240	-0.8205	-0.8224	-0.8223	0.0020
0	-0.9088	-0.9057	-0.9119	-0.9088	0.0035
10	-0.8924	-0.8928	-0.8946	-0.8933	0.0013
20	-0.7957	-0.8010	-0.7930	-0.7966	0.0046
30	-0.6651	-0.6640	-0.6624	-0.6638	0.0015

Table C.11 Closed circuit wind tunnel test 3: 240mm disks, 657mm front bridle, 422mm rear bridle, 9m/s flow, 34.8º pitch, 45º roll, varying dihedral.

Dihedral Angle (º)	M1 (Nm)	M2 (Nm)	M3 (Nm)	Avg. Moment (Nm)	95% C.I. (±Nm)
-30	-1.336	-1.339	-1.331	-1.335	0.005
-20	-1.865	-1.892	-1.900	-1.886	0.020
-10	-2.241	-2.234	-2.293	-2.256	0.036
0	-2.332	-2.298	-2.320	-2.317	0.020
10	-2.252	-2.241	-2.201	-2.231	0.030
20	-1.974	-1.981	-1.974	-1.977	0.004
30	-1.531	-1.531	-1.532	-1.531	0.001

Table C.12 Closed circuit wind tunnel test 4: 240mm disks, 657mm front bridle, 422mm rear bridle, 12m/s flow, 34.8º pitch, 45º roll, varying dihedral.

Dihedral Angle (º)	M1 (Nm)	M2 (Nm)	M3 (Nm)	Avg. Moment (Nm)	95% C.I. (±Nm)
-30	-2.401	-2.396	-2.401	-2.399	0.003
-20	-3.488	-3.469	-3.455	-3.471	0.019
-10	-4.174	-4.174	-4.208	-4.185	0.022
0	-4.300	-4.298	-4.298	-4.299	0.002
10	-4.106	-4.102	-4.021	-4.076	0.054
20	-3.583	-3.577	-3.590	-3.583	0.007
30	-2.791	-2.782	-2.781	-2.785	0.006

Table C.13 Closed circuit wind tunnel test 5: 240mm disks, 657mm front bridle, 422mm rear bridle, 9m/s flow, 34.8º pitch, -30º dihedral, varying roll.

Roll Angle (º)	M1 (Nm)	M2 (Nm)	M3 (Nm)	Avg. Moment (Nm)	95% C.I. (±Nm)
5	-0.4652	-0.4492	-0.4396	-0.4513	0.0146
15	-0.6535	-0.6478	-0.6245	-0.6419	0.0173
25	-0.6679	-0.6561	-0.667	-0.6637	0.0074
35	-0.9846	-0.9884	-0.9976	-0.9902	0.0075
45	-1.287	-1.242	-1.238	-1.255	0.031
55	-1.512	-1.502	-1.497	-1.504	0.008
65	-1.656	-1.665	-1.663	-1.661	0.005

Table C.14 Closed circuit wind tunnel test 6: 240mm disks, 657mm front bridle, 422mm rear bridle, 12m/s flow, 34.8º pitch, -30º dihedral, varying roll.

Roll Angle (º)	M1 (Nm)	M2 (Nm)	M3 (Nm)	Avg. Moment (Nm)	95% C.I. (±Nm)
5	-0.8118	-0.8149	-0.8187	-0.8151	0.0039
15	-1.171	-1.119	-1.180	-1.157	0.037
25	-1.209	-1.202	-1.213	-1.208	0.006
35	-1.810	-1.801	-1.814	-1.811	0.003
45	-2.299	-2.287	-2.289	-2.292	0.007
55	-2.743	-2.742	-2.767	-2.751	0.016
65	-3.074	-3.070	-3.062	-3.069	0.007

Table C.15 Closed circuit wind tunnel test 7: 240mm disks, 657mm front bridle, 422mm rear bridle, 9m/s flow, 34.8º pitch, 0º dihedral, varying roll.

Roll Angle (º)	M1 (Nm)	M2 (Nm)	M3 (Nm)	Avg. Moment (Nm)	95% C.I. (±Nm)
15	-0.808	-0.817	-0.803	-0.809	0.008
25	-1.275	-1.285	-1.336	-1.299	0.037
35	-1.903	-1.911	-1.999	-1.938	0.060
45	-2.332	-2.298	-2.320	-2.317	0.020
55	-2.662	-2.653	-2.650	-2.655	0.007
65	-2.859	-2.851	-2.865	-2.859	0.008
75	-3.013	-2.982	-2.950	-2.982	0.035

Table C.16 Closed circuit wind tunnel test 8: 240mm disks, 657mm front bridle, 422mm rear bridle, 12m/s flow, 34.8º pitch, 0º dihedral, varying roll.

Roll Angle (º)	M1 (Nm)	M2 (Nm)	M3 (Nm)	Avg. Moment (Nm)	95% C.I. (±Nm)
15	-1.379	-1.372	-1.390	-1.380	0.010
25	-2.205	-2.222	-2.189	-2.206	0.019
35	-3.329	-3.335	-3.443	-3.369	0.072
45	-4.300	-4.298	-4.298	-4.299	0.002
55	-4.903	-4.922	-4.913	-4.913	0.010
65	-5.248	-5.242	-5.217	-5.235	0.019
75	-5.473	-5.444	-5.405	-5.440	0.038

Table C.17 Closed circuit wind tunnel test 9: 240mm disks, 657mm front bridle, 422mm rear bridle, 9m/s flow, 34.8º pitch, 30º dihedral, varying roll.

Roll Angle (º)	M1 (Nm)	M2 (Nm)	M3 (Nm)	Avg. Moment (Nm)	95% C.I. (±Nm)
5	-0.115	-0.115	-0.115	-0.115	0.000
15	-0.611	-0.588	-0.589	-0.596	0.014
25	-0.930	-0.931	-0.945	-0.935	0.009
35	-1.277	-1.259	-1.256	-1.264	0.013
45	-1.531	-1.531	-1.532	-1.531	0.001
55	-1.739	-1.738	-1.739	-1.739	0.001
65	-1.872	-1.872	-1.877	-1.873	0.003

Table C.18 Closed circuit wind tunnel test 10: 240mm disks, 657mm front bridle, 422mm rear bridle, 12m/s flow, 34.8º pitch, 30º dihedral, varying roll.

Roll Angle (º)	**M1 (Nm)**	**M2 (Nm)**	**M3 (Nm)**	**Avg. Moment (Nm)**	**95% C.I. (±Nm)**
5	-0.224	-0.216	-0.215	-0.218	0.006
15	-1.070	-1.069	-1.068	-1.069	0.002
25	-1.712	-1.721	-1.717	-1.716	0.005
35	-2.324	-2.340	-2.321	-2.328	0.012
45	-2.791	-2.782	-2.781	-2.785	0.006
55	-3.178	-3.175	-3.168	-3.173	0.006
65	-3.446	-3.444	-3.444	-3.445	0.001